Design and Analysis of Quantum Dot Laser (InAsP) for Bio-photonic and Mode-Locking Applications

IVAN BAHNAM KAROMI

PhD Thesis

School of Physics and Astronomy

Cardiff University

May 2018

ABSTRACT

In this thesis, an original quantum dot material (InAsP) was introduced and characterised as a prospective laser material for applications in biophotonics and monolithic mode-locking. InAsP quantum dot material was grown in conditions that are appropriate for InP QD, which is the standard device in this study. The reasons for employing this material are to shift the emission to longer wavelengths than can be achieved with InP QD laser. In principle, by using both the InP and InAsP QDs in a single structure, a very wide gain spectrum can be produced that may be advantageous for passive mode-locking.

The characteristics of the InAsP QD lasers were determined and compared with the standard device (InP QD laser) in this work, such as threshold current density, laser efficiency, lasing wavelength and temperature dependency of the threshold current density for different cavity lengths (1, 2, 3 and 4mm). The results show a shifting in the emission wavelengths by 55 nm toward longer wavelengths, while maintaining useable threshold current density and laser efficiency. For example, the 2mm long InP laser has a threshold current density of 170 $A.cm^{-2}$ at room temperature, whereas for the same length, the InAsP QD laser has 260 $A.cm^{-2}$. Moreover, both samples delivered optical powers of at least 250 mW.

Edge-photo voltage spectroscopy (E-PVS measurements) confirmed deeper dot confinements for the InAsP materials by approximately 103 meV. The modal absorption spectra show a greater degree of inhomogeneous broadening for the InAsP QD materials, which was consistent with the dot size variation shown in TEM images for the InAsP wafer. This can support mode-locking in this material by broadening the optical gain spectra, which was also observed in this material.

Gain-current measurements at different temperatures; specifically, 150, 200, 250, 300, 350, and 400 K, illustrate that InAsP QD material has a wider gain band-width at all studied temperatures. The carrier distribution study shows that the InAsP QD material tends to be non-thermally populated at 150 K. And also the recombination rate of this material is faster than the InP QD materials. Both of these points can be positive in relation to mode-locked performance.

ACKNOWLEDGEMENTS

PAPERS AND CONFERENCES

Papers

1- Karomi, I., Smowton, P.M., Shutts, S., Krysa, A.B. and Beanland, R. **2015**. **"InAsP quantum dot lasers grown by MOVPE"** Optics Express 23(21), pp. 27282-27291

2- Krysa, A.B., Roberts, J.S., Devenson, J., Beanland, R., Karomi, I., Shutts, S. and Smowton, P.M. **2016** "**InAsP/AlGaInP/GaAs QD laser operating at 770 nm**" Journal of Physics: Conference Series 740(1),012008.

Conferences

1- Karomi, I., Shutts, S., Smowton, P.M. and Krysa, A.B. "**Fabrication and characterisation of 770 nm (InPAs) quantum dot lasers**" Semiconductor Integrated Optoelectronics, Cardiff, UK, 31March-2 April **2015.**

2- Karomi, I., Shutts, S., Smowton, P.M. and Krysa, A.B. **"Opening up spectrum with InPAs quantum dot lasers"** CLEO: Science and Innovations, CLEO-SI pp. 2267, **2015.**

3- Karomi, I., Shutts, S., Smowton, P.M., Krysa, A.B. and Beanland, R. "**InAsP quantum dot lasers**" 2015 IEEE Photonics Conference, IPC **7323595**, pp. 573-574 (**2015)**.

4- Karomi, I., Shutts, S., Smowton, P.M. and Krysa, A.B. "**Opening up spectrum with InPAs quantum dot lasers**" Conference on Lasers and Electro-Optics Europe - Technical Digest **2015**-August,7184392.

5- Smowton, P.M., Shutts, S., Thomas, R., *Beanland, R., Karomi, I.,* Gillgrass, S. and Krysa, A.B. "**Quantum dot lasers for integrated photonics**" Conference Digest - IEEE International Semiconductor Laser Conference7765729.

6- Krysa, A.B., Roberts, J.S., Devenson, J., Beanland, R., Karomi, I., Shutts, S. and Smowton, P.M. "**Growth and characterisation of InAsP/AlGaInP QD laser structures**" **2016** Compound Semiconductor Week, CSW 2016 - Includes 28th International Conference on Indium Phosphide and Related Materials, IPRM and 43rd International Symposium on Compound Semiconductors, ISCS 20167528566.

7- Karomi, I., Shutts, S., Smowton, P.M. and Krysa, A.B. "**InAsP Quantum Dot Material Compatible with InP Quantum Dot Structure for Monolithic Passive Mode-Locked Laser**" Semiconductor Integrated Optoelectronics, Cardiff, UK, 18-20 April **2017**

CONTENTS

TABLE OF ACRONYMS

AES	Amplifierd Spontanouse Emissiom
AFM	Atomic Force Microscopes
CDWM	coarse wavelength division multiplexing
E-PVS	Edge-Photo Voltage Spectroscopy
ES	Excited state
FCA	Free Carrier Absorption
FWHM	Full-Width at Half Maximum
GS	Ground state
HH	Heavy-hole
HREM	High-Resolution Episcopic Microscopy
I-L	Current-Light
I-P	Current-Power
I-V	Current-Light
IVBA	Intervalence Band Absorption
I-V-L	Current-Voltage-Light
J-L	Current density-Light
LH	Light-hole
MBE	Molecular Beam Epitaxy
ML	Monolayer

MOVPE	Metal Organic Vapour Phase Epitaxy
OCL	Optical Confinement Layer
OCT	optical coherence tomography
PL	Photoluminescence
QD	Quantum Dot
QDs	Quantum Dots
QW	Quantum Well
SCH	Separate Confinement Structure
SCM	Segmented Contact Method
SL	Supper lattice
SLD	Superluminescent diode
SOAs	Semiconductor optical amplifiers
TE	Transverse Electric
TEM	Transmission Electron Spectroscopy
TM	Transverse Magnetic

DEDICATED

TO ALL OF MY;

FAMILY

FRIENDS

COLLEAGUES

AND

TEACHERS

Chapter (1) Introduction

1.1 Aims and motivation

1.1.1 Toward longer wavelengths in InP quantum dot laser

InP quantum dots (QD) grown on GaAs substrates have been used as a semiconductor laser active region for output in the 630–750nm wavelength range (Smowton 2005) and also as single photon sources (Reischle et al. 2010). Threshold current density (J_{th}) can be low in the wavelength range from approximately 680-730nm, with for example a J_{th} of 130A.cm^{-2} being achieved for 2mm long, as-cleaved devices at 720nm (Kasim et al. 2015). However, InP QD laser material performance deteriorates for wavelengths longer than 740nm due to the larger dot size required and/or less suitable growth conditions such as lower growth temperatures, as illustrated in Figure 1:1 (Smowton et al. 2005).
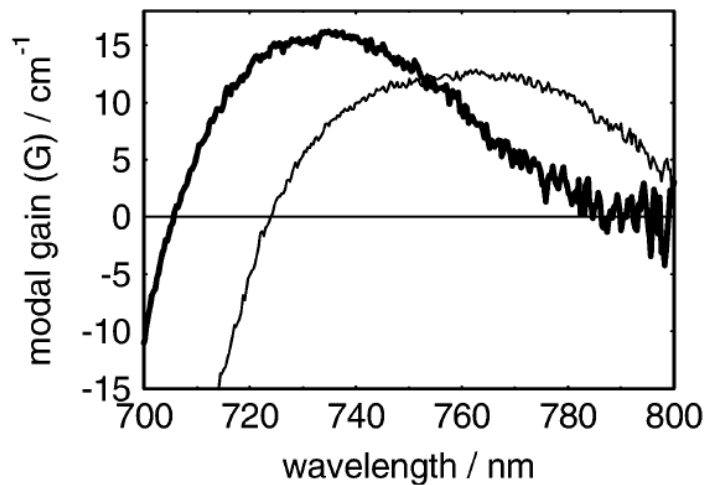
Figure 1:1 TE polarised modal gain spectra optimised for shorter wavelength injected current density of 290 A.cm^{-2} and longer wavelength injected current density of 3 kA.cm^{-2} (Smowton et al. 2005).

The low J_{th} lasers emitting at shorter wavelengths also have relatively broad gain spectra which support tunable or multi-wavelength sources that can be useful in bio-photonic applications. Since longer wavelengths towards 780nm transmit deeper into blood (Roggan et al. 1999), tissue and microvasculature (Bashkatov et al. 2005), longer wavelength from a similar active structure allow measurements at deeper or, with

multiple wavelengths, multiple depths. Additionally, AlGaAs quantum well (QW) based structures have been used to produce mode locked diode laser operation at 760nm for biophotonic applications (Wang et al. 2014). Indeed semiconductor lasers incorporating either $Al_xGa_{1-x}As$ QWs, (Singh et al. 2002) compressively strained InGaAsP QWs, (Mawst et al. 1999) or tensile strained GaAsP QWs, (Sumpf et al. 2004) can been used to produce wavelengths in the 720-780nm wavelength range. AlxGa1-xAs based structures tend to be more prone to reliability issues, including catastrophic optical degradation at high power densities (Singh et al. 2002), particularly for high Aluminium composition. InGaAsP structures, optimised for high power operation rather than low threshold current density, have been reported with J_{th} as low as 420 A.cm^{-2} being achieved for 1mm long cavities at 730nm and a reduced temperature dependence of threshold current compared to AlGaAs structures (Mawst et al. 1999). Moreover, GaAsP QW structures with J_{th} lower than 250 A.cm $^{-2}$ with 2mm long cavities emitting at 735nm have been reported (Sumpf et al. 2004). Adding aluminium to the usually longer wavelength emitting InGaAs quantum dots to form AlGaInAs quantum dots has produced emissions in the 760nm-920nm wavelength range (Schlereth et al. 2009).

This work explores the incorporation of Arsenic in the InP QDs as a means of producing longer wavelength laser emissions while still maintaining relatively low threshold currents, and moreover, in a structure compatible with the use of InP quantum dots. In fact, adding arsenic to InP QDs lowers the bandgap of the dot material and increases the lattice mismatch in respect to GaAs substrates, and thus, offers extra flexibility in engineering the above QD structures with a potential for extending their spectral operation range towards longer wavelengths in the near infra-red band.

1.1.2 Ultrafast pulse generation in quantum dot laser

Semiconductor lasers in general are convenient sources for generating picosecond or sub-picosecond optical pulses with moderate peak powers due to compatibility, reliability cost-effectivity and the availability over an extensive range of wavelengths using band gap engineering, allowing integration to occur with other optoelectronic devices and are electrically pumped. They are appropriate sources to use in diverse fields including optical communication, clock distribution, electro-optic sampling systems, photonic analogue-to-digital converters, microwave signal generation and diverse waveform generation (Avrutin et al. 2000).

However, solid-state lasers based on vibronic gain materials, for example, Yb:KGW, Ti:sapphire and Cr:Forsterite have demonstrated an improved performance in terms of optical pulse duration, high peak output power and low time jitter. For instance, when using the Yb:KGW laser, a pulse duration of 281 fs with a peak power of 3.9kW has been reported (Pekarek et al. 2010). Similarly in relation to Ti:sapphire, a pulse duration as short as 5 fs has been achieved by utilising a Kerr-lens mode-locking scheme (Morgner, 2001). In fact, these solid–state lasers exhibit several substantial limitations that have prohibited their common use in industrial applications. For example, the cost of ultrafast solid-state lasers is high, while the system design is complicated and heavy. Additionally, the size of these systems remains bulky, which means that integration with other optoelectronic devices for a compact setup is impossible. Furthermore, these systems regularly involve crystals which have low gain; therefore, there is a limitation regarding the crystal length which limits the pulse repletion frequency. Finally, electrical control of the output properties such as pulse duration and emission wavelength are hard to achieve in ultrafast solid-state lasers.

In contrast, semiconductor lasers in general can be compact, electrically pumped, fabricated easily and integrated with other optoelectronic devices to achieve a monolithic system. In effect, ultrafast pulse in a semiconductor laser can be achieved by means of three different techniques; specifically, gain-switching, Q-switching and mode-locking. The mode–locking method is generally the preferred technique to generate the ultrafast optical pulse with higher repetition rates, especially related to passive mode-locking where the element that forms the short pulses (the Saturable Absorber) can be obtained directly into the device structure during the fabrication process. Consequently, this makes monolithic passive mode-locking in semiconductor lasers easier to fabricate and operate and also offers the possibility of cost savings and lower power consumption in many applications which rely traditionally on solid-state lasers. Moreover, owing to short cavity length, these lasers offer a potential to generate high repetition rate for pulses.

However, mode-locked semiconductor lasers still have several issues to overcome. For instance, they remain unable to match the noise performance and pulse quality of the best solid-state mode-locked laser, whilst they also suffer from having asymmetric pulses, chirped spectra, larger timing jitter, low stability, wider pulse width and lower peak power (Yan et al. 2013). To improve the mode-locking in

semiconductor lasers, research on the material, device design and stabilisation mechanism is substantial.

In effect, using QD materials in a mode-locking laser exhibits several advantages over the bulk and QW materials and principally arises from the delta-like dos function and from the reduced active region volume. For example, the QD properties that can support the mode-locking system are low threshold current densities, broad emission spectra, low confinement factor, low linewidth enhancement factor, low internal optical loss, low absorption saturation energy, high gain saturation energy and ultrafast carrier dynamics (Yan et al. 2013). Each of these factors is crucial to improving mode-locking performance in terms of stability, pulse duration, chirp, noise and output power.

Stable passive mode-locking in two-section semiconductor lasers can be achieved via a careful balance between pulse broadening and pulse shortening within the device.

The absorption section which is usually biased reversely causes pulse shortening, while the gain section which is forward biased, produces pulse broadening. The levels of pulse broadening and pulse shortening owing to saturation are controlled by the saturation energies of these two sections (Thompson et al. 2009) and given by:

$$\rule{2cm}{0.4pt} \qquad\qquad\qquad 1{:}1$$

(Thompson et al., 2009)

where   is the photon energy,   is the modal area,   is the confinement factor and   is the material differential gain. The key factor for pulse shaping performance in mode-locked lasers is the ratio of the gain section to absorber section saturation energies. In semiconductor materials, the differential gain   decreases when carrier density increases owing to the limited density of available states; therefore, the differential gain in the modal absorption is higher than in the modal gain.

This effect is more defined in QWs than in bulk materials due to the step-like function, and is further exacerbated in QDs due to the discrete nature of the dot function. This is illustrated schematically in Figure 1:2, which represents the normalised modal gain against carrier density for bulk, QW, and QD material regimes (Thompson et al., 2009).
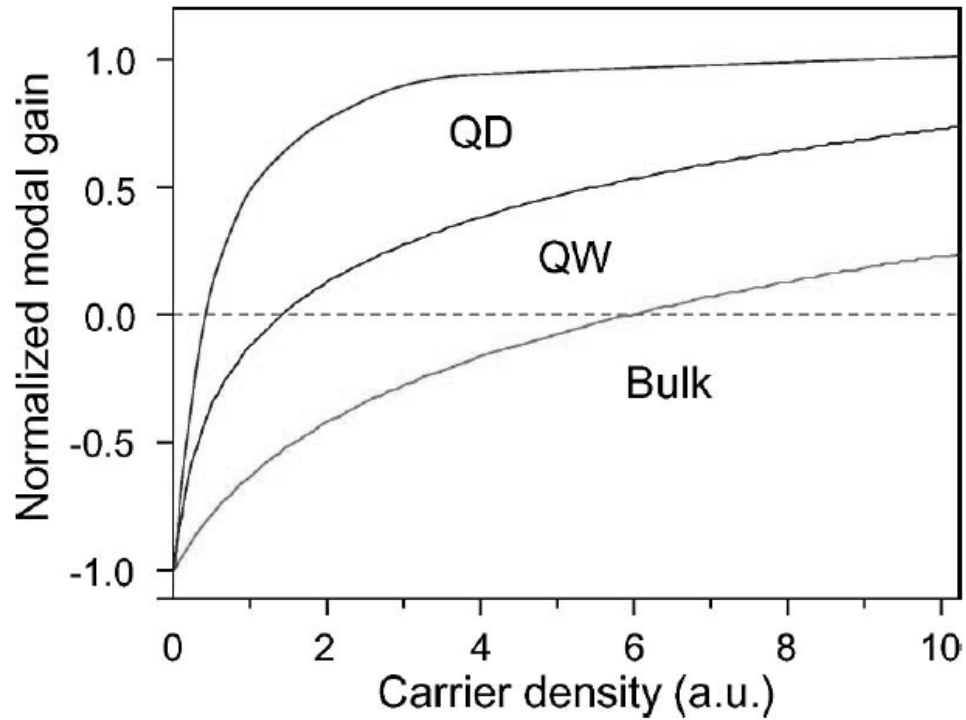
Figure 1:2 Schematic representation of the normalised modal gain versus carrier density for bulk, QW and QD material systems. (Thompson et al. 2009).

From Equation 1:1, if the modal area   and the confinement factor   remain constant for both the absorber and gain section, it can be deduced that the saturation energy of the absorber section will be lower than the saturation energy of the gain section. This ratio is higher for QW materials than for bulk materials, whilst QD materials is the highest for both bulk and QW materials.

This work introduces a new QD material (InAsP), which is grown in conditions appropriate with the standard InP QD materials to improve the mode-locking in the QD system. It is expected that the InAsP QD material will give short pulses due to deeper dots with high energy barriers. More recently it has been determined that by reducing the carrier escape rate, pulse duration can also be reduced. This can be accomplished at room temperature by making the dots deeper with high energy barriers (Finch et al. 2013). Moreover, it is expected, when a fraction of As is added to InP QD material the InAsP QD system displays a greater degree of inhomogeneous broadening which arises form dot size variations (Ribeiro et al. 2002). This can broaden both the optical gain bandwidth and the emission spectra of the laser which help to reduce the pulse duration in the case of mode locking system (Finch et al. 2013).

1.2 Literature review

1.2.1 Literature review for InP quantum dot laser

As the InP QD lasers are the standard devices in this study, it is worth mentioning some literature reviews concerning the growth and performance of such devices. Kurtenbach et al. (1994), studied the nanoscale InP island embedded in InGaP grown by (MBE). Their research revealed that InP island form due to the 3.7% lattice mismatch between InGaP and InP. Furthermore, the AFM measurements indicated that the island dot size is typically 50nm in diameter and 5nm in height for two normal monolayers. Moreover, they stated that the photoluminescence peak energy shifts from 1.85 to 1.53 eV, as the thickness increases from 2 to 10 (ML). Zundel et al. (1997), conducted a study regarding the effect of distance between dot layers on the shapes of dots for InP quantum dot embedded in a GaInP grown by MBE. Their research determined that with decreasing distance between dot layers the homogeneity of the dot size enhances the stacked InP dot system . Additionally, Johansson et al. (1998), studied the controlling of the dot size and dot density of self-assembled InP quantum dots grown by MOVPE. They stated that the dot density increases when growth temperature decreases and the deposition rate increases.

It should be specified that Porsche et al. (1998), grew self-assembling InP quantum islands on GaInP by means of low Pressure MOVPE under various growth conditions. From the AFM and PL measurements they described two types of coherently strained islands and mentioned that high growth rates and low growth temperature are necessary for small InP islands. They were able to achieve exclusively small islands with an average size of 20nm in diameter and 6nm in height. These QDs show luminous PL signals at 1.73 eV with a linewidth of 51 meV.

Jin-Phillipp and Phillipp (2000), studied the strain distribution in self-assembled InP quantum dots embedded in GaInP grown by MBE. Here, the HREM images revealed that the compressive strain in the QDs decreases when the spacing between the QD layers decreases. Consequently, this produces an increasing red shift related to the photoluminescence energy peak position of QDs of multi-layers when the thickness of the spacer layers decreases in comparison with that of single layer QDs. Manzt et al. (2000), considered the characterisations of room-temperature lasing via the ground state of InP/GaInP. They discovered that stimulated emission occurs via ground state at a

wavelength of 728nm for a 0.5mm cavity length. Threshold current density of 2.3 kA.cm^{-2} and external differential quantum efficiencies of 8.5% were observed for 2mm long devices. Additionally, light output power up to 250 mW without saturation effects was demonstrated . Ryou and Dupuis. (2001), completed a study of high density InP quantum dots embedded in InAlP grown by MOVPE at 650 ^{0}C and characterised the samples by AFM, PL measurement and TEM. At this point, they observed the formation of a high density of QDs on the order of 1010 cm^{-2} at certain growth conditions and also observed a gradual increase in QD size when deposition time increases. Zhang et al. (2003), deliberated the effect of the InAlGaP matrix on the growth of self-assembled InP quantum dots via MOVPE. They stated that the Al concentration has a significant effect on the size of InP QDs. Furthermore, they observed that the size of QDs decreases by increasing the Al concentration at a fixed volume of deposited InP. Lewis et al. (2004), considered the effect of the growth rate of InP/GaInP quantum dot lasers on substrate with different orientations. Their research revealed that growth conditions have a massive effect on the form of the gain spectrum. Moreover, they explained that at high growth rate on a 10° off (100) substrate, the gain spectrum are broad because of contributions from a bimodal dot size distribution.

Smowton et al. (2005), described the growth, material characterisation and device characterisation of InP-GaInP QD lasers operation in the wavelength range 690-750nm. They stated that growth conditions have a crucial influence on the form of gain spectrum. They achieved a relatively flat gain over a spectral width of 90nm at 300K for growth on (100) substrates with misorientation by 10° toward [111] because of the presence of a bimodal distribution of dot sizes. Additionally, a 2mm long device with uncoated facets can produce laser emissions over a (729-741 nm) range with 190 A.cm^{-2} of threshold current density. They also stated that by suppressing the bimodal distribution using (211)B substrates narrower gain spectra at shorter wavelengths can be achieved. Schulz et al. (2009), demonstrated the single layer InP quantum dot laser embedded in an $(Al_xGa_{1-x})_{0.5}1In_{0.49}P$ matrix lattice matched to GaAs at room temperature. The threshold current density was approximately 870 A.cm^{-2} at an emission wavelength of 638nm with output powers of more than 55 mW per facet.

Smowton et al. (2010), considered the effect of growth temperature on InP- QD laser 730nm grown by (MOVPE). In this case, they described the effect of growth temperature on the optical absorption, gain and threshold current density on two

different interlayer barriers of AlGaInP (8 and 16nm). In their research, they revealed that reducing the growth temperature from 750 to 690 ^{0}C increases the ground state absorption and shifts it to lower energy. They argued that this could be the result of increasing the dot size and number of dots. Moreover, they ascertained that 16nm barriers sample growing at 710 and 730 ^{o}C have sufficient dot states and gain which provide a lower threshold current density of roughly 165 A.cm^{-2} at 300 K for 2mm long lasers (uncoated facets).

1.2.2 Literature review of monolithic mode-locked lasers in QDs

As mentioned previously in this chapter, one of the aims behind InAsP QD lasers is to test their ability as a mode-locked regime. It is important here to show a few studies undertaken in the past regarding passive monolithic mode-locked in QD lasers which involve two sections (absorption and gain section). The first characterisation of the mode-locking in the QD material system was achieved by Huang et al. (2001), at 1.3 μm two-section InAs QD lasers with a repetition rate of 7.4 GHz, where a 17 ps pulse duration was obtained. Gubenko et al. (2004), attained a pulse duration as succinct as 1.7 ps with a repetition rate of 9.7 GHz from monolithic passive mode-lock (two–sections) of InAs/InGaAs (λ=1.28 μm) QD laser. They also reported that the pulse became brief by increasing the reverse bias on the observed section. Furthermore, Rafailov (2005), demonstrated two-section mode-locked lasers in InGaAs QD laser. Output power of 45 mW at 1260 nm was observed and the pulse duration varies from 2 ps to 400 fs at 21 GHz repetition rate depending on the driven current condition. Further studies conducted included Thompson et al. (2009), who studied passive monolithic mode-locking in InGaAs QD lasers. Here, they demonstrated pulse generation for repetition ranging from 310 MHz to 240 GHz with pulse duration varying from a picosecond to sub-400 fs. Their research stated that it is possible to improve the mode locked performance regime regarding pulse duration, output power and noise by controlling the gain to absorber section ratio in passive mode-locking and by increasing the reverse biased on absorber section. They also introduced a concept of the tapered waveguide structure that improved the performance of the mode-locking in terms of low timing jitter. Finch et al. (2013), deliberated the effects of temperature on passively mode-locked InAs QD lasers. They established that optical pulse duration can be reduced from 8.4 ps at 250 K to 290 fs at 20 K with a corresponding increase in optical bandwidth.

1.3 Thesis structure

This thesis contains seven chapters:

Chapter One introduces the motivations and the goals of this work, in addition to the literature review and the thesis structure.

Chapter Two gives an account of the theory and the background behind this work. It illustrates the physics of semiconductor lasers, and the growth and structure of the quantum dot lasers, as well as introduces threshold current density and semiconductor laser efficiency.

Similarly, the chapter mentions the important characteristics in connection with quantum dot lasers; specifically, modal absorption, modal gain, spontaneous emission and gain-current relation with several important equations related to this work. Moreover, the chapter outlines the occupational probability of the carriers in quantum dot system. To conclude, it finishes with the principles of mode-locking and conditions of passive mode-locking, along with the benefit of using QD lasers to produce ultra-fast pulses.

Chapter Three: This chapter reveals the sample structures and measurement techniques used in this work. The chapter reveals the processing of the samples and how they are prepared for tests. Subsequently, it begins with the growth of the InP and InAsP QD materials and illustrates the basic measurement of the wafers which are the TEM images and the Photoluminescence measurements. The chapter describes all the experimental setups used to collect the data in this work, specifically the segmented contact method which is described precisely.

Chapter Four: This chapter is concerned with the significant properties of the InP and InAsP QD lasers that is measured using the technique in Chapter three. It includes the (current-light) characteristics for 1, 2, 3 and 4mm cavity length of each structure and the Temperature dependence of threshold current density of the devices, besides the spectral measurement to determine the wavelengths of the devices. In addition, optical power and the efficiency of the samples are discussed in this chapter. Finally, the chapter depicts the modal absorption and modal gain of the materials, as well as the gain-current relations at room temperature. E-PVS measurement for InP and InAsP QD laser is also introduced in this chapter.

Chapter Five: This chapter focuses on the effect of temperature on modal absorption, modal gain and the gain-current relationship of the InP and InAsP materials. The chapter also involves the effect of the temperature on the optical gain bandwidth, in addition to the effect of the temperature on the emission peaks of the InP and InAsP materials is introduced in this chapter.

Chapter Six: Here, further analysis of the spontaneous emissions data includes the population inversion factor and spontaneous emissions in real units. Finally, the chapter analyses the carrier distribution and occupational probability at different values of temperatures for the materials namely (150, 200, 250, 300, 350, 400 K).

Chapter Seven: This chapter outlines the conclusions achieved from the last three chapters and the potential for further work related to this topic.

1.4 References

Avrutin, E.A., Marsh, J.H. and Portnoi, E.L. **2000**. Monolithic and multi-GigaHertz mode-locked semiconductor lasers : Constructions , experiments , models and applications. IEE Proceedings - Optoelectronic 147(4), pp.251-278

Bashkatov, A., Genina, W., Kochubey V. and Tuchin V. **2005**. Optical properties of human skin, subcutaneous and mucous tissues in the wavelength range from 400 to 2000nm. Journal of physics D: applied physics 38, pp 2543–2555.

Finch, P. Blood, P. Smowton, P. M. Sobiesierski, A. Gwilliam, R. M. and O'Driscol, I. **2013**. Femtosecond pulse generation in passively mode locked InAs quantum dot lasers. Applied Physics Letters 103(131109), pp.1–3.

Gubenko, A.E., Gadjiev, N.D. Iiinskaya, Yu.M. Zadiranov, A.E. Zhukov, Ustinov, Z.I. and Portnoi, E.L. **2004**. Mode-locking at 9.7 GHz repetition rate with 1.7 ps pulse duration in two-section QD lasers. Semiconductor Laser Conference, 2004. Conference Digest. 2004 IEEE 19th International, pp.51–52.

Huang, X., Stintz, A., Hua, L., Lester, L., Cheng, J. and Malloy, K. **2001**. Passive mode-locking in 1.3 µm two-section InAs quantum dot lasers. Applied Physics Letters 78(19), pp.2825–2827.

Jin-Phillipp, N. and Phillipp, F. **2000**. Strain distribution in self-assembled InP/GaInP quantum dots. Journal of Applied Physics 88(2), pp.710–715.

Johansson, J., Carlsson, N. and Seifert, W. **1998**. Manipulations of size and density of self-assembled quantum dots grown by MOVPE. Physica E: Low-dimensional Systems and Nanostructures 2(1-4), pp.667–671. Available at: http://linkinghub.elsevier.com/retrieve/pii/S1386947798001362.

Kasim, M., Elliott, S. N. Krysa, A. B. and Smowton, P. M. **2015**. Reducing thermal carrier spreading in inp quantum dot lasers. IEEE Journal of selected topics in quantum electronics 21(6), Article Sequence Number: 1900306.

Kurtenbach, A., Eberl, K. and Shitara, T. **1994**. Nanoscale InP island embedded in InGaP. Applied Physics Letters 66(3), pp.361–363.

Lewis, G., Lutti, J., Smowton, P. M. and Blood, P. **2004**. Optical properties of InP/GaInP quantum-dot laser structures. Applied Physics Letters 85(11), pp.1904–1906.

Manz, Y., Schmidt, G. and Eberl, K. **2000**. Room-temperature lasing via ground state of current-injected vertically aligned In/GaInP quantum dots. Applied Physics Letters 76(13), pp.3343–3345.

Mawst, J., Rusli, S., Al-Muhanna, A. and Wade, J. **1999**. Short-Wavelength (0.7μm < λ < 0.78 μm) High-Power InGaAsP-Active Diode Lasers. IEEE Journal of selected topics in quantum electronics 5(3), pp.785–791.

Morgner, E., Kärtner, F., Fujimoto, J., Ippen, E., Scheuer, V., Angelow, G.,Tschudi, T., Lederer, M., Boiko, A., and B.L.-D. **2001**. Generation of 5-fs pulses and octave-spanning spectra directly from a Ti:sapphire laser. Optics Letters 26(6), pp.373–375.

Pekarek, S., Fiebig, C., Stumpf, M., Oehler, A., Paschke, K., Erbert, G., Südmeyer, T. and Keller, U. **2010**. Diode-pumped gigahertz femtosecond Yb : KGW laser with a peak power of 3.9 kW. Optics Express 18(16), pp.16320–16326.

Porsche J., Ruf, A., Geiger M. andScholz, F. **1998**. Size control of self-assembled InP/GaInP quantum island. Journal of crystal growth, 195(1-4), pp.591–595.

Rafailov, U., Cataluna, M. and Sibbett, W. **2005**. High-power picosecond and femtosecond pulse generation from a two-section mode -locked quantum-dot laser. Applied Physics Letters, 87(081107), pp.1–3.

Reischle, M., Kessler, C., Schulz, W.-M., Eichfelder, M., Roßbach, R., Jetter, M.and Michler, P. **2010**. Triggered single-photon emission from electrically excited quantum dots in the red spectral range. Applied Physics Letters 97(14351), pp1-3.

Ribeiro, E., Maltez, R. L., Carvalho, W., Ugarte, D. and Medeiros-Ribeiro, G. **2002**. Optical and structural properties of InAsP ternary self-assembled quantum dots embedded in GaAs. Applied Physics Letters 81(16), pp.2953-2955.

Roggan, A., Friebel, M. Do¨ rschel, K. Hahn, A. and Mu¨ller,G. **1999**. Optical properties of circulating human blood in the wavelength r ange 400 – 2500 nm. Journal of biomedical optics 4(1), pp.36–46.

Ryou, J. and Dupuis, R.   **2001**. High-density InP self-assembled quantum dots embedded in In0.5Al0.5P grown by metalorganic chemical vapour deposition. Applied Physics Letters 78(22), pp.3526–3528.

Singh, R., Dabkowski, D., Clausen E. and Chin A. **1999**. High-power, reliable operation of 730 nm AlGaAs laser diodes. Applied Physics Letters 75(14), pp. 2002-2004.

Schlereth, T. W., Schneider, C., Gerhard, S., Hufling, S. and Forchel, A. **2009**. Short wavelength (760-920 nm)AlGaInAs Quantum Dot Lasers. IEEE J. Sel. Top. Quantum Electron. 15(3), pp. 792–798.

Smowton, P. M., Al-Ghamdi, M., Shutts, S., Edwards, G., Hutchings, M. and Krysa, A. B. **2010**. Effect of growth temperature on InP QD lasers. IEEE Photonics Technology Letters 22(2), pp.88–90.

Smowton, P. M., Lutti, J., Lewis, G., Krysa, A. B., Roberts J. , and Houston P. **2005**. InP–GaInP Quantum-Dot Lasers Emitting Between 690–750 nm. IEEE Journal of Selected Topics in Quantum Electronic 11(5), pp.1035–1040.

Sumpf, B., Beister, G., Erbert, G., Fricke, G., Knauer, A., Ressel, P. and Tränkle. G. **2004**. Reliable 1W CW operation of high-brightness tapered diode lasers at 735nm. IEEE Photonics Technol. Lett 16(4), pp.984–986.

Schulz., W-M. Eichfelder M., RoBbach, R., Jetter, M. and Michler, P. **2009**. Low threshold InP/AlGaInP quantum dot in-plane laser emitting at 638nm. Applied Physics Express 2, pp.112501-1125013.

Thompson, M., Rae, A., Xia, A., Penty, R. and White, I. **2009**. InGaAs Quantum-Dot Mode-Locked Laser Diodes. IEEE journal of selected topics in quantum electronics 15(3), pp.661–672.

Wang, H., Kong, H., Forrest, A., Bajek, D., Stephanie E. Wang, H., Jiaoqing Pan, P., Ding, Y. and Cataluna, M. **2014**. Ultrashort pulse generation by semiconductor mode-locked lasers at 760 nm. Optical Society of America 22(21), pp.25940–25946.

Yan, L., Lester, L., Chang, D., Langrock, C., Fejer, M., and Kane, D. **2013**. Characteristics and instabilities of mode-locked quantum-dot diode lasers. Optics Express 21(7), pp.477–485.

Zhang, X., Heller, R., Noh, M., Dupuis, R., Walter, G. and Holonyak, N. **2003**. Effect of the InAlGaP matrix on the growth of self-assembled InP quantum dots by metalorganic chemical vapour deposition. Applied Physics Letters 83(7), pp.1349–1351.

Zundel, M., Specht, P., Eberl, K., Jin-Phillipp, N. and Phillipp, F. **1997**. Structural and optical properties of vertically aligned InP quantum dots. Applied Physics Letters 71(20), pp.2972–2974.

Chapter (2) Background and theory

2.1 Introduction

This chapter discusses the general principles of semiconductor lasers, especially the quantum dot laser which was used in this work. Firstly, the chapter starts from optical transmission in a two-level system and subsequently moves to the band structure of the semiconductor materials. Important terms have been outlined in this chapter, such as Fermi-Dirac statistics and population inversion. Additionally, the principles of semiconductor laser are illustrated, for instance density of state in a quantum system and quantum confinement, as well as the threshold gain in semiconductor lasers. Secondly, the quantum dot system has been introduced with the growth technique and quantum dot active region, whilst it also covers broadening mechanisms in the quantum dot system. The most important concepts in quantum dot lasers, such as model gain, modal absorption, spontaneous emission and gain-current relation and several important equations are examined in this chapter. Moreover, the population inversion factor and occupational probability are illustrated in this chapter. Finally, the chapter describes the mode-locking principles in a laser, conditions of mode-locking and likewise describes the passive mode-locking in semiconductor lasers. The chapter concludes with the benefits of using QD materials in a mode-locking system.

2.2 Fundamentals of lasers

2.2.1 Components of a laser

The word LASER is an acronym of the phrase (Light Amplification by Stimulated Emission of Radiation). To produce laser emissions three basic elements should be available (see Figure 2:1). The first element is the medium of the laser (active medium) which could be gas, liquid or solid that allows the population inversion and amplification to occur. The choice of medium materials affects the emission wavelength. The second component is the pumping, which is a process to achieve population inversion. Pumping can be performed either electrically or optically by the external source. The third element is the resonator that provides feedback for the light generated inside the medium. At each end of the active medium there is a mirror. At least one must be partially reflective to allow the coherent light to be emitted.
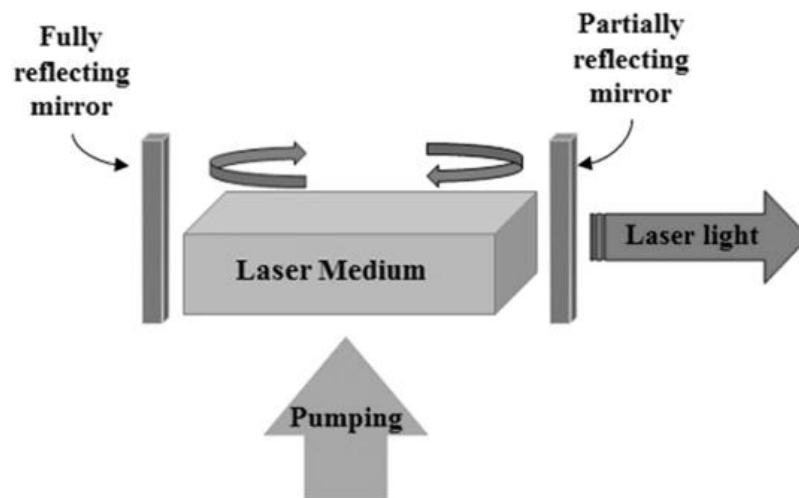
Figure 2:1 Basic elements of a laser system.

The laser used in this study is the semiconductor laser which is pumped electrically. The mirrors were formed by cleaving the edges of the chip during the fabrication process. Semiconductor lasers can be classified into four groups according to the materials used in the active region when they are grown: bulk, quantum well, quantum wire and quantum dot. Quantum dot materials were used to grow the laser samples that were used in this work.

2.2.2 Optical transmission in a two-level system

Figure 2:2 illustrates three possible processes that can occur between a two-level system (ground and excited state) when there is an interaction between a photon and matter. These are absorption, spontaneous emission and stimulated emission.
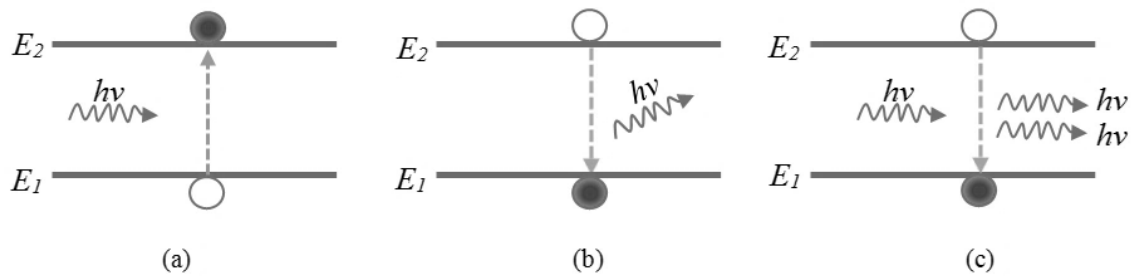
Figure 2:2 Energy level diagram illustrates (a) absorption (b) spontaneous emission and (c) stimulated emission.

In the case of absorption, an electron occupying an energy state in the lower level (E_1) absorbs a photon that has an energy equal to (E_2-E_1= hv); hence, the electron will move to an empty state in the upper energy level (E_2). The absorption rate $\quad$ depends on the number of photons with adequate energy $\quad$, number of electrons in the lower energy level $\quad$ and the number of empty states in the upper energy level $\quad$. The total rate of the absorption processes is given by:

$$2:1$$

where $\quad$ is a probability coefficient of absorption.

A spontaneous emission occurs when an electron occupying an energy state in the upper level falls to the lower energy level spontaneously and releases a photon with energy equal to (E_2-E_1= hv). The phase and the direction of the photons that are produced in this process are random. The spontaneous emission rate $\quad$ is only controlled by the number of electrons in the upper energy level $\quad$ and the available empty states in the lower energy level $\quad$ as presented below:

$$2:2$$

where $\quad$ is a probability coefficient of the spontaneous emission. It is important here to mention that electrons can fall to a lower energy state via non-radiative processes,

such as Auger recombination or recombination via a defect state, which will be described in detail later in this chapter (see Section 2.5.4).

Stimulated emission occurs when an income photon with energy equal to (E_2-E_1= hv) disturbs an electron occupying an energy state in the upper level and releases another photon with the same energy (E_2-E_1= hv); moreover, the produced photon has the same phase as the incident photon and travels in the same direction. The stimulated emission rate   is therefore controlled by the number of electrons in the upper energy level   the available empty states in the lower energy level   and the photon density, as shown below:

$$2:3$$

where   is a probability coefficient of the stimulated emission.

In equilibrium conditions the absorption rate must balance the emission rates, so:

$$2:4$$

The rate of downward transitions is equal to the rate of the upward transitions. And it can be show that   The laser produces a coherent ray by allowing stimulated emission to dominate over absorption and spontaneous emission. Consequently, this means there must be more carriers in the upper state than the lower one, so called "population inversion", which will be comprehensively described in this chapter later (see Section 2.3.2 and Section 2.6).

2.3 Semiconductor lasers

2.3.1 Band structure and materials for semiconductor lasers

Since the electrical and optical properties are determined by the crystal structure, it is beneficial to introduce the band structure of the semiconductor materials. At 0 K the valence band states are fully occupied by electrons and the conduction band states are fully empty. However, at a temperature above 0 K a few electrons obtain thermal energy to move to the conduction band. Additionally, unoccupied states in the valence band are thought of as 'holes' which behave as positive charges of an electron. The semiconductor materials used in semiconductor lasers should have a direct energy gap

which means the minimum conduction band state and the maximum valence band state are at the same value of the wave vector (k), as shown in the E-k relationship in Figure 2:3. This means that when a recombination between election and hole occurs to produce a photon the momentum and energy are conserved. The relationship between E-k can be given by:

$$\underline{\qquad} \qquad\qquad\qquad 2:5$$

(Coldren et al. 2012)

where   is the effective mass of the carrier (electron or hole) and the electron momentum (P) can be given by:

$$2:6$$

If the semiconductor materials are under strain the valence bands splits heavy–hole (HH) and light-hole (LH).
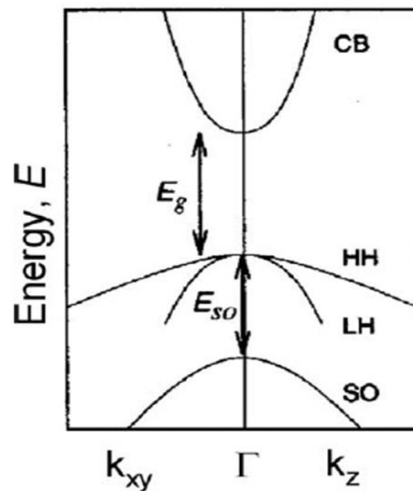
Figure 2:3 In a direct band gap, bulk, unstrained structure, the HH band and the LH band are degenerate at the valence band maximum at the Brillouin zone center (Alfred 2011).

Materials used in fabricating semiconductor laser play a significant role as they determine the optical and electrical properties, and optimising the materials involved is necessary to ensure the laser operates satisfactorily. For a double heterostructure laser (see Section 2.3.3) at least two compatible materials are required, one for the cladding layers and another for the active region. For a separate-confinement heterostructure, 3 or 4 different bandgaps should be required within the same structure. The essential

requirement for these different materials is to have the same crystal structure with virtually the same lattice constant, so that it can be easily epitaxially grown with negligible interface trapping. Figure 2:4 plots the band gap versus lattice constant for several materials of III-V semiconductor groups that are extensively studied and developed in optoelectronic applications. The dash lines on Figure 2:4 indicate the region of associated with the indirect gap. GaAs was the first semiconductor material used to produce laser radiation. Ternary compounds can be formed from binary materials by motion along the line joining two points that represent the binary materials. The lattice constant for GaAs is 5.6533°A when used as a substrate, while the ternary compound $Al_xGa_{1-x}As$ has a lattice mismatch of approximately 0.1 %. Similarly, with InP as a substrate with a lattice constant of 5.8687°A, the quaternary compound $Ga_xIn_{1-x}As_yP_{1-y}$, also has a virtually perfect lattice match for particular values of x and y. Usually materials that used in semiconductor lasers need to be doped to become degenerate materials in order to achieve population inversion.
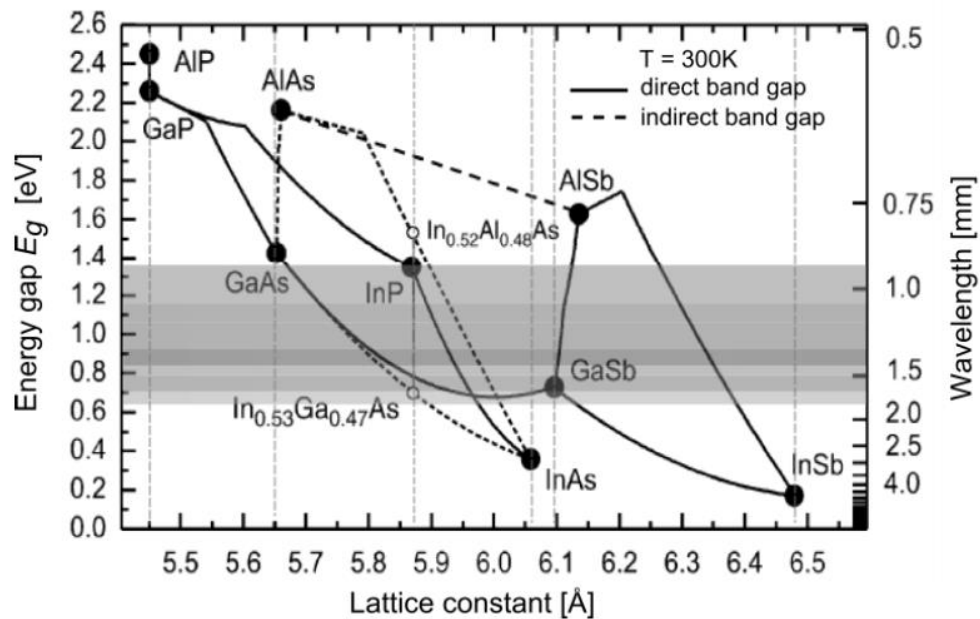
Figure 2:4 Lattice constant, band gap energy and band gap wavelength for several common III-V compound semiconductors (Coldren et al. 2012).

2.3.2 Fermi-Dirac statistics and population inversion

The probability that an electron occupies a state of energy E can be described by Fermi-Dirac statistics. Figure 2:3a illustrates the energy level for intrinsic semiconductor material, where the Fermi level E_F is in the middle of the energy gap.

For n-type semiconductors, the Femi energy is closer to the conduction band, whereas for p-type semiconductors, the Fermi energy is closer to the valance band. The Fermi–Dirac statistic in thermal equilibrium can be given as:

$$ \underline{\qquad\qquad} \qquad\qquad\qquad\qquad\qquad\qquad 2{:}7 $$

$$ \text{(Coldren et al. 2012)} $$

In case of a p-n junction, which is the principal system with regards to the laser diode, in non-thermal equilibrium conditions (forward bias) it is worth identifying a separate Fermi-level for conduction and valence bands as:

$$ \underline{\qquad\qquad} \quad 2{:}8 \quad \text{and} \qquad \underline{\qquad\qquad} \quad 2{:}9 $$

$$ \text{(Coldren et al. 2012)} $$

where   are the valence and conduction band quasi-Fermi levels respectively. When the forward bias is applied to p-n junction   is separated by slightly less energy than the applied voltage energy. To achieve population inversion in a semiconductor, the occupation probability of carriers in the conduction band level require more than the occupation probability in the valence band level; in other words, $>$ So:

$$ \underline{\qquad} \quad \underline{\qquad} \qquad\qquad\qquad\qquad 2{:}10 $$

and this leads to:

$$ \qquad\qquad\qquad\qquad\qquad\qquad\qquad\qquad\qquad 2{:}11 $$

where   is the quasi-Fermi level separation, Equation 2:11 signifies that the optical gain will become positive only if the quasi-Fermi level separation is greater than the photon energy of interest. In the other words to achieve gain in semiconductor laser it must be had   . Therefore, this needs the voltage across the p-n junction to be greater than the band gap (Coldren et al. 2012).

2.3.3 Semiconductor lasers

The semiconductor laser is one of the most crucial inventions of the 20th century. In its simplest form it is fabricated by growing a p-doped layer on an n-doped semiconductor substrate generating so-called p-n junction, as shown in Figure 2:5. It is occasionally termed the junction laser or laser diode. Figure 2:6 illustrates a separate confinement double heterostructure semiconductor laser. The active region is made of semiconductor materials that have a narrower energy gap than that of the confined barriers. Electrons are injected into the n-side, while holes are injected into the p-side. When the current is being transmitted through the device, electrons and holes recombine through either spontaneous or stimulated recombination. As a result, photons are generated. The generation emission is confined to the waveguide structure due to the refractive index step between the cladding layer and the core. Moreover, the photons leave the cavity from the facet(s) producing a laser ray (Williams and R. H. 1991).

The laser produces a coherent ray by allowing stimulated emissions to dominate over absorption and spontaneous emission. A semiconductor laser is formed by placing the active region in a resonant cavity, with partially reflecting mirrors. Electrons in the active layer are usually excited electrically.
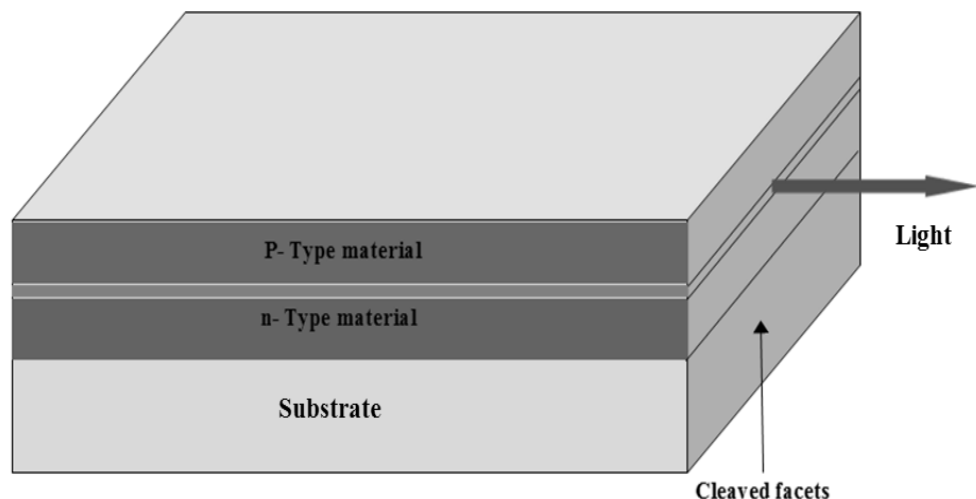
Figure 2:5 Schematic diagram of a simple semiconductor.
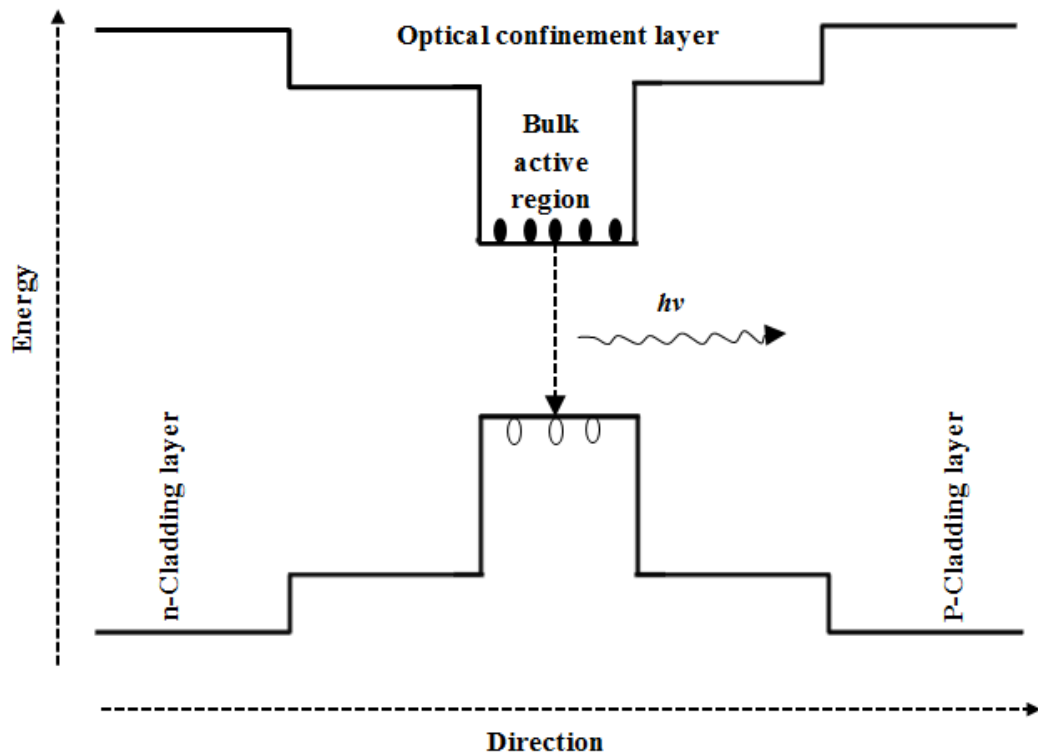
**Figure 2:6 Schematic of a separate confinement double
heterostructure laser (Williams and R.H 1991).**

The significant parameters of the semiconductor laser are threshold current (I_{th}) and external differential quantum efficiency (   ), which can both can be computed from the (light power-versus- current) relationship (P-I) curve, as shown in Figure 2:7. The threshold current can be found from the intercept of the above-threshold curve with the x-axis, whereas differential quantum efficiency can be calculated from the following equation:

$$\qquad\qquad\qquad\qquad \text{—}\ \text{—} \qquad\qquad\qquad\qquad\qquad 2:12$$

(Casey and Panish 1978)

where   is the electron charge,   Planck constant,   frequency of output light, and $\Delta\ /\Delta$ is the slope of the (P- I) curve above the threshold, as revealed in Figure 2:7. (   ) is the rate of increasing emission photons to increase the injected carriers.
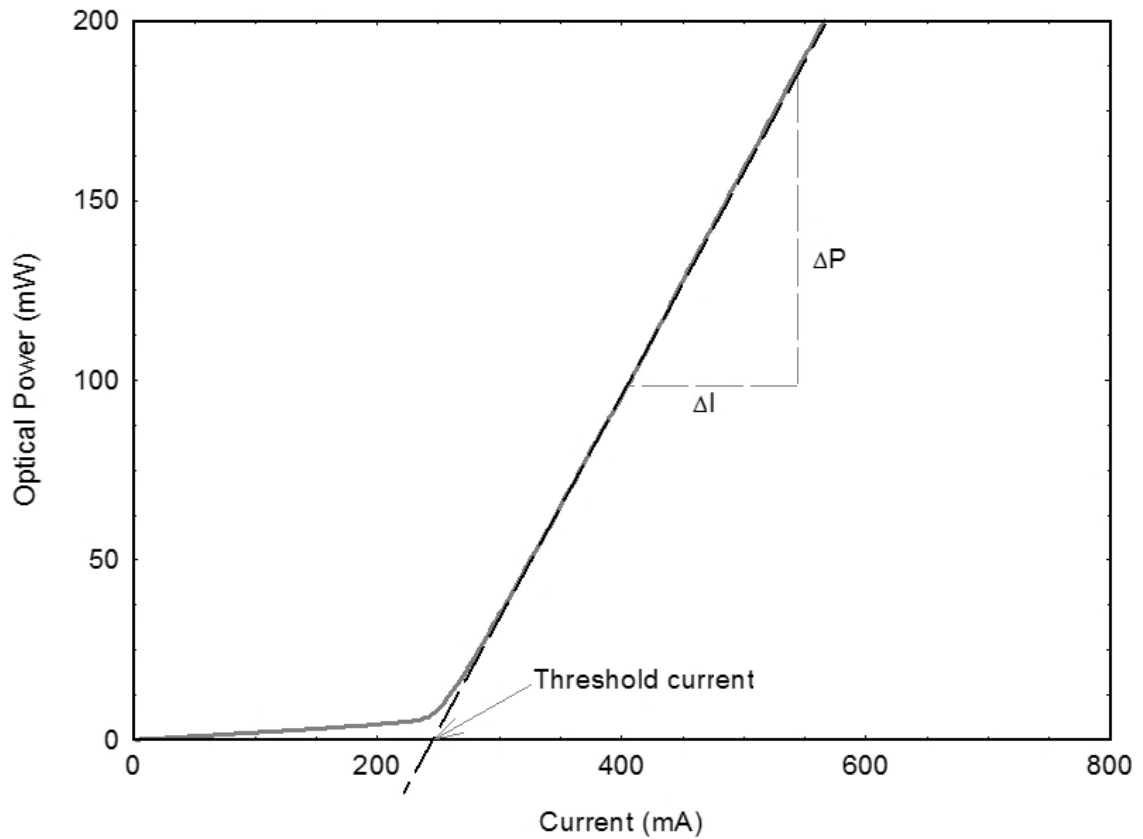
Figure 2:7 (Light power – Current) relationship in semiconductor lasers.

Furthermore, it is possible to measure the internal optical loss ( ) and the internal differential quantum efficiency ( ) of the laser, by means of different cavity lengths (L) that are made of same materials, by plotting the inverse of   vs L, as illustrated in Figure 2:8, according to the following relationship:

$$\qquad \rule{1cm}{0.4pt} \quad \rule{2cm}{0.4pt} \quad \rule{1cm}{0.4pt} \qquad\qquad 2:13$$

(Kressel amd Butler, 1977)

where (R) is the mean mirror reflectivity of the facets. Although Equation 2:13 is still the most convenient method to measure the internal differential quantum efficiency ( ) and internal optical loss ( ), research indicates that this method is not necessarily valid, seeing that it relies on the assumption that   and   do not depend on cavity length (L) (Smowton and Blood 1997) (Piprek et al. 1999).
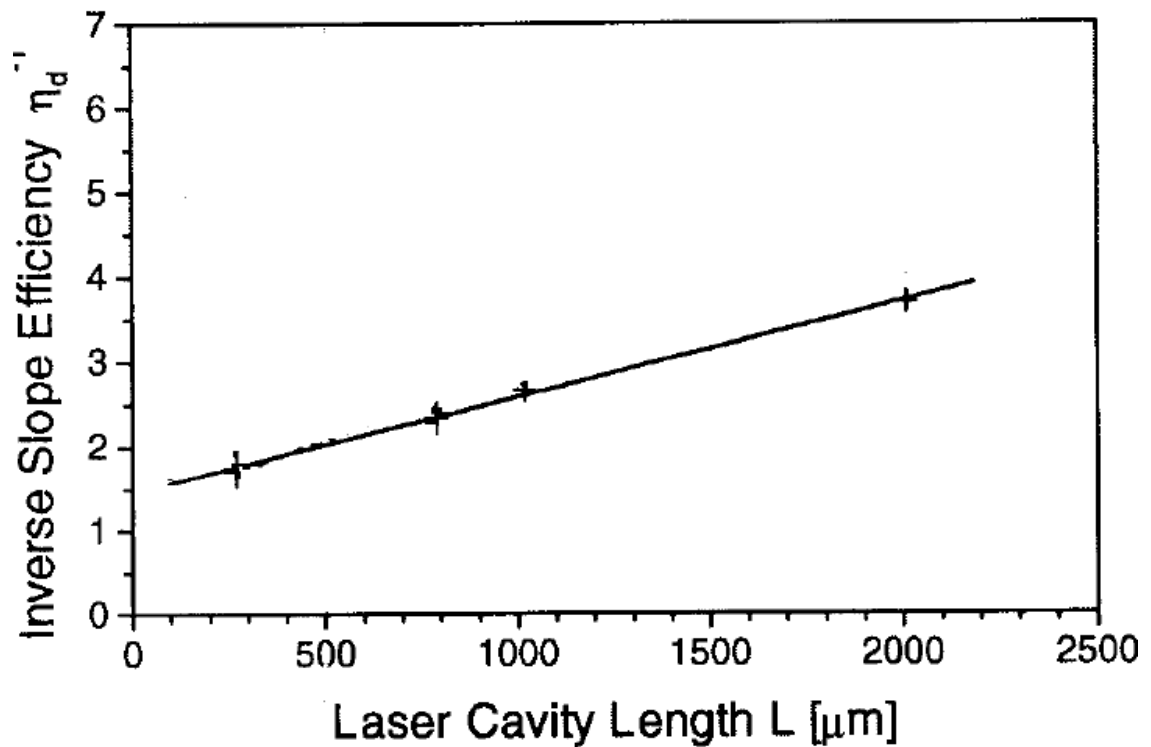
Figure 2:8 Cavity length dependence of the inverse differential quantum efficiency (inverse of the slope efficiency) (Piprek et al. 1999).

2.3.4   Threshold gain in Fabry-Perot semiconductor laser

Presume an optical resonator of a semiconductor medium of length (L), as shown in Figure 2:9 is cleaved along its crystallographic axis to form two parallel facets with reflectivity (R_1, R_2) to provide optical feedback. A refractive index step of approximately 3.5 (of semiconductor material) produces approximately 30% reflectivity. To achieve threshold, the optical modal gain (G), which is an increase in photon density per unit length (cm^{-1}) must equal the optical losses that arises from absorption, scattering and roughness, in addition to mirror loss (α_m) during a round trip.

All losses except mirror loss (α_m) are known as internal optical loss (α_i) which is defined as the loss of light from the lasing optical mode of the laser as it propagates down the waveguide structure. However an optical loss, is still incurred due to mechanisms which persist for photon energies below the band gap, such as free carrier absorption. (FCA) and intervalence band absorption (IVBA), (Pikhtin et al. 2003).
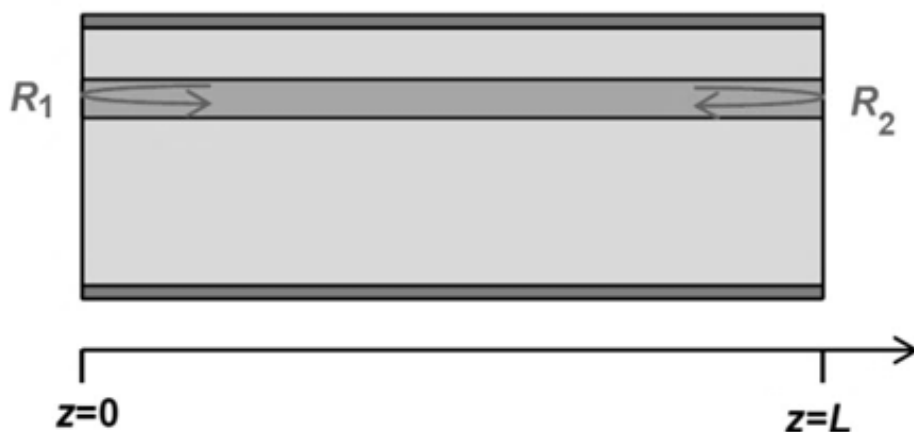
Figure 2:9 Fabry-Perot solid medium.

The round trip gain (cm^{-1}) is given by:

$$$$ 2:14

The round trip loss is given by:

$$$$ 2:15

In a threshold condition ($G_{th} = G$):

So:

$$$$ 2:16

Or:

$$$$ 2:17

where,

In semiconductor laser $R_1 \approx R_2 \approx 0.3$; therefore, for laser diode:

$$$$ 2:18

2.4 Quantum dot laser

2.4.1 Quantum confinement and density of state

The semiconductor laser in Figure 2:5 is a conventional laser, termed a bulk device. Such devices have a high threshold current density due to the high thickness of the active region. However, nowadays most semiconductor lasers are grown using thin layers in the active region called quantum wells or quantum dots. To understand the quantum concept, one should firstly consider the quantum confinement effects on electrons. Quantum confinement takes place if one or more of the dimensions of a crystal approach the Bohr exciton radius (a few nanometres) (Chukwuocha, 2012). According to the dimensions of the confinement, three categories of confined structures are defined: quantum well, quantum wire and quantum dot, although the concepts of band structure in semiconductors still apply. The electron energy level should be treated as discrete instead of continuous, as shown in Figure 2:10.
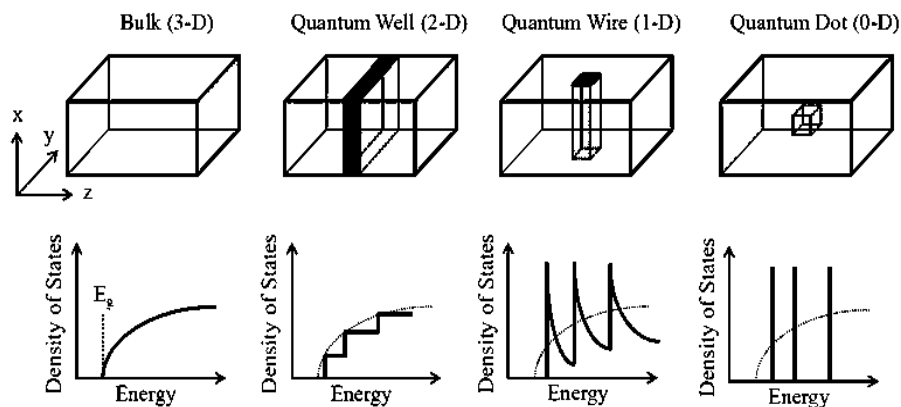
Figure 2:10 Density of states for; bulk structure, quantum well, quantum wire and quantum dot (Alivisatos, 1996).

The quantum well structure gives electrons 2 dimensions of freedom, while for quantum wire there is only one direction of freedom. However, the quantum dot structure is totally quantised (the electron is squeezed in 3 dimensions). The most important difference between traditional semiconductor lasers and quantum lasers, is that the emission wavelengths of the quantum confined lasers are highly sensitive to confined size, as well as composition. To understand how the emission energy depends on the size of the quantum confined materials, it would be beneficial to start with the particle

in a box which is the platform of the quantum mechanics. The particle in a box model defines a particle free to move in a small space surrounded by impassable barriers. The simplest form of the particle in a box model considers a one dimensional system. This is a theoretical situation where a particle of mass m is confined between two walls at x=0 and x=L as shown in Figure 2:11. The potential energy is zero within the box but it is infinity at the walls. The particle cannot be found in a region where the potential is infinite as the particle would have infinity energy.
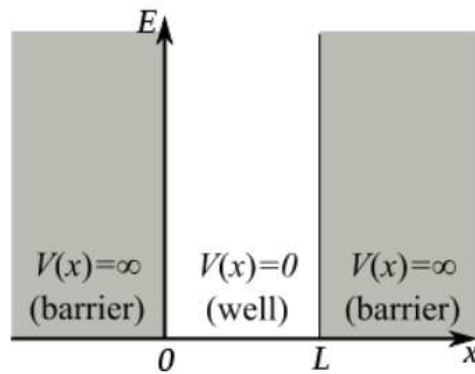
Figure 2:11 Particle in a box.

The Schrodinger equation can be used to obtain the wavefunction and energy levels of particle confined in one dimensional box without approximations. The energy of the confined particle in one dimensional box is given as:

$$\overline{\qquad}$$

$$2:19$$

where n is the quantum number and n=1 for the ground state. Just like the particle in a box, the electron and hole in quantum dot system are confined so that they cannot move out of the dot. However, there are some adjustments to correct their difference; Firstly, there are actually two particles within the each quantum dot (electron and hole) rather than one as it is in the particle in a box. Secondly, QDs are geometrically spherical in shape rather than square or sometimes the dots formed as a pyramid shape as shown in Figure 2:12, hence the length of the box L is replaced with radius R and thirdly, the masses of the electron and hole are replaced by their effective masses due to their interaction with the crystal lattice. The confinement energy of the electrons in QDs thus, becomes:

$$\rule{3em}{0.4pt} \quad \rule{3em}{0.4pt} \qquad\qquad 2{:}20$$

(Onyia et al. 2018)

So the ground state energy in QDs (n=1) can be written as:

$$\rule{3em}{0.4pt} \quad \rule{3em}{0.4pt} \qquad\qquad 2{:}21$$

However, electrons in QDs do not move in a vacuum in contrast to the particle in a box, rather inside bulk semiconductor crystals. Therefore, energy gap of the bulk accounts for the baseline energy of the system. The energy gap of QDs is thus the energy gap of the bulk semiconductor and the confinement energy of both electrons and holes as shown below:

$$\rule{2em}{0.4pt} \ \rule{2em}{0.4pt} \ \rule{2em}{0.4pt} \qquad\qquad 2{:}22$$

((Ikeri et al., 2017)

where $(\quad)$ is the energy gap of the bulk. The simple models in equation 2:22 show that discrete electronic states arise at conduction and valence bands and the energy gap of QDs becomes size dependent and larger with decreasing size due to the confinement of electrons and holes within the QDs.
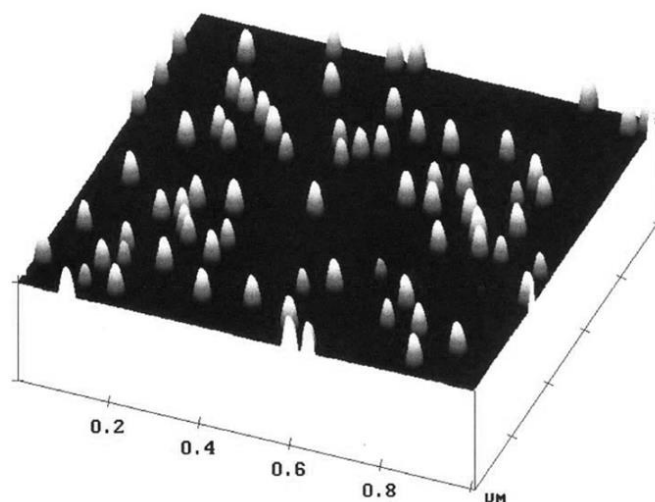
Figure 2:12 An atomic force micrograph of InAs quantum dots on a GaAs substrate The InAs dots were grown by MBE at a growth temperature of 5308C.The vertical scale is expanded relative to the horizontal scale (Warburton 2002)

2.4.2 Quantum dot growth

Self-assembly using the Stranski-Krastanow growth mode is the most common method used to grow the QD lasers. This method offers the potential for growing semiconductor material epitaxially onto another semiconductor material with a different lattice constant. This lattice mismatch leads to the occurrence of strain field in the heterostructure of the system (for example, there is a mismatch of approximately 7 % when InAs QD is deposited onto GaAs, this mismatch creates highly strained 3D layer (Roberts 2017). This strain encourages the formation of islands on the top of a thin layer called wetting layer as revealed in Figure 2:12. The formation of the islands minimises the strain and forms the QDs. In the device the wetting layer works as a carrier reservoir and allows electrons and holes to be transported between the dots. The self-assembly technique allows limited control of the size, density and composition of the dots by controlling limited growth conditions and/or materials used, leading to control of the emission wavelength. Variation of the parameters of the QDs has a direct influence on the operating characteristics of the laser structures. The typical self-assembly process can form dot densities of 10^{10}-10^{11} cm^2 (Kim and Jeong 2005), with dimensions 5nm high and base dimensions 20nm x 20nm. These structures are normally grown by either Molecular Beam Epitaxy (MBE) or Metal Organic Vapour Phase Epitaxy (MOVPE). The samples in this study were grown by (MOVPE) for arsenides and phosphides. InP QDs have been used in this study and are considered the standard device. The lattice mismatch of approximately 3.8 % occurs because InP has a lattice constant of 5.869 A^o and GaAs has 5.653 A^o (Derbali 1997). The wavelength of this laser at 300 K is approximately 720nm. In this study, we added a small fraction of As around 25% to InP in order to design InAs$_x$P$_{1-x.}$ The new structure is compatible with the wafer of the standard device (InP). Moreover, growth for both structures was conducted under conditions appropriate for InP dots.

2.4.3 Quantum dot active region

The active region is usually placed between the wider band gap n and p type of the semiconductor layers forming a double heterostructure, as demonstrated in Figure 2:13. As mentioned previously, during the growth process, the dots formed on the wetting layer is the same material as the dots. The entire structure (dots and wetting layer) planted in a wider band gap quantum well which forms a so-called dot –in- a- well

structure. This is embedded in the waveguide of high refractive index material surrounded by a low refractive index material. This structure supports both optical and electrical confinement, so it is known as a separate confinement heterostructure (SCH).
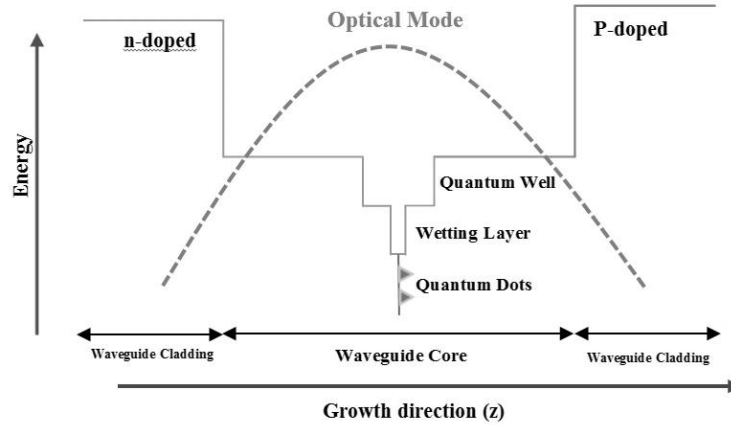
Figure 2:13 Active region of the Quantum dots.

2.4.4 Broadening in the quantum dot system

The perfect quantum dot should provide a sharp delta function in the transition spectrum; however, the transition spectrum is broadened by several factors. In fact, there are two basic types of broadening that the dots can experience. The initial one is homogeneous broadening, that arises from the Heisenberg uncertainty principle (   ) where   is uncertainty of the energy level occupied by the carrier and   is the life time of the carrier. In the other word the energy of an electron or hole is not precisely equal to the energy state in the dot due to collisions. This kind of broadening can be described in terms of a normalised Lorentzian function. The value of this broadening in the quantum dots system is typically in the order of meV at room temperature (Blood 2009). The second broadening which the quantum dot ensembles can experience is inhomogeneous broadening. This arises from the difference between the individual dots in terms of size, shape and composition as shown in Figure 2:14. This difference is due to fluctuations in surface roughness, surface temperature or ion concentrations during the self-formation process (Sugawara et al., 2000). Inhomogeneous broadening can be described by Gaussian distribution over the ensemble. The dot ensemble has inhomogeneous broadening of the quantized energies due to size fluctuation of the dots, while the optical gain of a single dot shows homogeneous broadening with a width that is proportional to the polarization

dephasing rate. Figure 2:15 shows The interaction between the cavity-mode photons and the carriers in the quantum dots via homogeneous broadening of gain (Sugawara et al. 2000).
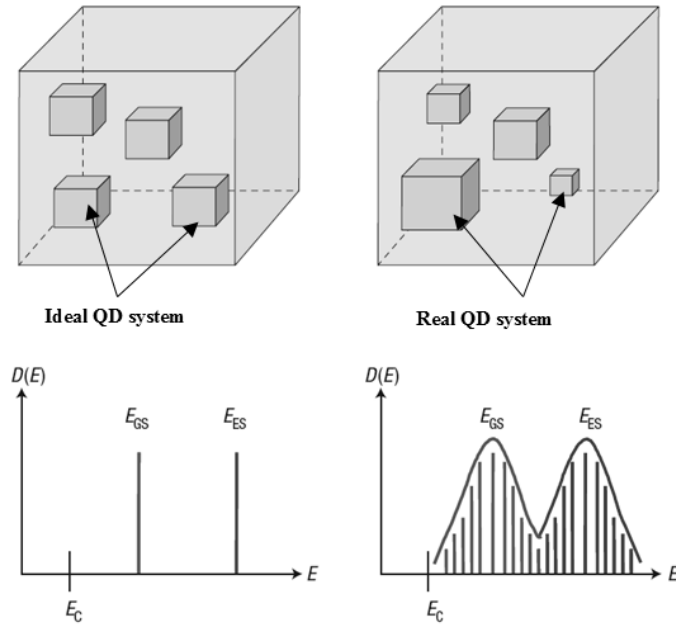
Figure 2:14 These effects lead to inhomogeneous broadening. a, A schematic of an ideal QD system and, b, a real QD system, where inhomogeneous broadening is illustrated. (EGS: ground-state energy; EES: excited-state energy; EC: the bottom of the conduction band (Rafailov et al. 2007).
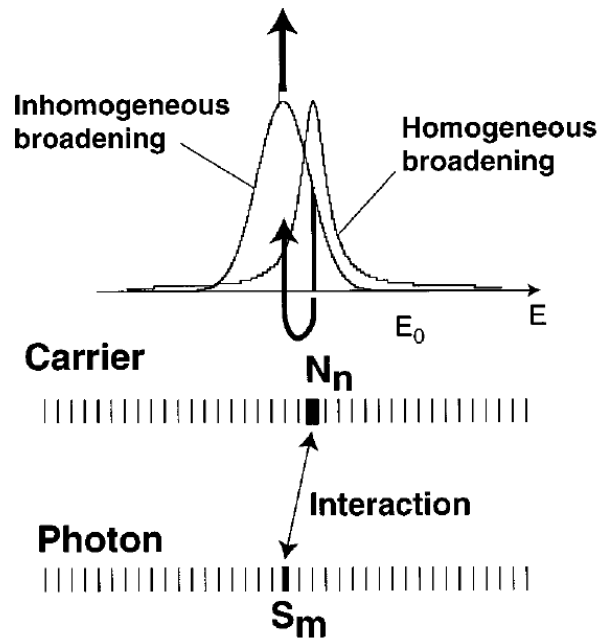
Figure 2:15 The interaction between the cavity-mode photons and the carriers in the quantum dots via homogeneous broadening of gain (Sugawara et al. 2000).

2.5 Modal gain, modal absorption and spontaneous emission

This section will discuss modal gain, modal absorption and spontaneous emission which are crucial features related to quantum dot lasers. Gain measurement is key to understanding the underlying physical behaviour of the materials and structures of the active region. Various static and dynamic characteristics can be analysed from gain spectral measurement, such as differential gain, quasi-Fermi level separation, and others. The spectral gain is generally measured as a function of current density and temperature. For mode-locking purposes material gain is a critical factor because the wider the gain bandwidth is, the shorter the pulse width that can be achieved. Conversely, the measure of modal absorption spectrum is also fundamental in identifying the transitions in the QD material. This, in principle, means that there are no carriers in the conduction band states and the valence band states are full. Therefore, the model absorption will offer a full picture of the energy transitions unlike the model gain and the spontaneous emission which have the effect of the carrier distribution and interaction. Spontaneous emission is also significant, especially when measured as a function of the current density in real units that can help to determine the internal efficiency of the device. Calculation using the measured spontaneous emission spectrum can give information for carrier distribution and population inversion, which will be described in detail later in this chapter.

There are numerous methods available to measure modal gain, absorption and spontaneous emission. These can be classified into two types. The first is High Resolution Spectroscopy that includes the Hakki-Paoli method (Hakka and Paoli 1974) and modified Cassidy methods (Cassidy 1984). The second is Variable Stripe Length Techniques, which consist of Shaklee and Leheney, Variable stripe length (Shaklee and Leheny 1971), the integrated mode filter method, besides the segmented contact method). The segmented contact method was used in this work to measure modal gain, absorption and spontaneous emission. The techniques and the experimental setup are described accurately in the subsequent chapter.

2.5.1 Model gain in quantum dot system

Optical gain is defined and measured as a fractional increase in energy in an optical mode per unit distance of propagation. The model gain (G) is related to the local gain (g), which can be obtained from many calculations through the relation

, where   is the optical confinement factor. Basically, the optical gain is controlled by population inversion; therefore, a measurement of model gain should be performed as a function of the pumping level.

In an edge emitting laser, the light is guided through the dots layer over the cavity length, which is very much larger than the optical wavelength, as shown in Figure 2:16a. Moreover, in this geometry, it is possible to define the gain coefficient along the axis of the waveguide as:

$$\overline{}\ \overline{} \qquad\qquad 2{:}23$$

where W is the energy in the mode and (*dW/dL*) is the increasing of energy per unit distance. The model gain of an ensemble of N identical dots per unit area in the plane of layer is given as:

$$\frac{\bullet}{\bullet}\ \overline{} \qquad\qquad 2{:}24$$

(Blood 2015)

where   is the gain cross section, in the same direction of propagation and polarisation, •   is the profile of the optical field across the waveguide (see Figure 2:16b) and •   is the optical field at the layer of dots. The term in the square brackets is defined as an effective mode width (   ), as illustrated in Figure 2:16b.
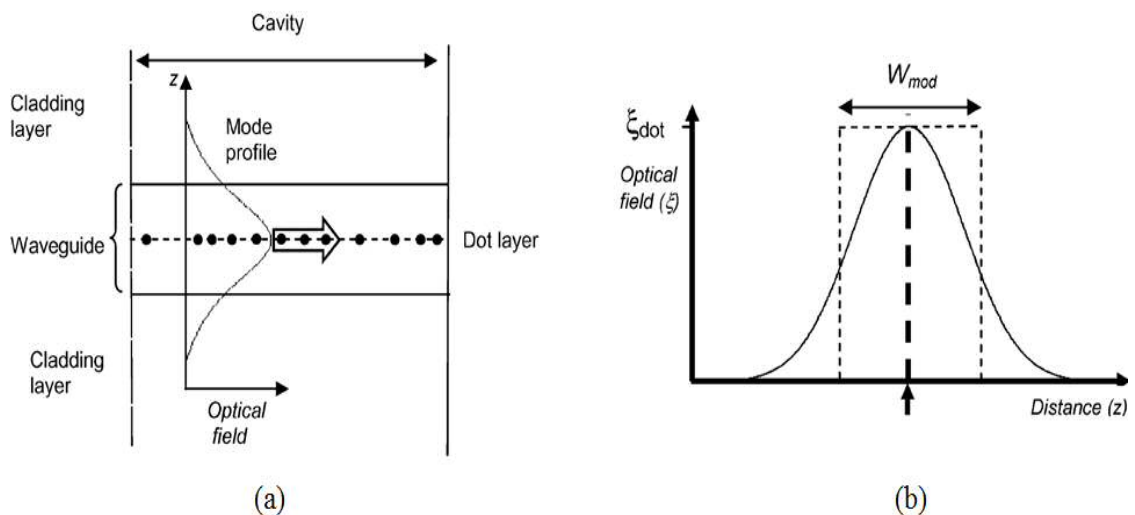
**Figure 2:16 (a) layer of dots within a waveguide of diode laser,
(b) The effective mode width (Blood 2009).**

The material gain of a single dot cannot be defined; thus, the cross section shows a comparison between different dot systems in terms of size, shape and composition. However, the modal gain provides ground for evaluation of the laser's operation because this determines the threshold of the laser and reveals inhomogeneous size distribution.

2.5.2 Model absorption in quantum dot laser

The number of photon absorbed per unit time for the light incident normal to layer of dots ($\Delta\Phi$) is given by:

$$ \overline{\quad\quad} \tag{2:25} $$

(Blood 2009)

where N is the number of the dots per unit area,   is the area under the cross-section peak and represents the total absorption strength of a single dot.   is the normalised probability of absorption occurring for photon energy hv per unit energy interval and   is the energy separation of the dot states. Additionally,   and   are given respectively as (Blood, 2009):

$$ \overline{\quad\quad} \; \overline{\quad} \tag{2:26} $$

$$ \text{–} \; \overline{\quad\quad\quad\quad} \tag{2:27} $$

(Blood, 2015)

where n is the refractive index,   is the permittivity of free space, e is the electron charge,   is the electron mass, M is the optical matrix element,   are the normalised envelope function of the upper (conduction) and lower (valance) state respectively,   is the homogenous Lorentzian linewidth.

In this case,   shows that there is a potential for interaction, even when the photon energy is not equal to   Equation 2:27 is plotted in Figure 2:17 as a function of photon energy relative to photon energy separation   .
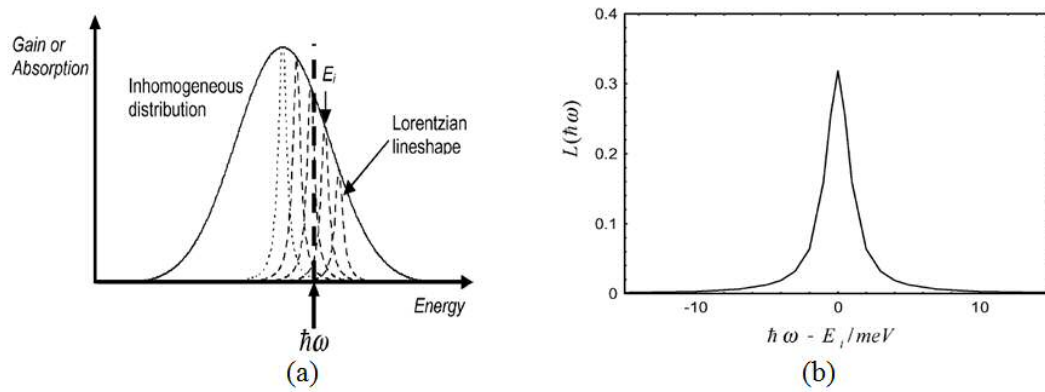
Figure 2:17 (a) absorption or gain at photon energy *hv* is determined by contributions from dots of different sizes, with energy separation Ei in the inhomogeneous distribution by virtue of their homogeneous Lorentzian lineshape, (b) Normalised Lorentzian homogeneous lineshape function plotted as a function of the photon energy relative to the dot energy level eparation Ei (Blood 2009).

If the homogeneous linewidth is smaller than the inhomogeneous linewidth in the quantum dots system, the modal absorption cross section (A_m) at a given photon energy of optical mode propagation along the waveguide is given as:

$$\underline{\qquad}$$

2:28

(Blood 2015)

where   is the number of dots per unit energy interval, the area under the modal absorption for a single transition gives the integrated cross section   which is a distinctive property of the dot and does not depend on homogeneous broadening. Thus:

$$\underline{\qquad}$$

2:29

(Blood 2015)

2.5.3 Spontaneous emission spectrum

As shown previously, the spontaneous emission rate   is proportional to the Einstein coefficient A_{21} and the population of the states f_2, f_1, as seen in Equation 2:1.

In quantum dot structures, spontaneous emission occurs in all directions. In this case spontaneous emission propagates normally to the layer of dots and is not amplified, this can be used to characterise the spontaneous emission spectra. Meanwhile, the

propagation along the dots layers causes an Amplified Spontaneous Emission (ASE), which is a significant factor with regards to obtaining the modal gain, modal absorption, population inversion factor and the spontaneous emission in real units of the quantum dot lasers. The procedure and the equations used for that will be discussed in the following chapter.

2.5.4   Non-radiative recombinations

When the electrons in the conduction band and the holes in the valence band recombine non-radiative (without photon emission), this is termed non-radiative recombination. Such processes raise the required current to achieve threshold in the laser and reduce the efficiency of the device; therefore, it should be identified and minimised. Owing to the absence of the light in these processes, the measurements of this process cannot be performed directly.

There are two general types of non-radiative recombination; specifically, Auger recombination and recombination by defects. Auger recombination occurs due to the recombination of the electron and the hole indirectly, where momentum and energy are conserved in this process by interacting with a second electron or hole in the conduction or valence band. Subsequently, it relaxes by way of multi-phonon emission or lattice vibrations. This process is usually negligible in wide band gap materials, although it is tremendously important in narrow band gap ones (Stoneham 1981).

Conversely, recombination by defects is due to real semiconductor structure impurities or defects that form. This creates a localised defect state in the crystal, and forms a so-called "forbidden energy gap", so that the defect can capture carriers and release phonons (Abakumov 1991).

2.5.5   Gain–current relation in quantum dot laser

One of the most important characteristics of a semiconductor laser is the gain-current relationship. This relationship can be useful to determine the threshold current density, gain saturation effects, differential gain and transparency current density of the laser. The plot in Figure 2:18 illustrate the typical gain-current curve, which can be obtained experimentally from the model gain spectra at different pumped levels.
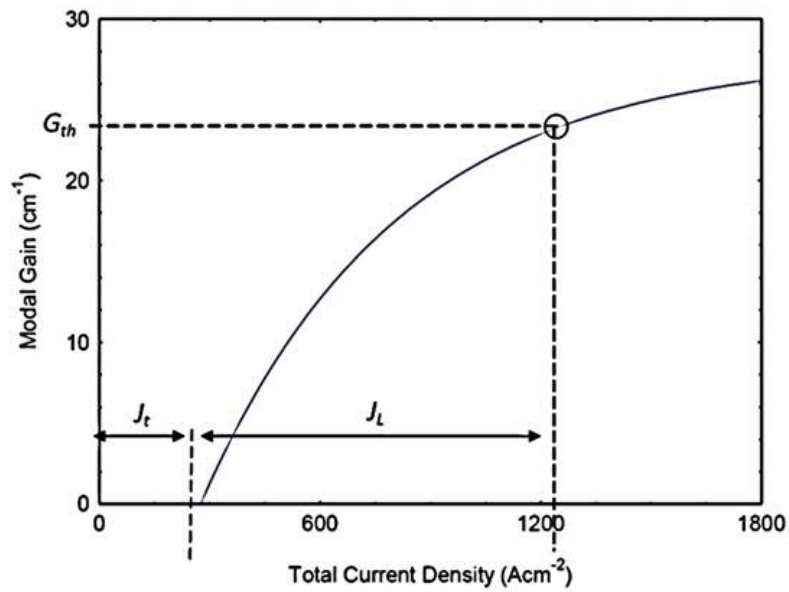
Figure 2:18 Plot of a typical gain-current relation showing the transparency current(J_t) and the current required to reach the threshold (J_L)in a device of a specific length.

The relationship between gain and current in a quantum dot laser can be approximated as:

$$\overline{\qquad}$$

2:30

(Zhukov et al. 1999)

where   represents the saturated modal gain for a specific QD state and   is a dimensionless fitting parameter that account for the interaction between QD states and the inhomogeneous broadening. This Equation 2:30, will be used to calculate   and   in Chapter four to assist with a comparison.

2.6   Population inversion factor

The population inversion factor (P_f) provides a description of the occupation probability of the states at different energies. It therefore provides information of the carrier's distribution in the active region. In general P_f is given as:

$$\underline{\qquad}$$

2:31

(Summers et al. 2001)

The   value can range from 0 to1. Additionally, unity is achieved if the upper state is occupied fully (   ) or if the lower state is empty (   ), where both these assumptions are satisfied the system, it is said to be fully inverted.

In the case of a quasi-equilibrium system, the occupation probability is given by Fermi-Dirac statistics and takes the form:

$$\underline{\hspace{3cm}} \qquad\qquad 2{:}32$$

(Summers et al. 2001)

where E is photon energy and   is quasi-Fermi level separation, Equation 2:32 can be written in a more general form as:

$$\underline{\hspace{1.5cm}} \qquad \underline{\hspace{1.5cm}} \qquad\qquad 2{:}33$$

(Hutchings et al. 2014)

From Equation 2:33, if a plot of   versus   is linear, this means all states which participate in the transition across the spectrum have occupation probabilities, according to quasi-equilibrium. Emission temperature   can be determined from the slope of this plot.   is a characteristic of the gain and emission spectra and emerges from the energy distribution of the carriers participating in these transmissions. It may not have the same temperature as the temperature of the lattice (T_L). The intercept of the plot gives a value of   which indicates the energy separation of populated electrons and holes states participating in the transitions. In the case of quasi-equilibrium   .

 As the occupation probability of the carriers is an extremely significant factor in mode-locked quantum dot lasers, it is beneficial to define three regions of occupation distribution in the quantum dot system, based on Equation 2:33 (Hutchings et al., 2014).

Thermal Occupancy: versus   plots are linear, and the slope gives   equivalent to the temperature of the lattice (T_L). This implies the wetting layer and the quantum dot states are all in thermal equilibrium and occupation of all the states can be described by means of Fermi-Dirac statistics.

Quasi-Thermal Occupancy: versus   plots are linear, although   is not equivalent to the temperature of the lattice (T_L). The system can be described by way of Fermi-Dirac statistics.

Random Occupancy: The value of   is very much greater than the Lattice Temperature (T_L). Moreover, the QD states are decoupled from the wetting layer states. The rate of recombination from the dots is very much faster than the thermal excitation of the carriers to the wetting layer, therefore the system cannot be described by Fermi-Dirac statistics. It has been shown recently that random population in a QD system can support mode-locked laser operation, where a pulse width of 290 fs was observed from the QD laser sample at 20 K; though it was operating in random occupation (Finch et al. 2013).

2.7 Mode-locking in semiconductor laser

2.7.1 Mode-locking in laser

Lasers usually output light continuously as long as the excitation is present. However, lasers can also output pulses of light, the easiest way to do that would be to pulse the excitation source. For example, in injection pulsed lasers, modulating the electrical current will modulate the output light. In Q-switched lasers, the cavity loss is modulated, and this gives pulsed operation. Mode-locked lasers are a more interesting type of pulsed laser, as these lasers produce ultra-short pulses. These ultra-short pulses also have very high peak optical power, seeing that for the same average output power the light is now concentrated into very narrow pulse periods instead of being output continuously

Mode-locking is the technique employed to lock the phase relationship of longitudinal modes in a laser cavity to generate ultra-short optical pulses in the order of picoseconds to femtoseconds. A further significant feature of mode-locked lasers is that the energy which was dispersed in several modes in cw operation is now concentrated in short pulses of light. This means that although the output average power (P_{av}) may be low, the pulse peak power (P_{peak}) can be significantly higher. The mode-locked lasers are exclusively beneficial in numerous photonic applications, for instance optical clock

distribution, clock recovery, radio over fibre signal distribution, optical sampling, optical data communication networks, high-speed optical communication systems, high speed optical interconnects, optical time division multiplexed transmissions and ultrafast signal processing. Additional applications include optoelectronic measurement applications, such as analogue to digital conversion, electro-optic sampling and impulse response testing of optical components, THz generation and others (Finch et al. 2013).

2.7.2 Principle of mode-locking

The production of the shortest pulse durations and the highest repetition rates is usually described as ultrafast lasing. In standing wave resonator, the repetition rate can be given as:

$$\qquad\qquad\overline{\qquad\qquad}\qquad\qquad\qquad\qquad 2\text{:}34$$

where c is the speed of light in the vacuum, n is the refractive index and L is the length of the laser cavity.

A schematic of the gain spectrum profile, the longitudinal modes and the lasing output of the laser are shown in Figure 2:19, the longitudinal modes   are given as:

$$\qquad\qquad\overline{\qquad\qquad}\qquad\qquad\qquad\qquad 2\text{:}35$$

where m is the integrated mode number, the laser action can occur only for the cavity modes that are placed within the gain bandwidth of the laser material. These modes undergo optical gain and are also resonant with the cavity.

 For a mode to take place in laser action, the optical gain must be greater than the optical loss for that mode. Under high enough pumping, a few modes experience net optical gain and start lasing.
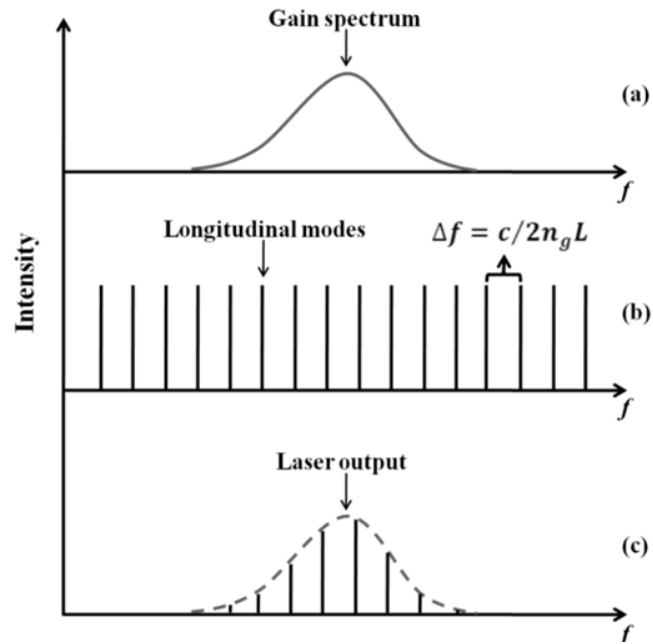
Figure 2:19 (a) gain spectrum profile, (b) the longitudinal modes and (c) the lasing output.

For a normal laser operating in continuous wave (CW) mode, the modes lase in random style; thus, the laser output is a random intensity fluctuated over some average value. In case of a mode-locking situation, the relationship between the phases of the modes is constant, so all the lasing modes are locked together in phase. These modes can constructively interfere, which subsequently makes the output light pulsed, as revealed in Figure 2:20.
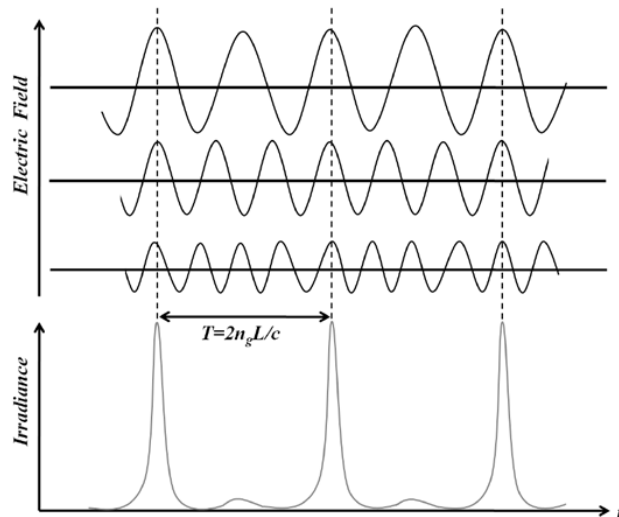
Figure 2:20 Illustration of mode-locked laser output in the time domain.

What happens in a mode-locked laser is that the cavity modes have frequencies that are integer multiples of the inverse roundtrip time. When the laser is mode-locked, these modes are lasing in harmony, locked together, and hence, the output of the laser is a periodic train of pulses which have period equals to the cavity round trip time   as shown in Figure 2:20.

There are two basic types of mode-locking mechanism in a semiconductor laser, which are distinguished by the means of the pulse–shaping mechanism; specifically, active mode-locking and passive mode-locking. Active mode-locking can be achieved by an external electrical signal to modulate the gain or losses of the semiconductor laser.

The frequency of the external electrical signal must correspond with the cavity round trip ( ). High repetition rates cannot be easily achieved in the active mode-locking technique because of the limitation of high frequency electrical signal generators. Passive mode-locking can be obtained by combining a saturable absorber (SA) in the laser cavity that does not require any external modulated source. Passive mode-locking will be described in detail in the subsequent section as it is the technique that has been used to achieve mode-locking in this thesis.

2.7.3   Passive mode-locking in semiconductor laser

The passive mode-locked laser diode consists of two-sections which are electrically insulated: one termed the gain section that is normally forward biased to produce gain for lasing, whereas the other section is known as the saturable absorber section (SA), which is regularly supplied by a DC reverse bias voltage in order to decrease the absorber recovery time. The SA section is a crucial element owing to the nonlinear properties of the material, which provides the self-starting mode-locking and shortening pulse mechanisms.

Figure 2:21 shows the two-section regime of the semiconductor laser processed for passive mode-locking in a form entitled "monolithic passive mode-locking". The dynamics of gain and loss in the pulse shaping is shown in Figure 2:22.
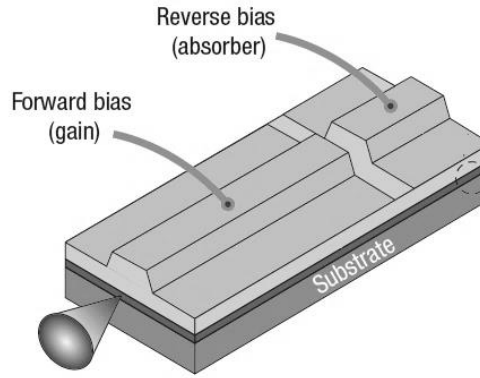
Figure 2:21 Two-section monolithic mode-locked laser diode regime (Rafailov et al. 2007).

At a steady state, the leading edge of the pulse reaches the cavity; the loss is unsaturated and higher than the gain. However, the leading edge of the pulse saturates the absorber quicker than the gain, leaving a net gain window around the pulse peak area. The absorber in turn, recovers from saturation to the highly loss state more speedily than the gain, consequently, the trailing edge of the pulse is attenuated by the absorber. The saturation power and recovery time of the absorber are two significant parameters in the pulse formation and shaping. By means of the reversely biased voltage, generated carriers can be ejected from the SA section speedily and thus, the absorber recovery time is decreased. By increasing the reverse bias on the SA, pulse widths can also be shortened owing to the reduction of the net gain window (Smith et al 1985).
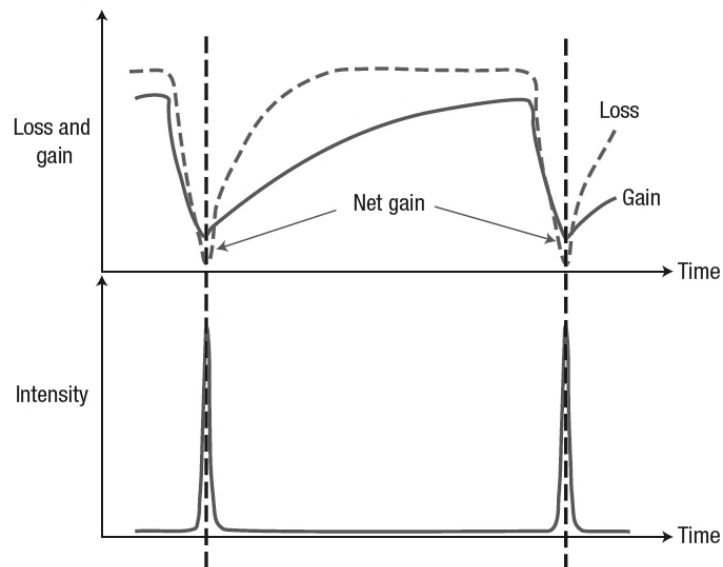
Figure 2:22 Gain and loss dynamics during passive mode-locking operation in a semiconductor QD laser ((Rafailov et al. 2007).

2.7.4 Mode-locking condition

An increase in injected current into the gain section causes pulse broadening, whereas the increases in reverse bias into the SA section affects the pulse shortening. Stability of the mode-locking depends on the balance between pulse shortening and pulse broadening. In order to generate optical pulses in passive mode-locking, the loss has to saturate faster than the gain, which can be described by the stability condition of passive mode-locking. In the other words, the saturation energy of the gain section must be more than the saturation energy of the SA section , which are given as:

$$ \quad\quad\quad\quad\quad\quad \overline{\quad\quad\quad} \quad\quad\quad \overline{\quad\quad} \quad\quad\quad\quad\quad 2:36 $$

(Lin et al. 2009)

where *A* is the optical mode cross-sectional area, and are the differential loss and gain, respectively. Figure 2:23, shows the differential absorption and gain as a function of the carrier density in the semiconductor laser. It can be visibly seen from the tangent lines of the gain and absorption curves that > which is a substantial requirement for passive mode-locking.
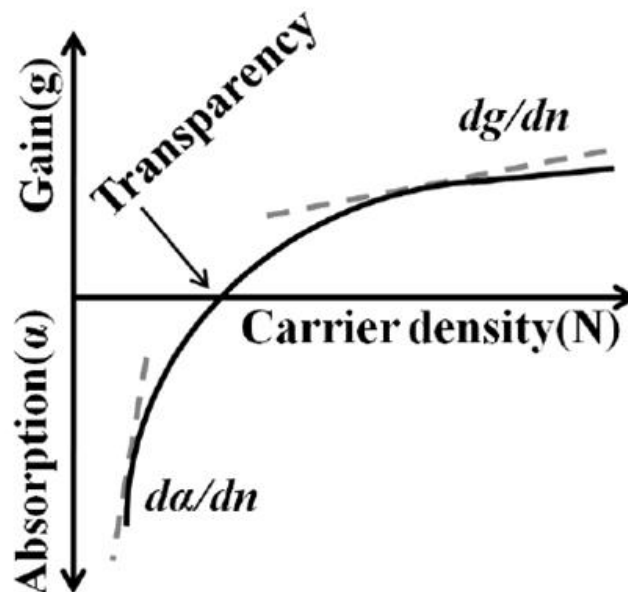
Figure 2:23 Gain and absorption as a function of the carrier density.

2.7.5 Quantum dot materials as a mode-locked medium

Passive mode locking of monolithic quantum dot lasers has been shown to have several advantages owing to the three-dimensional confinement nature, which generate improvements in the mode-locking performance in comparison with the conventional bulk and QW materials. I now describe in brief the important advantages for the quantum dot material that support mode locking in lasers in terms of stability, pulse duration, chirp, output power and noise (Rafailov & Cataluna 2011).

Advantage of QD saturable absorbers: The advantages of broadband absorption, ultrafast absorption recovery and low saturation fluence for the quantum dot system, is that they can all be exploited positively to support mode-locking when quantum dot material is used as a saturable absorber.

Broad gain bandwidth: The quantum dot semiconductor materials are also exciting materials for generation and amplifications of femtosecond pulses due to spectral broadening associated with the inhomogeneous broadening. The highly broad bandwidth available in QD mode-locked lasers presents the potential for generating sub-100fs pulses providing all the band can be engaged coherently and dispersion effects can be effectively minimised.

Low threshold current: QD lasers have the advantage of low threshold current requirement. This attribute also applies to operations in a mode-locking regime. A low threshold current is clearly advantageous because this can offer a device which is compatible as an effective and compact source of ultrafast pulses.

Low Temperature Sensitivity: Owing to the discrete density of states in a QD system, QD lasers exhibit low temperature sensitivity, making excellent candidates for many applications including mode-locking.

Suppressed carrier diffusion: Carrier diffusion in the gain material in the QDs system is highly suppressed due to the localised nature of QDs, compared with QW materials.

Lower level of amplified spontaneous emission: Ultrafast pulse generation in semiconductor materials can be affected by timing jitter, especially in passive mode-locked devices because of the lack of synchronization with an electrical signal. ASE is the primary cause of jitter because it produces random fluctuation in photon density,

gain and index of refraction, which can lead to variation in the round-trip time. Furthermore, QD materials have an overall lower level of ASE in comparison with QW materials.

Linewidth enhancement factor: The QD materials have an extremely low value of linewidth enhancement factor due to the symmetry of the gain associated with QD structures. The low value of linewidth enhancement factor means lower chirp, lower sensitivity to optical feedback effects and suppressed beam filamentation.

Ultrafast carrier dynamics: In zero-dimensional QDs, the electron-phonon scattering rate is reduced due to the delta function-like ODs, which is known as a phonon bottleneck effect. It is subsequently predicted that the low scattering rate will lead to longer relaxation time (ps order) between QD states than in QW and bulk materials. The long relaxation time will strongly restrict the application of QDs in lasers and amplifiers. Nevertheless, contrary to the predictions, fast carrier dynamics have been demonstrated by pump-probe experiments. In QDs, two distinct recovery times exist related to the absorption. A fast recovery (1 ps) was ascertained to be followed by a slow decay (100 ps), as shown in Figure 2:24. An ultrafast recovery time of ~100 fs is also measured and attributed to Auger scattering, which provides a channel for carriers relaxing from ES into GS.
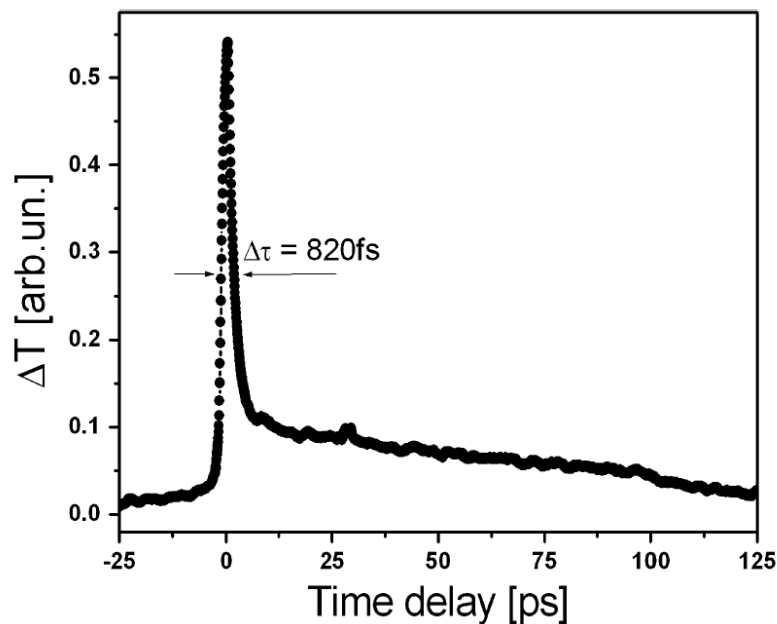
Figure 2:24 Illustration of two recovery times of a QD-based device by pump-probe measurements. ΔT is the change in the transmission of the probe due to absorption saturation of the pump (Rafailov et al. 2004).

2.8 Summary

This chapter contributed background theory regarding the principles of semiconductor materials, quantum dot lasers and a mode-locked laser. The chapter has provided the relevant theory and equations required to understand and explicate the experimental results shown in the following chapters, starting from optical transmission in a two levels system and band structure of the semiconductor materials. Fermi-Dirac statistics and population inversion as well as the principles of semiconductor laser, such as the density of state in a quantum system and quantum confinement, were introduced in this chapter. The quantum dot system has been introduced, besides the quantum dot active region. The most important concepts in quantum dot lasers, such as modal gain, modal absorption, spontaneous emission and gain-current relation. Moreover, several important equations were presented in this chapter as well as the population inversion factor and the occupational probability. Finally, the chapter described the mode-locking principles in semiconductor laser.

2.9 References

Abakumov, V.N., Perel, V.I. and Yassievich, I.N.**1991**.Nonradiative irecombination in semiconductors. Amsterdam: Elsevier.

Alfred, A **2011**. Strained-layer quantum-well lasers. IEEE Journal of selected topics in quantum electronics 17(5), pp. 1364-1372.

Alivisatos, A., **1996**. Perspectives on the Physical Chemistry of Semiconductor Nanocrystals. J. Phys. Chem, 100, pp.13226–13239.

Blood, P. **2009**. gain and recombination in quantum dot lasers. IEEE Journal of selected topics in quantum electronics, 15(3), pp.808–818.

Blood, P. **2015**. Quantum Confined Laser Devices, Oxford: Oxford University Press. UK.

Casey, H. C. and Panish, M. B. **1978**. Heterostructure Lasers: Part A: Fundamental Principles Academic, San Diego.USA

Cassidy, D.T.**1984**. Technique for measurement of the gain spectra of semiconductordiode lasers. Journal of Applied Physics 56 (11), pp.3096-3099.

Chukwuocha, E. and Onyeaju, M. **2012**. Simulation of quantum dots (QDs) in the confinement regime. Int. Journal of Applied Sciences and Engineering Research 1(6), pp.784–792.

Coldren, L., Corzine, S., and Masanovic, M., **2012**. Diode Lasers and Photonic Integrated Circuits, New Jersey: Johon Wiley and Sons. USA.

Derbali, M.B., Hassen, F., Meddeb, J., Maaref, H. and Abraham, P. **1997**. Optical characterization of highly mismatched InP/GaAs(111)B epitaxial heterostructures. Microelectronics Journal 28, pp.1005-1009.

Finch, P. Blood, P. Smowton, P. M. Sobiesierski, A. Gwilliam, R. M. and O'Driscol, I. **2013**. Femtosecond pulse generation in passively mode locked InAs quantum dot lasers. Applied Physics Letters 103(131109), pp.1-4.

Hutchings, M., O'Driscoll, I., Smowton, P., and Blood, P. **2014**. Fermi-dirac and random carrier distributions in quantum dot lasers. Applied Physics Letters 104, pp.031103:1–031103:4.

Hakki, B. W., and Paoli, T. L.**1975**. Gain spectra in GaAs double-heterostructure injection lasers. Journal of Applied Physics 46(3), P.1299-1306.

Ikeri, H. I., Onyia, A. I. and Asogwa U.P. **2017**. theoretical investigation of the size effect on energy gap of CdSe, ZnS and GaAs quantum dots using particle in a box model. Journal of Ovonic Research 14(2), pp. 49-54.

Kim, H. D. and Jeong, W. G. **2005**. Growth of InAs and InGaAs quantum dots on (001) InP and their photoluminescence properties. Journal of the Korean Physical Society 47(5), pp. 852-856.

Kressel, H. and Butler, J. **1977**. Semiconductor laser and heterojunction LEDs. New York: Academic, UAS.

Lin, C.-Y., Xin, Y.-C., Li, Y., Chiragh, F. L.and Lester, L. F. **2009**. Cavity design and characteristics of monolithic long-wavelength InAs/InP quantum dash passively mode-locked lasers. Optics Express 17(22), pp.19739 -19748.

Onyia, A. I. Ikeri, H. I. and Nwobodo A. N. **2018** theoretical study of the quantum confinement effects on quantum dots using particle in a box model. Journal of Ovonic Research 14(1), pp. 49 - 54.

Pikhtin, N. A., Slipchenko, S. O., Sokolova, Z. N. and Tarasov I. S. **2004**. Internal Optical Loss in Semiconductor Lasers. Semiconductors 38(3), pp. 360–367.

Piprek, J., Abraham, P. and Bowers, J., **1999**. Cavity length effects on internal loss and quantum efficiency of multiquantum-well lasers. IEEE Journal of selected topics in quantum electronics, 5(3), pp.634–647.

Rafailov, E., Cataluna, M. and Sibbett, W., **2007**. mode-locked quantum-dot lasers. nature photonics 1, pp.395–401.

Rafailov, E., White, S., Lagatsky, A., Miller, A., Sibbett, W.,Livshits, D., Zhukov, A. and Ustinov, V. **2004**. fast quantum-dot saturable absorber for passive mode-locking of solid-state lasers. IEEE Photonics Technology Letters 16(11), pp.2439-2441.

Rafailov, E., Cataluna, M. and Eugene, A. **2011**. Ultrafast Lasers Based on Quantum Dot Structures. Weinheim: Wiley-VCH Verlag and Co.KGaA. Darmstadt, Germany.

Roberts, T. S., Stevens, B.J., Clarke, E., Tooley, I., Orchard, J., Farrer, I., Childs D.T., Babazadeh, N., Ozaki, N., Mowbray, D. and Hogg, R.A. **2017**. Strain balancing of metal-organic vapour phase epitaxy InAs/GaAs quantum dot lasers. IEEE Journal of selected topics in quantum electronics 23(6), pp.1-8.

Smith, P., Silberberg, Y. and Miller, D. **1985**. Mode locking of semiconductor diode lasers using saturable excitonic nonlinearities. Journal of the Optical Society of America B, 2(7), pp.1228-1236.

Smowton, P. M., and Blood .B. **1997**. Fermi level pinning and differential efficiency in GaInP quantum well laser diodes. Applied Physics Letters, 70(9), pp.1073-1075.

Summers, H., Thomson, J., Smowton, P. M., Blood, P. and Hopkinson, M. **2001**. thermodynamic balance in quantum dot. Semiconductor science and technology, 16, pp.140–143.

Sugawara, M., Mukai, K. Nakata,Y.and Ishikawa, I. **2000**. Effect of homogeneous broadening of optical gain on lasing spectra in self-assembled In_xGa_{1-x}/GaAs quantum dot lasers. Physical review B 61(11), pp. 7595 -7603.

Stoneham, A. M. **1981**. Non-radiative transitions in semiconductors. Reports on Progress in Physics.44, pp.1253-1291.

Shaklee, K. L.and Leheny R. F. **1971**. Direct determination of optical gain in semiconductor crystals. Applied Physics Letters 18(11), pp.475-477.

Warburton, R. J. **2002**. Self-assembled semiconductor quantum dots. Contemporary Physics 43(5), pp.351-364.

Williams, D. M. and R.H. **1991**. Physics and technology of Heterojunction devices, Ltd, Peter Peregrinus.

Zhukov, A., Kovsh, A., Ustinov, V., Egorov, A., Ledentsov N., Tsatsul'nikov, A., Maximov, M., Shernyakov, Y., Kopchatov V. Lunev, A., Kop'ev, P., Bimbergdag, D. and Alferov Z. **1999**. Gain characteristics of quantum dot injection lasers. Semicond. Sci. Technol, 14, pp.118–123.

Chapter (3) Sample structure and experimental procedures

3.1 Introduction

The chapter introduces the devices structures and experimental techniques used in this work. The chapter begins with growing wafers and explaining the materials used, along with the samples that were fabricated and prepared. Some important measurements for the wafers such as Transmission Electron Microscopy (TEM), Photoluminescence measurements (PL) and the Calibration of P and As fraction in ODs are shown in this chapter. The chapter also presents the experimental techniques and equipment used to collect data in this work, as well as same raw data. These include Current-Voltage-Light (IVL) temperature, near-field, spectrum and Edge-Photo Voltage Spectroscopy (E-PVS) measurements. The Segmented Contact Method (SCM) technique is illustrated in detail in this chapter, with various important equations used to process the data. Finally, the chapter introduces some important raw data to clarify the work in Chapters: four five and six.

3.2 Sample growing and fabrication

3.2.1   Growing and samples structure

The samples in this study were grown by Dr. Andrey B. Krysa in the EPSRC National Centre for III-V Technologies, the University of Sheffield. The Stranski-Krastanov mode (MOVPE) technique for arsenides and phosphides was used. InP QDs have been used in this study as the standard device, while InAsP QDs is a desired device. The active region of the laser structures consisted of 5 InP or InAsP QD sheets (see Figure 3:1) with a $Ga_{0.54}In_{0.46}P$ quantum well with a thickness of 8nm grown above each QD sheet and separated by a layer of $(Al_{0.3}Ga_{0.7})_{0.52}In_{0.48}P$ with a thickness of 16nm. The active region was sandwiched with an $Al_{0.52}In_{0.48}P$ clad / $(Al_{0.3}Ga_{0.7})_{0.52}In_{0.48}P$ core waveguide.
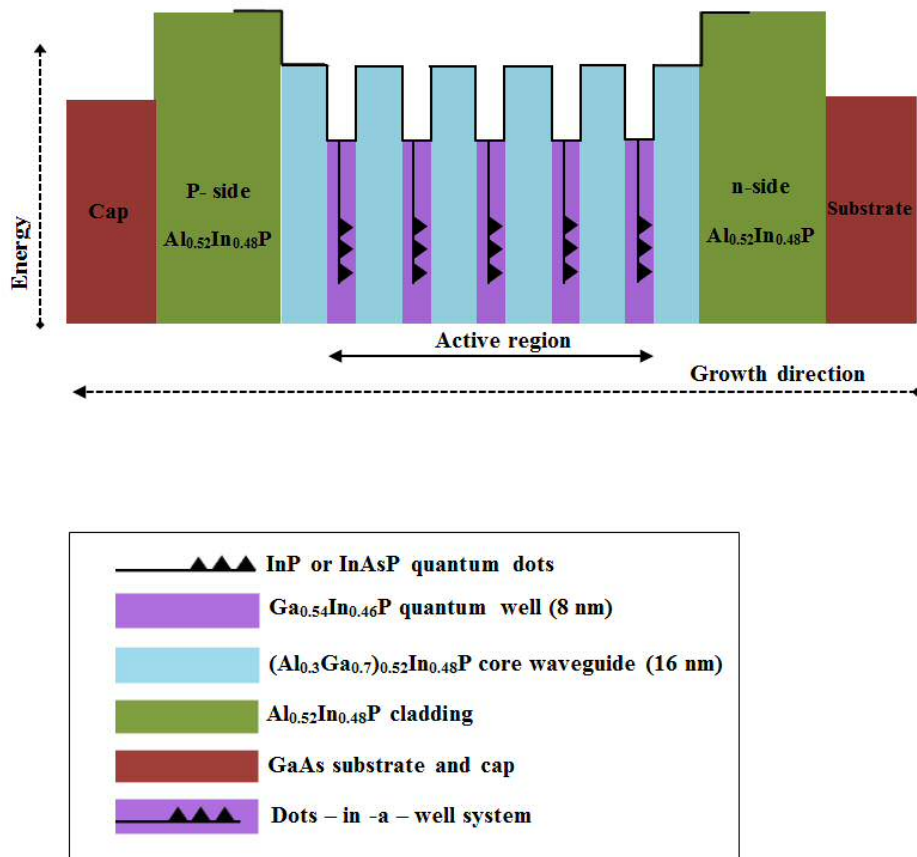
Figure 3:1 Schema of epitaxial growth structure.

Table 3:1 reveals the description of layers used. Figure 3:2 displays the schema of the layers structure of the wafer.

Reps	Material	Thickness, nm
1	P-GaAs	50
1	P-Ga$_{0.52}$In$_{0.48}$P	50
1	P-Al$_{0.52}$In$_{0.48}$P	1000
1	(Al$_{0.3}$Ga$_{0.7}$)$_{0.52}$InP	84
5	(Al$_{0.3}$Ga$_{0.7}$)$_{0.52}$InP	16
5	Ga$_{0.52}$In$_{0.48}$P	8
5	InP or InAsP	0.76
1	(Al$_{0.3}$Ga$_{0.7}$)$_{0.52}$InP	100
1	n-Al$_{0.52}$In$_{0.48}$P	1000
1	n-Ga$_{0.52}$In$_{0.48}$P	50
1	n-GaAs buffer	500
	n-GaAs substrate	

Table 3:1 Materials for the structure of the wafer.

Figure 3:2 Schema of the layers structure of the wafer.

The epitaxy of laser structures was performed on (100) GaAs substrates with a miscut angle of 10o towards <111>A in a low pressure (150 Torr) horizontal flow reactor. The growth temperatu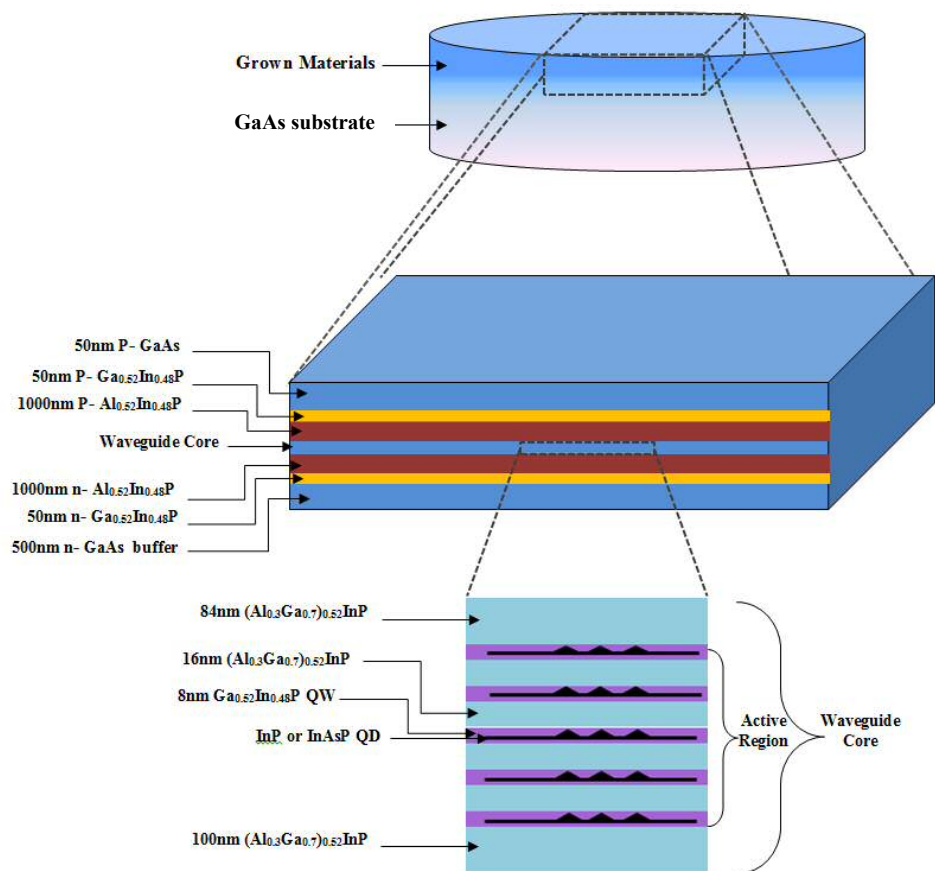res measured by a thermocouple inside the graphite susceptor were 710 ^{o}C. disilane and dimethylzinc are used as aprecursors for n- and p-type doping, respectively.

The phosphine flow was kept constant at 300 sccm throughout the growth of the core regions, and the arsine flow of 6.25 sscm was introduced to the reactor during the growth of the InAsP QD layers. Based on θ-2 θ X-ray diffraction scans near 004 of bulk InAs$_x$P$_{1-x}$ grown with the same growth conditions as the InAsP QDs, a solid molar fraction of arsenic of roughly 25% would be expected. Such a proportion of As would be expected to produce an increase in emission wavelength of approximately 120nm compared to the InP bulk material.

When As is added to InP this makes the lattice constant higher. Consequently, InAsP has a higher lattice mismatch with GaAs (which has a lattice constant of 5.653 A^o) than InP. The between two layers can be calculated from the relation: ___ (Colema 200), where is the lattice constant of the substrate layer (GaAs) and is the lattice constant of the deposited layer (InP or InAsP in this cause). This can affect the dots size shape and hence, the wavelength emission.

3.2.2 Calibrations of P and As fractions in QDs

To evaluate the molar fraction of arsenic in the InAsP QD layers, a calibration sample comprising 20 periods of alternating InAsP (3.2nm) and InP (29.2nm) layers was grown on on-axis (100) InP substrates and analysed by a Bede QC2a X-ray diffractometer around the (004) plane. The reason for using such InP-InAsP crystalline superlattice (SL) rather than bulk InAsP layers in our calibrations was to "dilute" the average strain in the grown structures and consequently, to avoid complications in the X-ray diffraction analysis due to strain relaxation in the crystalline lattice.

Similarly, regarding the InAsP QD laser active region, the calibration sample was grown at 710°C and the same constant phosphine flow. Arsine was switched to the reactor during growth of the InAsP layers. A θ-2 θ diffraction scan of the calibration sample is presented in Figure 3:3, bottom curve. The "zero" order peak of the SL is

offset towards smaller diffraction angles by 216" which corresponds to a moderate compressive strain of 0.08%.

 Assuming there are no strain relaxation and abrupt reagents' switching, the calculated diffraction spectrum (bottom curve) resulted in a good agreement with the measured one at an arsenic fraction of ~25% in the group V crystalline sublattice. The corresponding decrease of the bandgap energy of InAsP is ~250 meV.
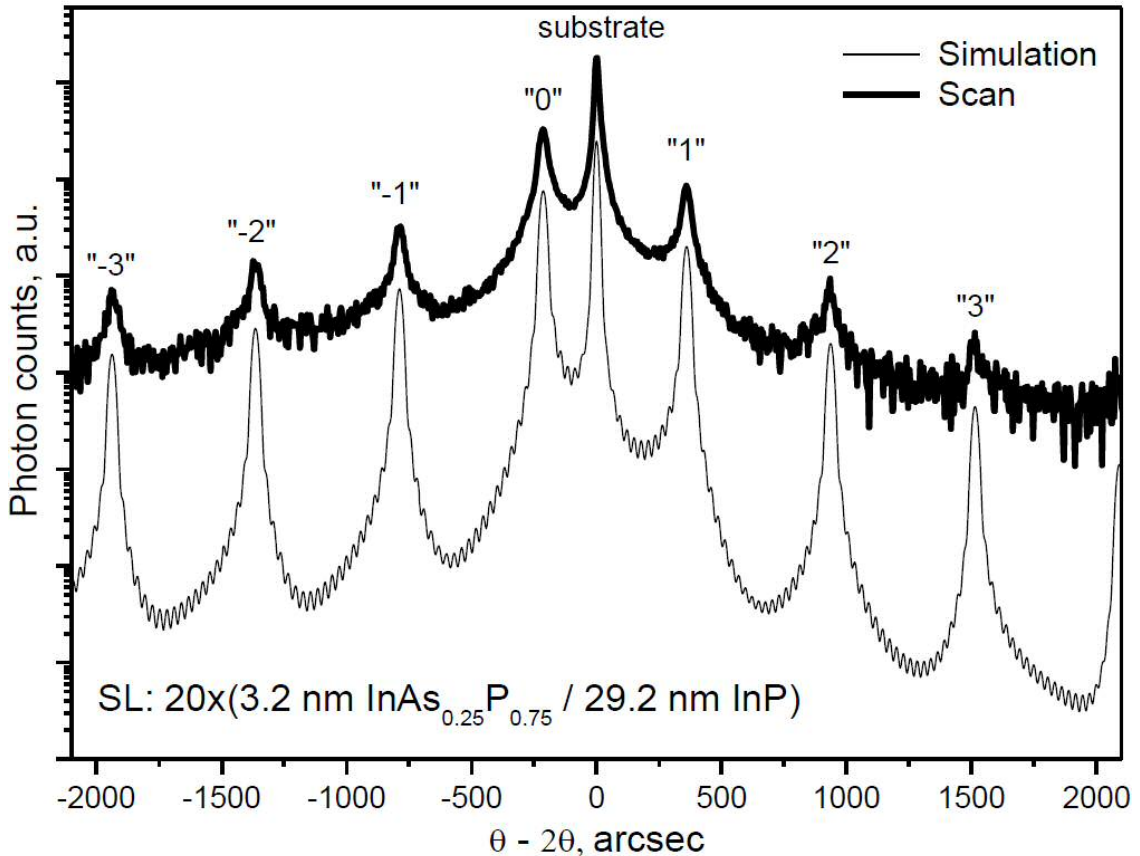
Figure 3:3 Theta-2theta scans of InP/InAsP SL: measured (top) and simulated (bottom) assuming an arsenic fraction of 25%.

3.2.3 Transmission Electron Microscopy (TEM)

Transmission electron microscopy (TEM) is a powerful and unique technique for structure characterization.The most important application of TEM is the atomic-resolution real-space imaging of nanoparticles (**Wang 2000**). Figure 3:4 shows the TEM images for the samples. The dots densities of the samples were calculated, and it is the same order of 10^9 -10^{10} cm^{-2}. The dot density was calculated by counting their number

in a length of cross section TEM specimen, converted into a real density using an estimate of the specimen thickness obtained by tilting 15 degrees about the [-110] axis and measuring the projected width of (001) interfacial or surface planes.
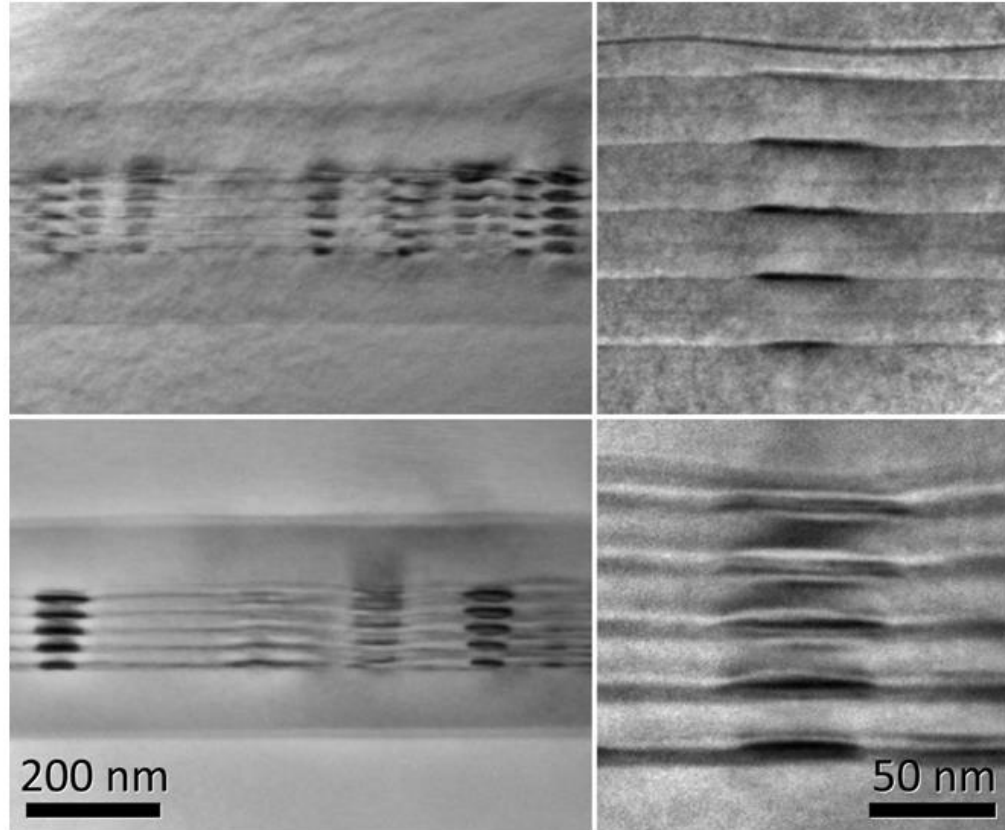
Figure 3:4 Transmission electron microscope images of 5 layers of InAsP dots (upper) and InP dots (lower). Left: bright field, g = 004 image showing several stacks of dots; right: dark field, g =002, displaying the changes in dot size and shape of an individual stack

The InP dots generally appear larger and the stacks more regular than the InAsP dots, with a height of 4-5nm and a lowermost dot diameter of 40-50nm, whereas the InAsP dots have a height of 2-3nm, a lowermost dot diameter of 20-30nm and greater variability in dot diameter through the stack. It is thought that the smaller dot size and greater size variation of the InAsP dots is due to the higher lattice mismatch.

3.2.4 Photoluminescence (PL) measurements

Photoluminescence (PL) measurements taken at room temperature using a Biorad PL mapper with a 532nm excitation laser are shown in Figure 3:5. While the width of the PL spectrum is dependent on the carrier density within the sample, that depends on both the collected pump power, which was nominally the same, and the non-radiative

recombination rates, these results do indicate both an increased broadening of the InAsP dot material spectrum and a shift to longer emission wavelengths as shown in Figure 3:5. Ribeiro et al. (2000) shown that the PL measurement for the of InAsP self-assemble QD shift toward low photon energy in comparison to InP QD material at 77 K.
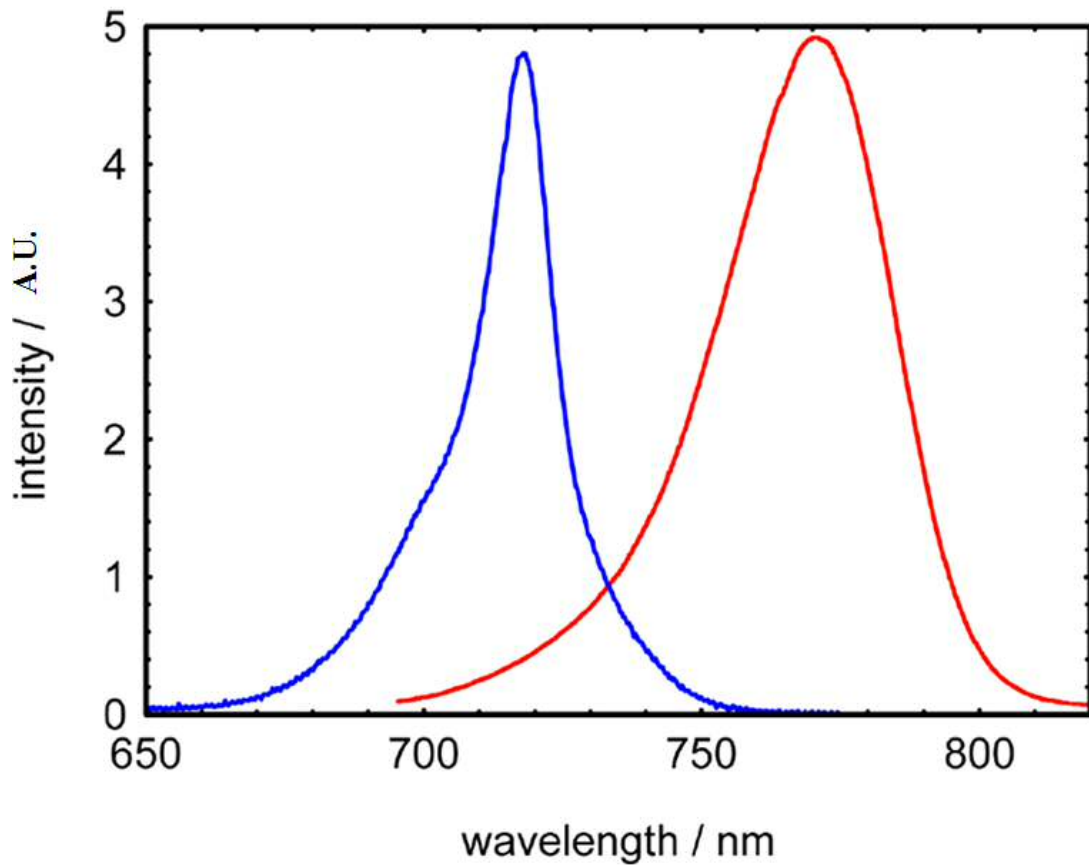
Figure 3:5 Photoluminescence measurements taken at room temperature with an excitation wavelength of 532nm. Data for the InP dot material in blue and the InAsP dot material in red (longer wavelength broader spectrum).

3.2.5 Fabrication and preparing the samples

Each of the samples used in this work were processed in the clean room at Cardiff University (School of Physics and Astronomy) by the technical staff (Dr. Sam Shutts and Dr Angela Sobiesierski). two different samples were prepared:

The first samples are oxide-stripe laser devices with 4 different cavity lengths 1, 2, 3 and 4mm, as shown in Figure 3:6-a. These devices were prepared in order to measure

the fundamental properties of the laser, such as threshold current density, quantum efficiency, lasing wavelength, device temperature dependency and others.

The second samples are multi-section devices which are used in the Segmented Contact Method (SCM) to measure the modal gain, modal loss, spontaneous emission of the samples. as well as carrier distribution in InP and InAsP QD materials The (SCM) will be detailed in this chapter later.

 Additionally, the multi-section samples were formed by dividing the top electrical contact of the 2mm length device into a 300 µm long section separated by etched gaps of 4 µm to create electrically isolated sections to allow each section to be driven separately in (SCM) measurements. Figure 3:6-c indicates the multi-section sample.

Once the samples were received, they were checked under a travelling microscope to measure the total lengths, the sections lengths, sample width and stripe width. Additionally, they were also examined to investigate the facets of the samples to ensure that the facets are clear and undamaged on both sides, particularly under the 50 µm stripe region of the facet. After the good samples were chosen, they were mounted under the microscope onto suitable copper blocks according to their lengths, using metal containing conductive epoxy that was heated to 175 ^{o}C for 45 seconds or more.

The coper blocks were already mounted on a T05 transistor header that has 3 pins or more to make the sample suitable for driving and testing. For the lasers samples, two chips of laser comprising the same material and the same cavity length were mounted on the copper block. Each one is connected to each pin of the header by a gold wire of 50 µm in diameter as shown in Figure 3:6b. For 300 µm multi-section devices Section 1 and Section 2 were connected to the two pins separately as shown in Figure 3:6d.

It is important that the measurements of any sample used are checked for different aspects. For example, the (I-V) characteristics should not indicate any electrical problems or leakage path, whereas the (I-L) characteristics should not display any sign of mode hopping at high driven currents. Moreover, the near field profile of the samples should show no evidence of filamentation and should be homogenous to ensure that the current is being pumped uniformly along the device. These properties and others will be precisely illustrated in the following sections.
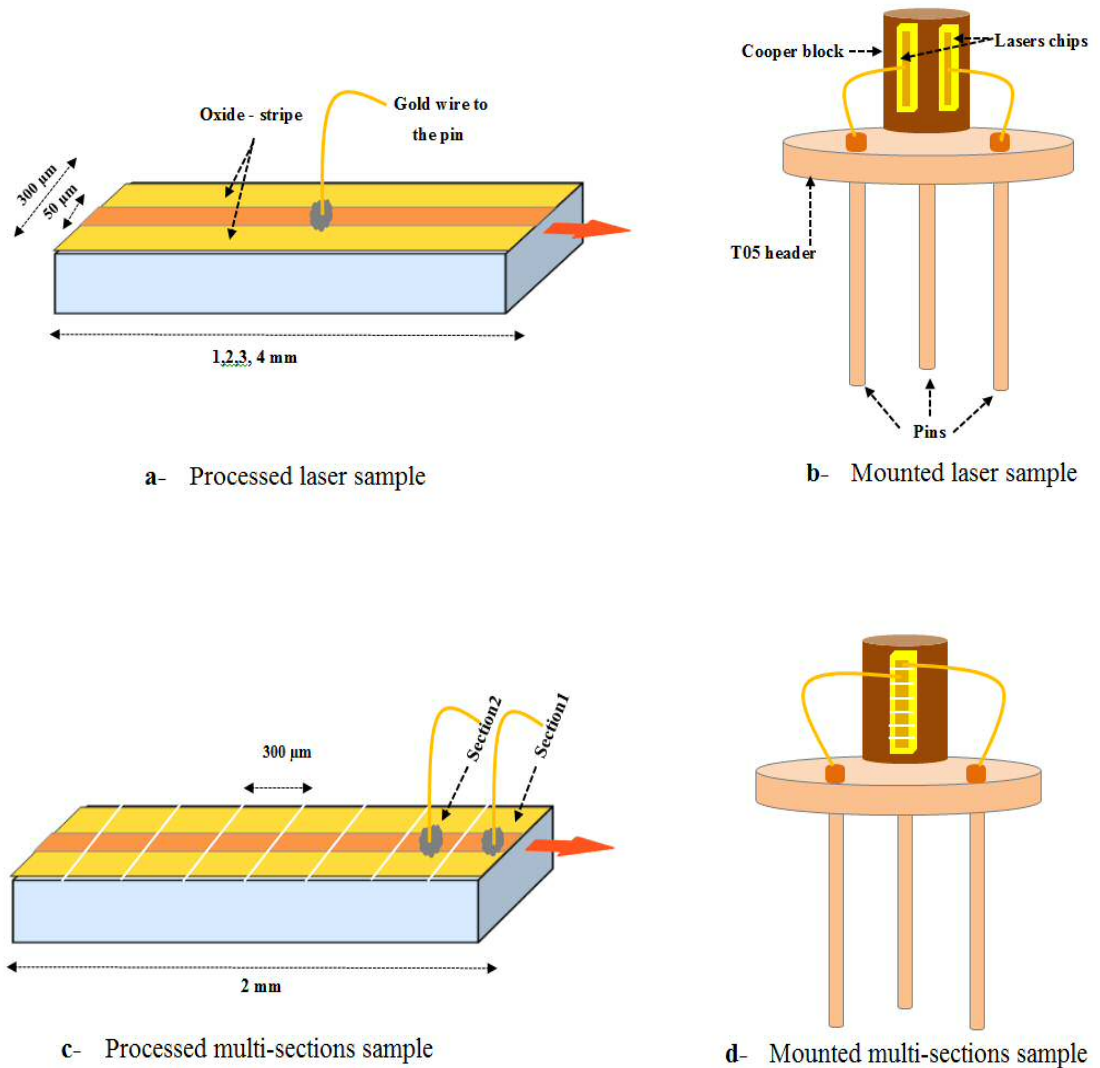
Figure 3:6 Diagram of processing and mounting of the samples.

3.3 Current-Voltage-Light (IVL) temperature measurements

Measuring (IVL) characteristics at room temperature and as a function of temperature is important in understanding the operation of semiconductor lasers. An existing computer controlled setup, as shown in Figure 3:7, was applied to measure (IVL) as a function of temperature.

The mounted laser devices were fixed inside the vacuum chamber, which has a neutral density filter window to allow a fraction of emitted light to be collected by the photodiode detector. The gates of the three channels of the boxcar integrator were aligned within a stable signal coming from the device via an oscilloscope.

Figure 3:7 Schematic diagram of IVL kit setup.

Pulse mode operation was used to run the lasers with a repetition rate of 1kHz and pulse width of 1μs, in order to avoid self-heating effects. The pulse generator produces voltage pulses, which are amplitude controlled with a computer contro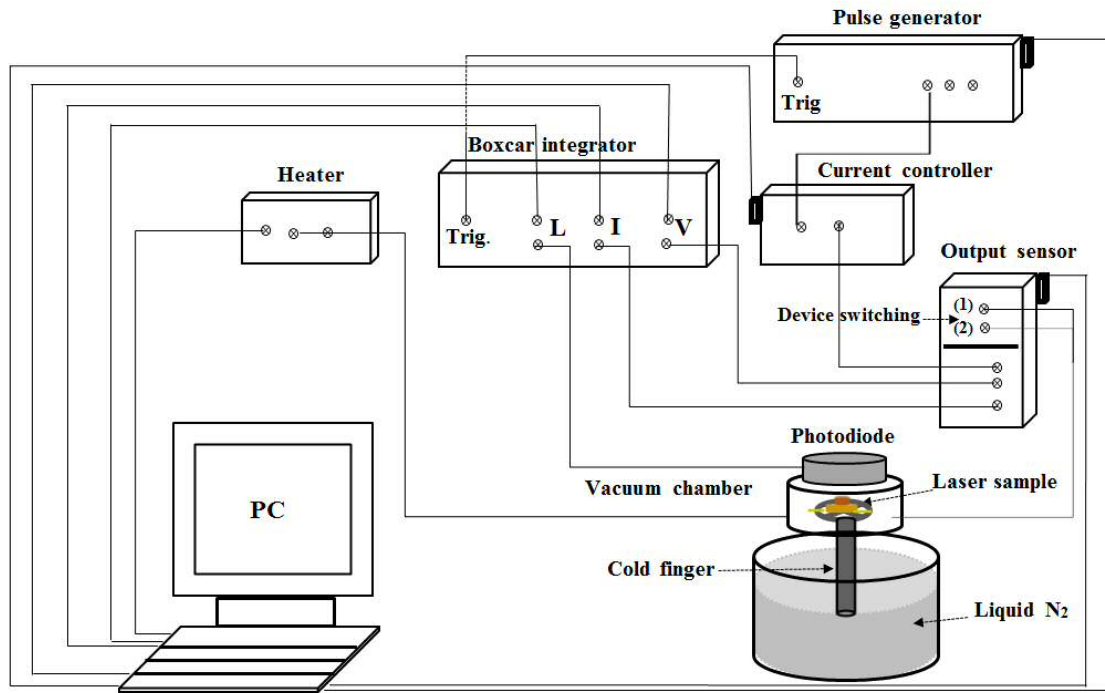lled potentiometer. The PC reads the IVL signals coming from the boxcar integrator and provides feedback to the potentiometer based on the current and the maximum light level detected. The software saves (I-V) and (I-L) files. When the kit is used to measure IVL at different temperatures, the device is cooled down to the lowest temperature required using liquid nitrogen, which cools the cold finger, attached to the laser sample. Temperatures above room temperature are achieved using a resistive heater embedded in the cold finger. In this work, the system was run under a software condition of (minimum temperature 150, maximum 400 and step 10 K). At the lowest temperature required, the nitrogen is removed, and the system allowed to warm up. The temperature of the sensor of the cold finger is monitored and computer controlled measurements are taken at the desired temperature. A maximum 0.03 of arbitrary light level is used, seeing as it is known that the photodiode detector is within the linear range.

An example of this measurement is shown in Figure 3:8, which is I-L characteristics as a function of temperature for the 1mm device InP quantum dot laser.
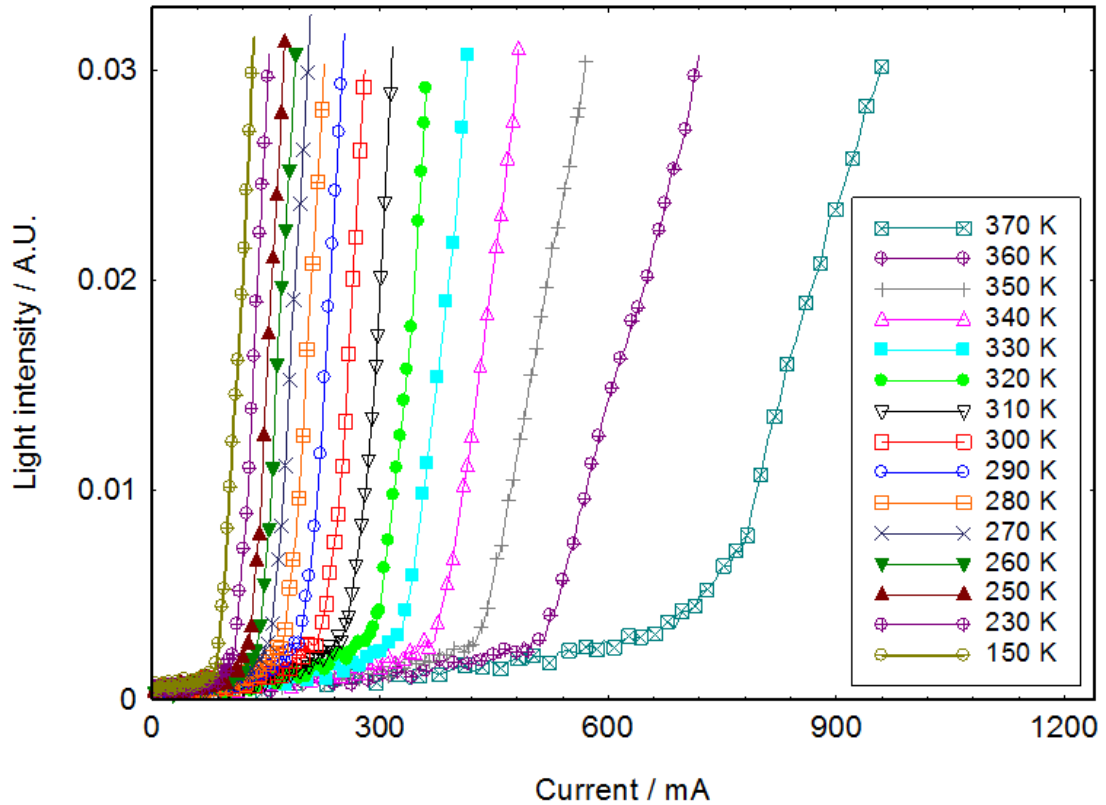
Figure 3:8 (I-L) characteristics as a function of temperature for 1mm InP QD laser.

From Figure 3:8 it can be clearly seen that the threshold current increases and the slope efficiency decreases when temperature increases, for more details about the effect of the temperature on the (I-L) characteristics of the semiconductor laser see (Vail et al. 1994). The (IVL) kit can also be used to measure the optical output power of the lasers in real units by replacing the photodiode detector via a calibrated integrated sphere. The integrated sphere measures the average optical power and it is possible to convert this to the peak optical power using the known duty cycle. An example is shown in Figure 3:9, which is the peak optical power in (mW) as a function of the injection current in (mA) for a 1mm long InP quantum dot laser at room temperature. At low levels of current the optical output power is small. This is where spontaneous emission is dominant. When the injection current is increased up to specific value called threshold current a tiny increase in the current causes a huge increase in optical power and the device emits as a laser where the stimulated emission is dominant. Threshold current is the point when optical gain in laser media compensates the optical loss. Threshold current can be determined by a (I-P) curve which is the intercept of the linear part of the curve with the x-axis as shown in Figure 3:9, which is in this case is approximately 245 mA. To compare material properties, this is converted to the threshold current density which is

the threshold current per unit area. The device area is deduced from the length of the device that is measured using a travelling microscope and the pumped strip width which is usually determined from near-field measurements.These are described in the subsequent section. The slope of the (I-P) curve above threshold is also important, seeing as it represents the differential efficiency of the laser see Equation 2:12 in Chapter two. This will be described in the next chapter in Section 4.4.
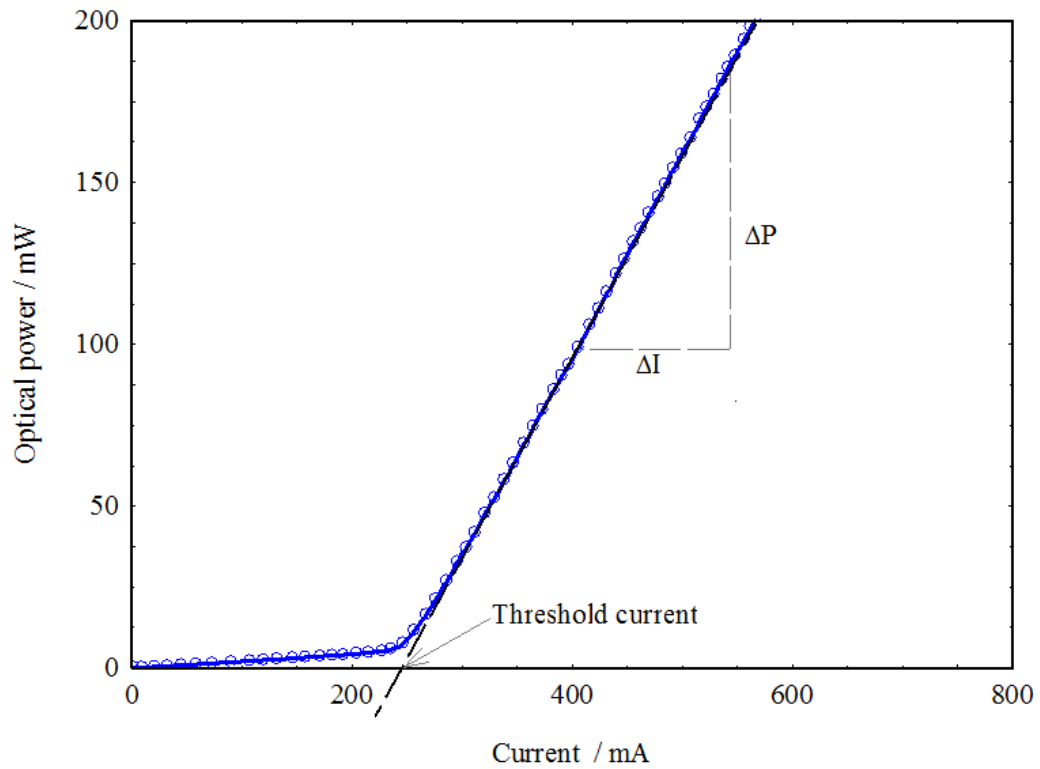
Figure 3:9 (I-P) characteristics using integrated sphere.

Regarding Figure 3:8, it can be clearly seen that the threshold current decreases and the differential quantum efficiency increases, when the temperature decreases. In general, the threshold current density in the semiconductor laser increases exponentially with temperature, according to the following formula:

$$ — $$

3:1

(Asryan and Suris, 1998)

where T_0 is the characteristic temperature of the device and   is a constant, this is studied preciseily in Section 4.2.2 in Chapter four.

Figure 3:10 displays the (I-V) characteristics at different temperature for a I mm long InP QD laser. It can be visibly seen that the slpoe of the curves decreases when the temperture increases, so the differential resistance (R) of the device increases with temperture, for more details about the effect of the temperature on the (I-V) characteristics of the diode see (Korucu 2010)
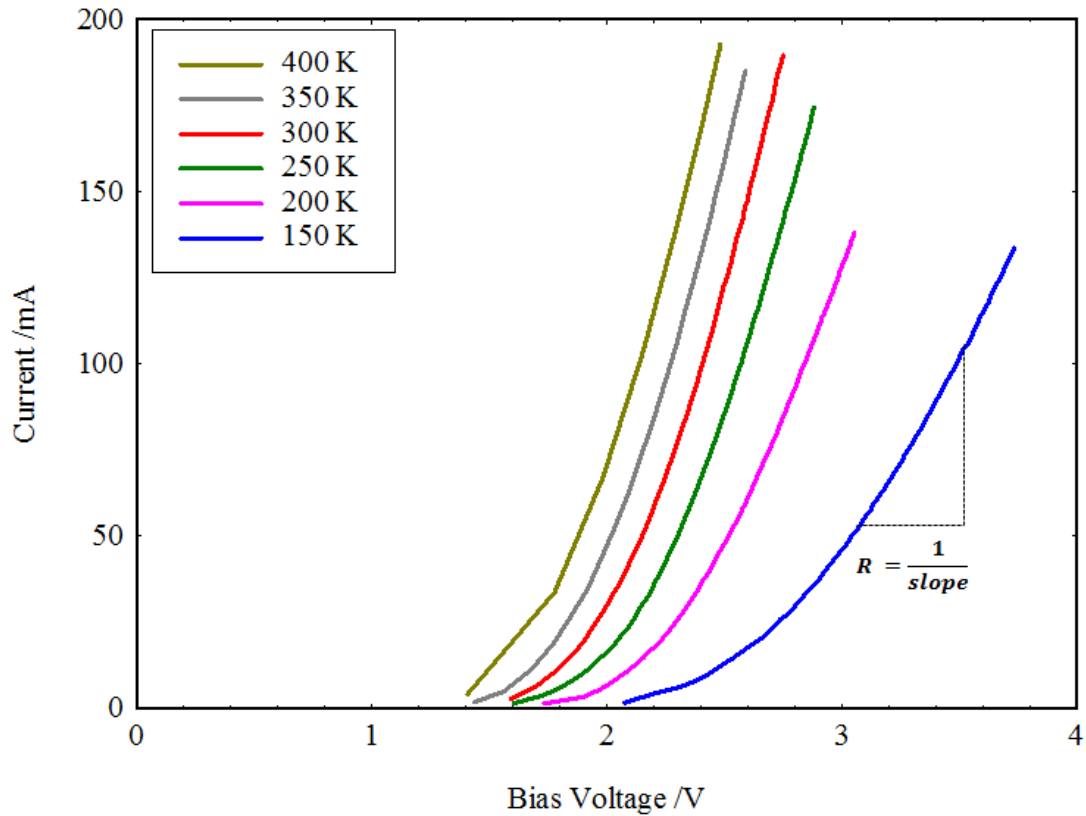
Figure 3:10 (I-V) characteristics of 1mm InP QD laser.

3.4 Near-field measurement

The near–field is the profile of the output light that emerges from the device facet. The experimental setup that is used to analysis the near- field profile of the devices is shown in Figure 3:11, the device which can be either the laser or the multi-section is mounted onto a micro-position stage and driven by a suitable pulse (using the same range of pulsed currents used in the (I-V-L) kit) from the pulse generator. A lens of magnification 20 was used to couple the emitted light coming from the device into the CCD camera and neutral density filters were placed between the lens and the camera to avoid saturation.
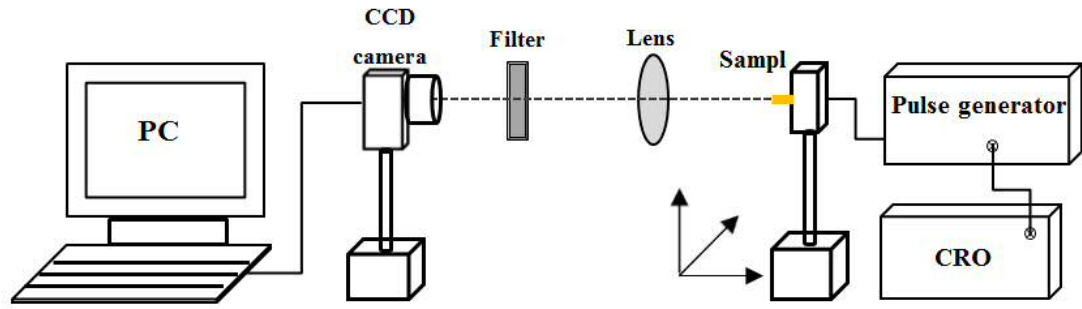
Figure 3:11 Near-field experimental setup.

The near-field distribution of light provides information on the carrier's distribution and hence, on the current spreading between the oxide stripe and the active region of the device. The full width at half maximum (FWHM) of the profile of near-field is typically used on a measure of the effect of the pumped width. Figure 3:12 illustrates the near-field profile of the 2mm InAsP quantum dot laser.
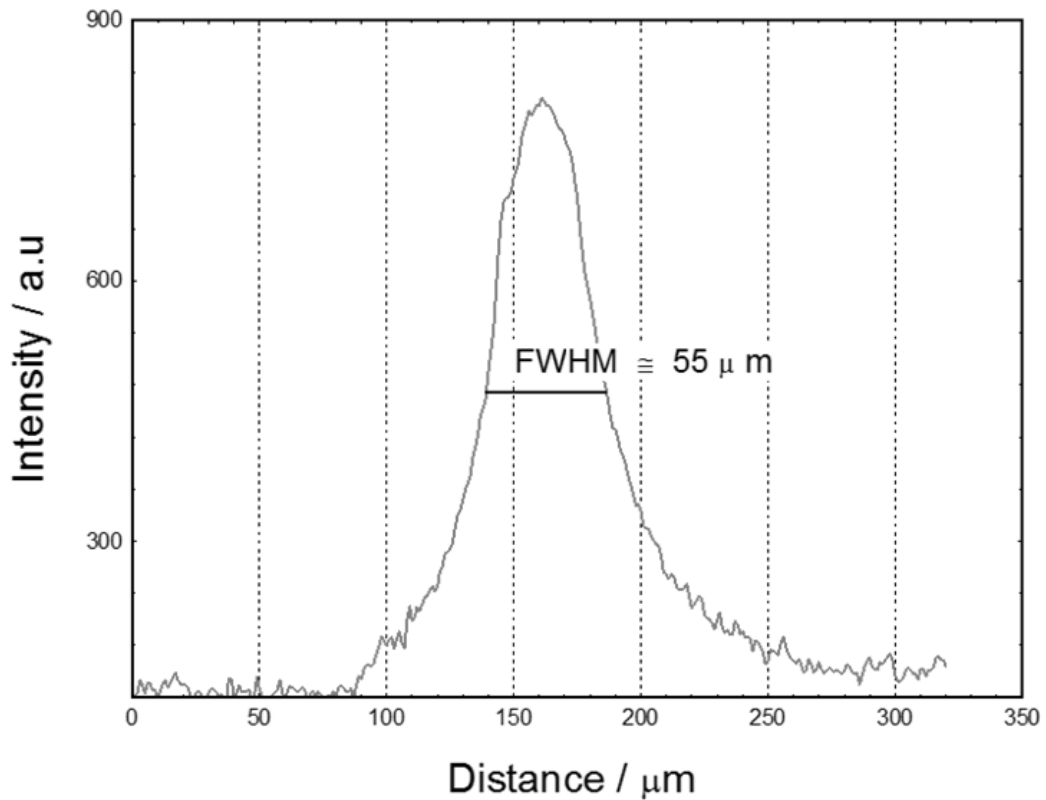
Figure 3:12 Near-field profile of the 2mm InAsP quantum dot laser.

In fact, the x-axis of the profile measured by the camera is originally in pixel numbers. This was converted to distance units using the measured width of the facet and by capturing an image of the facet at the same focused distance as the near-field was measured.

Figure 3:13a is the captured image of the output light, while Figure 3:13b is the facet image captured of the 2 mm InAsP quantum dot laser.

a   b
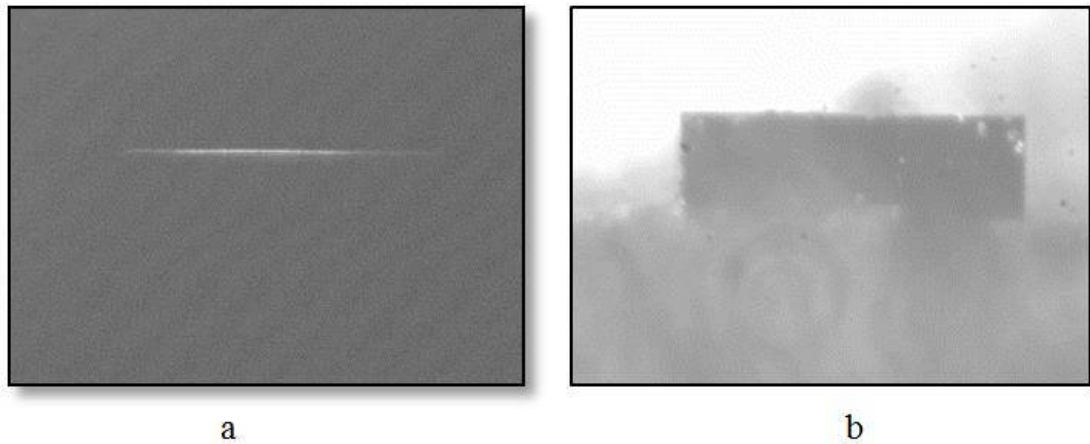
Figure 3:13 (a) image of the near-field light, (b) image of laser facet.

From Figure 3:12, the (FWHM) is 55 ±10 µm. The result can be used to convert the threshold current to threshold current density. The near-field test is also important to make sure that the current is pumped homogenously along the device. Additionally, for the multi-section device, it is crucial to have an identical near-field profile for both sections.

3.5 Spectrum measurements

To measure the emission wavelengths of the laser, a spectrum analyser was used with the experimental setup shown in Figure 3:14.
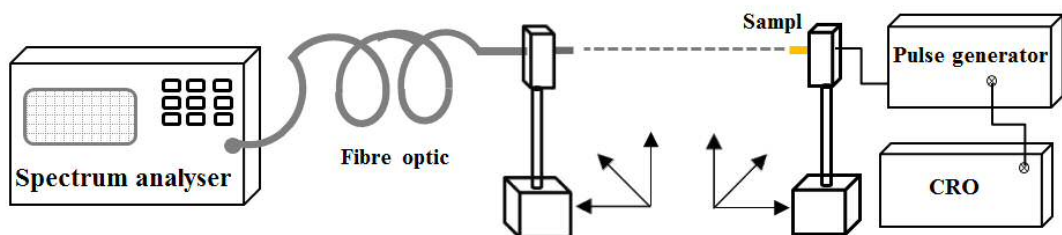
Figure 3:14 Experimental setup for spectrum measurements.

The laser samples were driven in a pulse mode at a current level of 1.1 of the valve of threshold current for each sample. The sample is aligned with the fibre optic before ligth is collected by the spectrum analyser. Figure 3:15 shows an example of the InP 2mm quantum dot laser spectrum at room temperature. The spectrum was measured with a resolution of 0.02nm, whilst the emission wavelength was approximately 720nm.
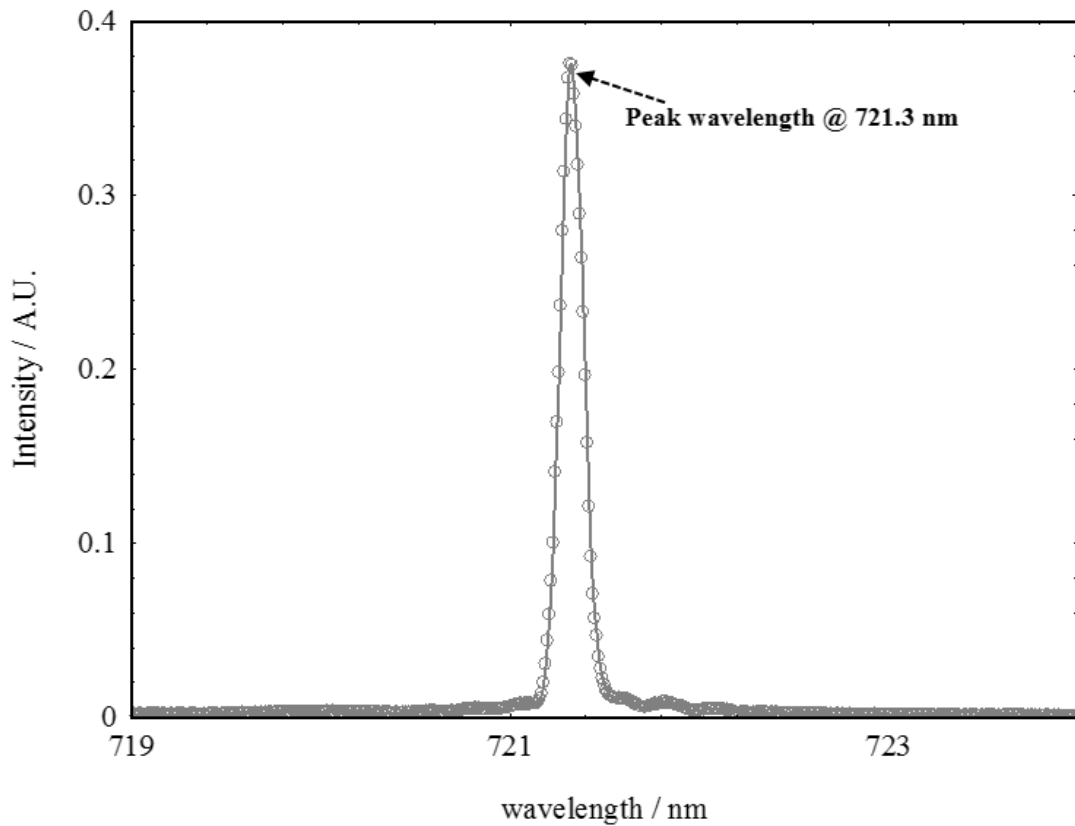
Figure 3:15 Spectrum emission of the 2mm InP quantum dot laser.

3.6 E-PVS (Edge-Photovoltage Spectroscopy) measurements

The E-PVS (Edge-Photovoltage Spectroscopy) measures the absorption of the incident light in arbitrary units, as a function of the wavelength. The experimental setup is shown in Figure 3:16. The light from a halogen lamp, which is operating at 24V passes the chopper and the grating monochromator (the resolution of light can be controlled by the widths of entrance and exit slits), then passes through a polarizer and is focused by the lens on the edge of the waveguide p-n hetero-junction of the laser sample (the laser sample is mounted onto a micro-position stage with three freedom degree of rotation in order to achieve maximum alignment).

 Subsequently the light is guided inside the structure and absorbed if the incident photon energy overtakes the transition energy of the structure. As a result, electron-hole pairs are created. These can be separated by the junction electric field, generating an external photovoltage, that is amplified by a phase–sensitive detector.

The monochromator was connected to the PC via a stepping motor to allow selection of the wavelengths. The polariser, lens and device are all placed inside a metal box which works as a Faraday cage to minimise electrical interference. When the polariser is placed in TE mode, the light polarised parallel to the growth plane, whereas TM mode light polarised perpendicular to the growth plane.
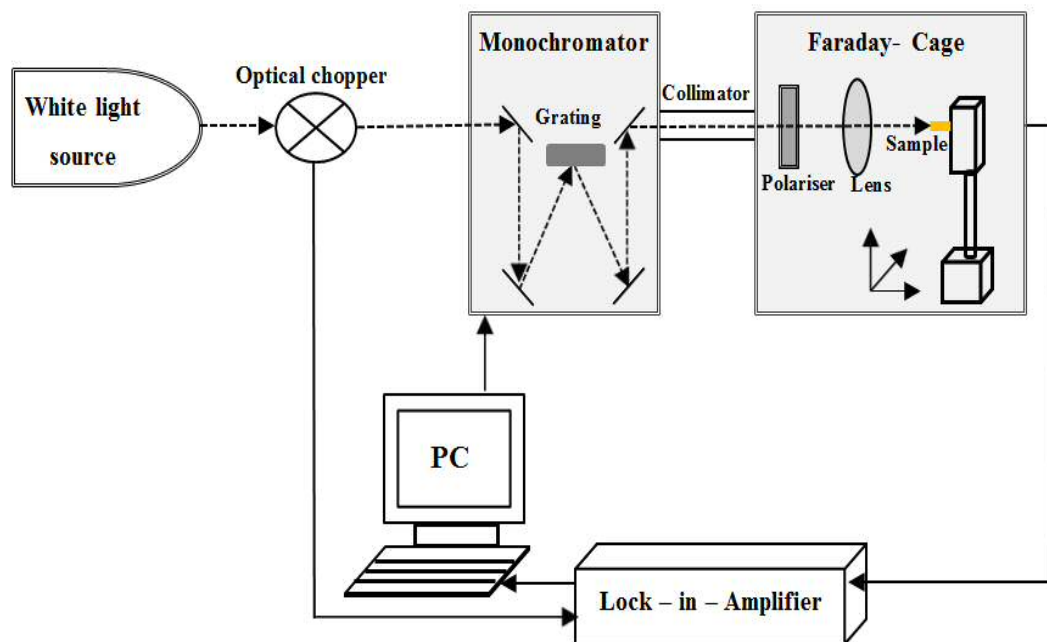
Figure 3:16 Experimental setup of E-PVS measurements.

3.7 Segmented contact method technique

The segmented contact method (SCM) was used in this work to characterise the modal gain, modal absorption, spontaneous emission and inversion factor spectra in real units of the InP and the InAsP QD material at room temperture and different temperture (150, 200,250,300, 350, 400 K) using the sample mentioned in Figure 3:6d. The technique and all the equations that will be introduced in this section dependent on (Blood et al. 2003).

3.7.1 Basis of the segmented contact method

Figure 3:17 is a schematic diagram of the segmented contact structure. Presume a total rate of spontaneous emission I_{sp} in the active region of a device for a particular polarisation of light per unit photon energy interval per unit area of the active region; consequently,
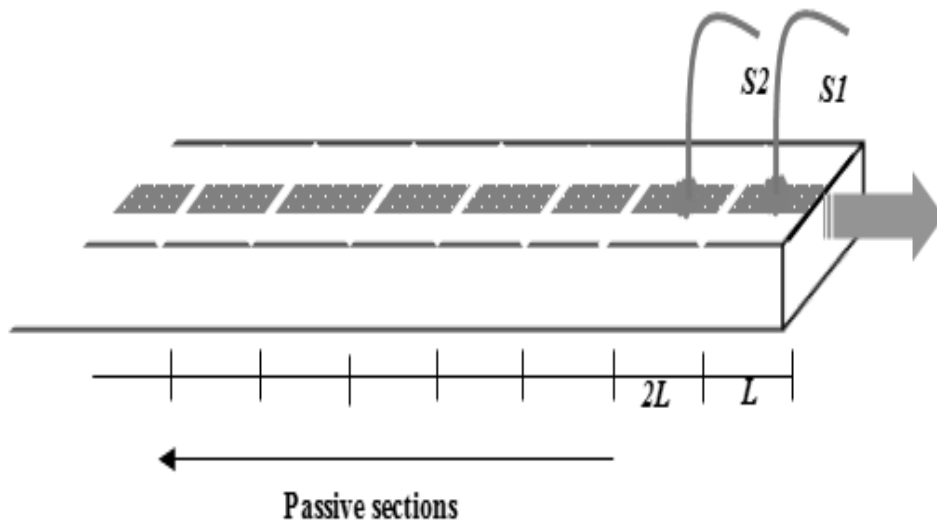
Figure 3:17 Segmented contact structure.

the emission rate in the waveguide at the end of the stripe (I_{sp}) over an element of thickness Δx at a distance x from the facet of the device is:

$$3:3$$

(Blood et al., 2003)

where   is the fraction of spontaneous emission coupled into the waveguide,   is the modal gain and   is the optical internal loss. Providing   is constant along the stripe, the total intensity of the (ASE) of the specific polarisation emitted from length L of pumped material per unit stripe width is given as:

$$3:4$$

The top electrical contact of the sample in Figure 3:17 is divided into separate electrical injection areas (termed sections). The facets angle of 10° was chosen to avoid the round-trip amplification. The stripe contact width is 50 µm and the section length is (L = 300 µm). Section 1 and Section 2 in the front of the device were driven with a specific amount of current density separately to measure the amplified spontaneous emission spectrum (ASE) for Section 1, Section 2 (I_{ASE1}, I_{ASE1}) and with the same overall specific current density simultaneously to measure I_{ASE12}. Equation 3:4 can be used to derive the following:

$$\overline{} \qquad\qquad 3{:}5$$

$$\overline{} \qquad\qquad 3{:}6$$

$$\overline{} \qquad\qquad 3{:}7$$

where A is the modal absorption of the non-pumped cavity. The experimental set up for measuring the ASEs of the segmented contact device is described in Figure 3:18. The multi-section device is placed on a micro-positioning stage capable of alignment over 6 degrees of freedom. When Section 1 or Section 2 is driven by a specific current density AES (Amplifierd Spontanouse Emissiom) light emerges from the facet of the device and is focused on a 5X magnification and subsequently filtered by a polariser prior to entering the slit on the monochromator. Inside the monochromator box, the grating of 1200 lines splits the ASE light into a wavelength spectrum.

 The diffracted light is detected by a temperature controlled ICCD camera which can keep temperature stability and low noise to signal ratio. The pulse of 1µs width with repetition frequency of 1 kHz is supplied by the main pulse generator to drive the sections

(the pulse pumping to the section is used to reduced the heatself effect inside the chip which can effect the result the duty cycle of 0.1 % is used which is recommended) (Shutts et al. 2013). The switch box is used to drive either Section 1 separately and Section 2 separately, or Section 1 and Section 2 simultaneously. The second pulse generator controls the ICDD camera and matches its signal with the signal from the main pulse generator, then the aligned signal pulses are recorded by a computer program as ASE spectra.

The temperature can be modified by using the temperature controller and cycle of liquid nitrogen that flows into the cryostat to liquid nitrogen transfer tube. on the other hand the cryostat should be keep under the low vacuum condition using vacuum pump.
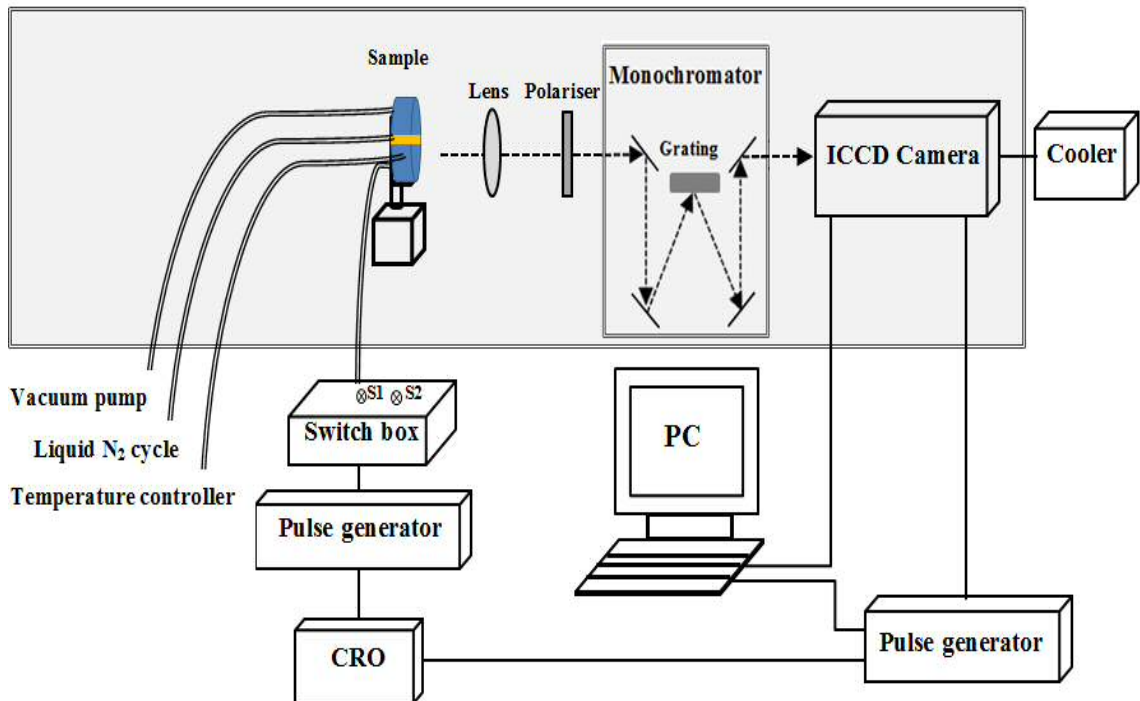
Figure 3:18 Experimental setup of SCM.

Figure 3:19 shows the ASE spectra in arbitrary unit for Section 1, Section 2 and Section 12 for the InAsP quantum dot multi-section sample under TE polarisation at pumped current density of 1500 A.cm^{-2} at room temperature using the expermintal set up shown in Figure 3:18.
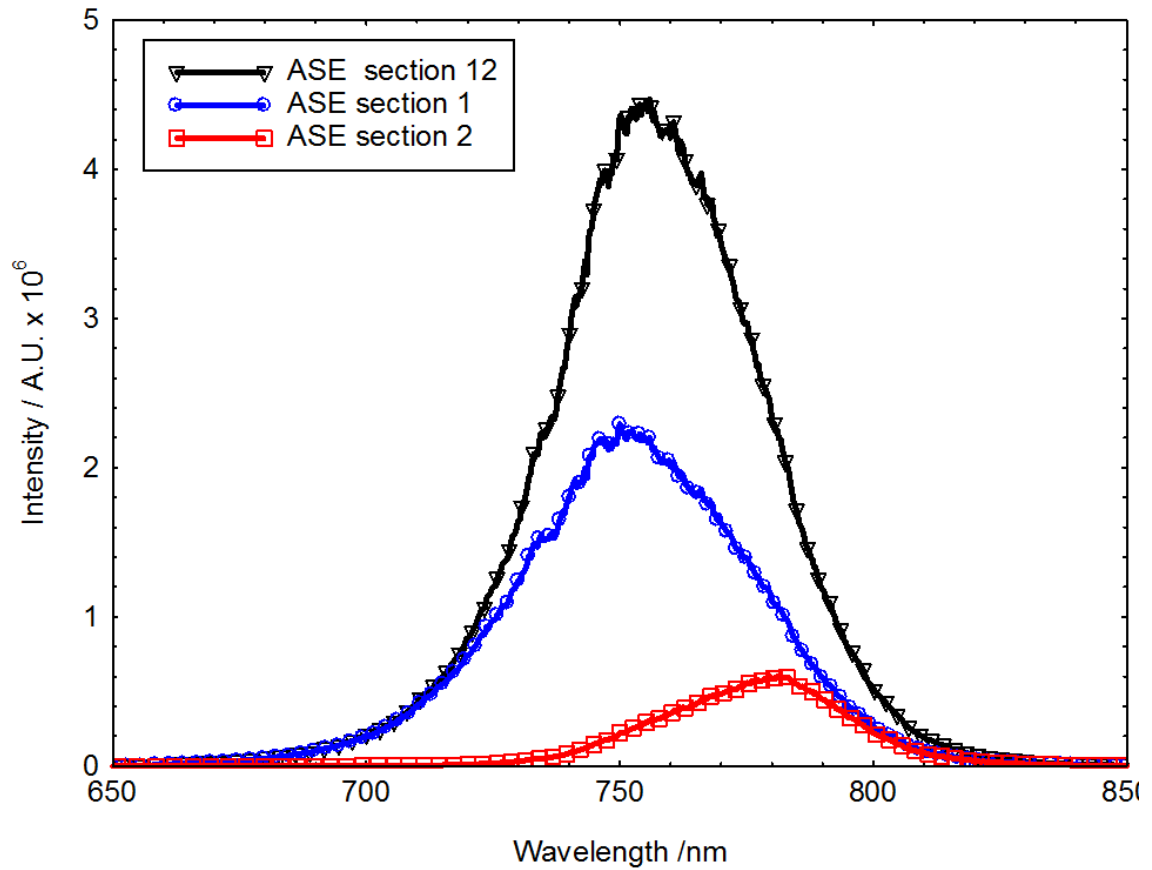
**Figure 3:19 Amplified spontaneous emission of InAsP quantumdot sample
for Section 1, Section 2 and Section 12 at room temperture.**

The (I-V) curves for both Section 1 and Section 2 must exhibit high agreement to ensure that both sections are being driven with the same amount of current during the measurement. At a fixed voltage level, the difference must not be more than 4% to make surre that both sections are deiven by the same amout of currunt when they are driven separeatly.

Figure 3:20 is an example of the (I-V) curves (Section 1(S1) and Section 2(S2)) for the multi-section device of InAsP quantum dot for the front sections. It is also important that the near-field of Section 1 and Section 2 are as identical as possible, as this is assumed in the equations used to derive net modal gain (-) and positive modal absorption and   .
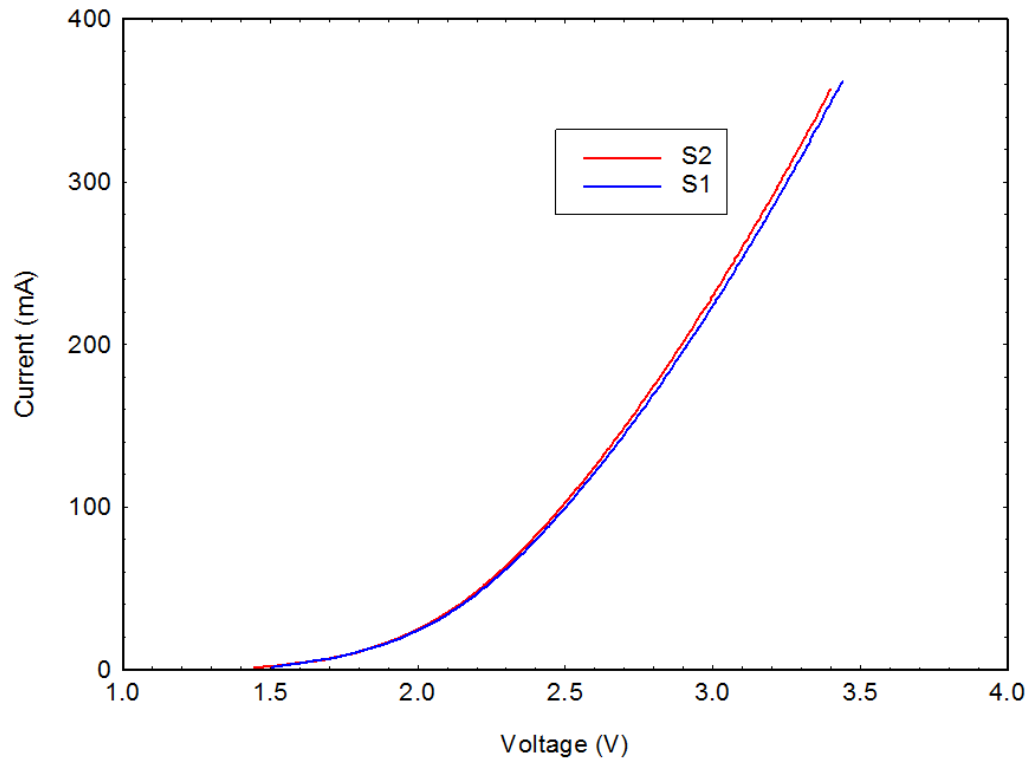
Figure 3:20 (I-V) Characteristics of Section 1 and Section 2 of the segmented contact sample.

3.7.2 Modal absorption and modal gain

It is possible to get an expression for net modal absorption   -   by dividing Equation 3:6 by Equation 3:5, as can be seen below:

$$ - \quad \overline{\quad\quad} \qquad\qquad\qquad 3:8 $$

Moreover, in a similar way, the modal gain expression can be obtained by dividing Equation 3:7 by Equation 3:5 as:

$$ - \quad \overline{\quad\quad} \qquad\qquad\qquad 3:9 $$

Therefore, it is possible to obtain modal absorption and modal gain spectra from Figure 3:19 using Equations 3:8 and 3:9. Figure 3:21 shows the modal absorption for the InAsP quantum dot laser material as a function of the wavelength.
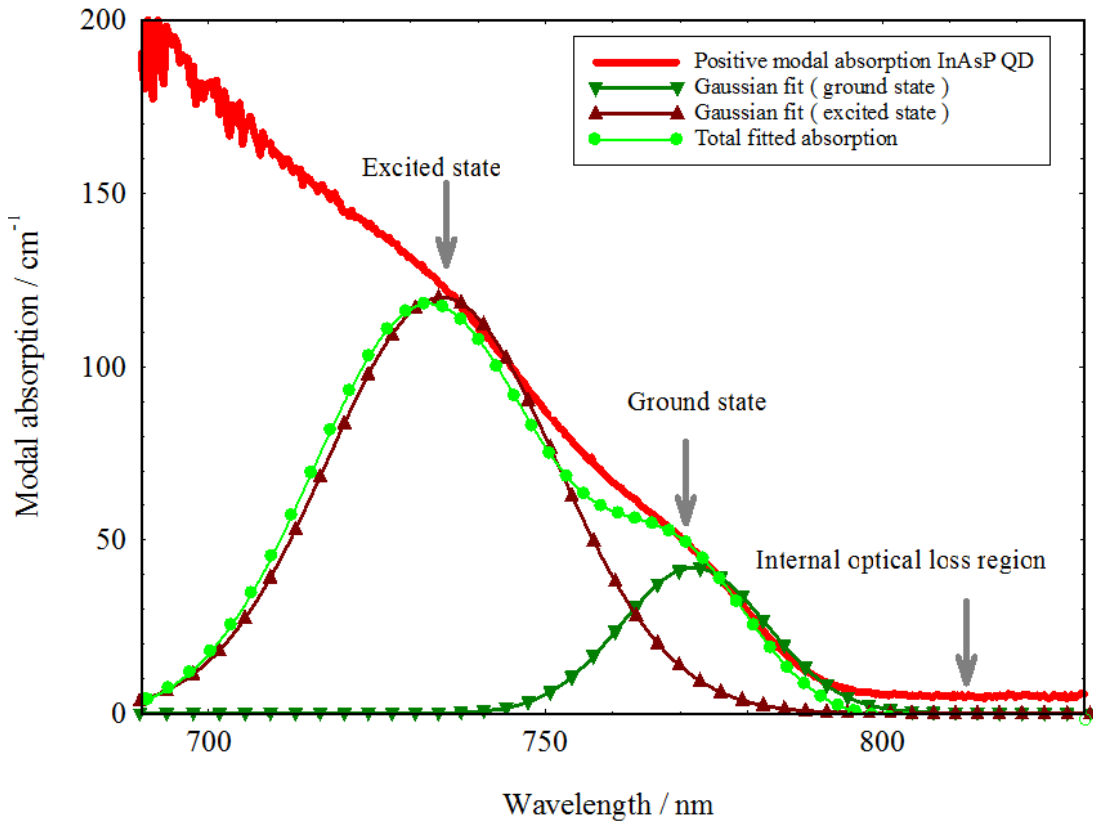
**Figure 3:21 Positive modal absorption spectrum for the InAsP quantum dot laser
indicates the ground state, excited state and internal optical losses region.**

In Figure 3:21, two features can be observed which are thought to be due to the inhomogeneous broadened of the dots distrubution which indicate the ground state and excited state of the quantum dot transitions. From the same figure, it is also possible to extract the internal optical loss   (which was introduced in Section 2.3.4 in Chapter two) from the long wavelength region where the absorption of states   is negligible. Hence, at these photon energies there is no amplification by way of the cavity, so the loss only comes from scattering or othe absorption mechanisms as mentioned in Section 2.3.4. The modal absorption is a passive measurement; therefore, the spectrum is dependent on the pumped current.

To avoid the effect of excess carriers in the passive section due to self-pumping, the passive section is grounded to 0 V when the other section is being pumped. The ground and excited state are fitted to a Gaussian distribution in Figure 3:21 according to the parameters shown in table 3:2.

State	Amplitued (cm^{-1})	Peak Position (nm)	Standard diveation (nm)
Ground	42	772	10
Excited	120	735	17

Table 3:2 Fitting parameters used for Gaussian distribution in Figure 3:21.

Finger 3:22 is the net modal gain spectrum of the InAsP quantum dot at a current density level of 380 A.cm^{-2}. From the gain spectrum, it is possible to extract the   from the long wavelength region. This should agree with the absorption spectrum. In contrast to the absorption spectrum, the gain spectrum is sensitive to pumped current density (carrier concentration). When the current density is increased, the peak gain coefficient and the gain bandwidth increase.

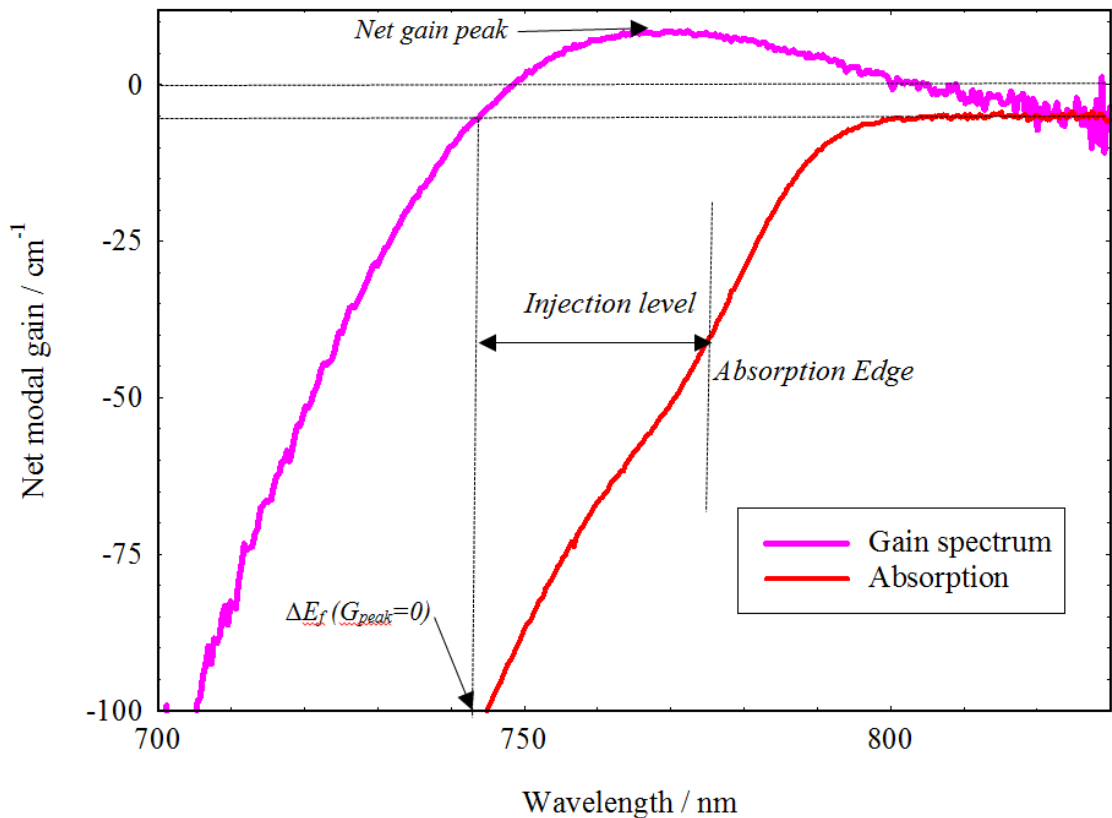

Figure 3:22 Net modal gain spectrum for the InAsP quantum dot laser at a current density of 380 A.cm^{-2} together with modal absorption spectrum indicates; net modal gain, absorption edge, quasi-Fermi level separation and injection level.

The peak energy of the gain position is the lasing photon energy of the output light of the laser. The modal gain spectrum also allows the quasi-Fermi level separation (ΔE_f) to be determined where this is assumed to equal to the transparency energy, if the device is in thermal equilibrium.

The transparency point is the point when the medium moves from absorbing to gain, which means (G_{peak}=0 or -   -). This can be extracted from the gain curves at the value of -   level at a short wavelength.

In Figure 3:22 the injection level is also labelled which is the value of the quasi-Fermi level separation minus absorption edge. Also the absorption edge is indecated in Figure 3:22 which is the half energy region from the end of the   region to the end of the ground state peak, as difiend in (Shutts et al. 2013).

3.7.3 Spontaneous emission

The SCM can be used also to measure non-amplified spontaneous emission spectra (   ) by using Equations 3:5 and 3:7 as simultaneous equations and solving to obtain   as:

$$\rule{3cm}{0.4pt} \; - \; \rule{1.5cm}{0.4pt} \qquad\qquad 3{:}10$$

An example of non-amplified spontaneous emission spectrum formed from the ASE spectra of Figure 3:19 is illustrated in Figure 3:23 for the InAsP QD material at room temperture at different level of injected current density (230, 250 and 270 A.cm^{-2}).

Figure 3.23 shows the spotanouse emission spectra increse when injected current density increases (carrier concentration) and the area under the curves also increases with current density.
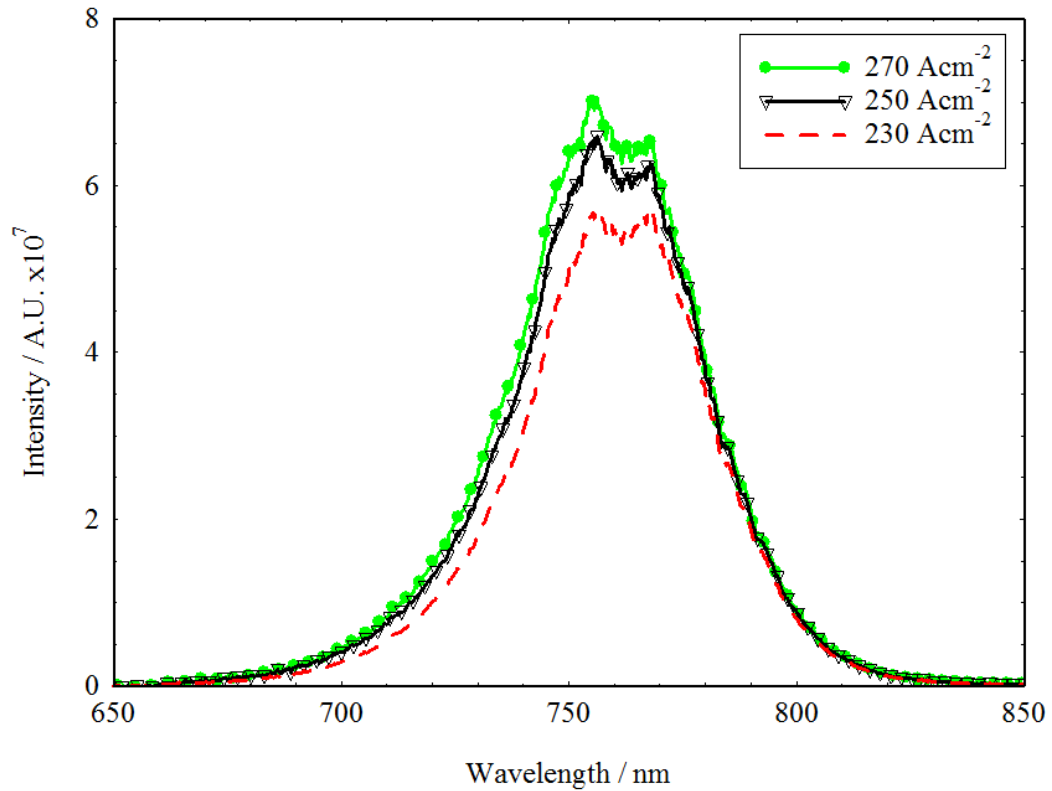
**Figure 3:23 Spontaneous emission spectr of the InAsP quantum dot laser
at different current density levels.**

3.7.4 Population inversion factor

The population inversion factor   mentioned in Chapter two (see Section 2.7) can be calculated from the following expression:

$$\qquad \rule{2cm}{0.4pt} \ \ \text{--} \ \ \rule{2cm}{0.4pt} \qquad\qquad\qquad 3:11$$

where n is the effective refractive index of the semiconductor structure,   is the quantum well width and   is the optical confinement factor. Figure 3:24 represents the experimental data for the population inversion spectrum of the InAsP QD materials at room temperature at 380 A.cm^{-2} of the driven current density.
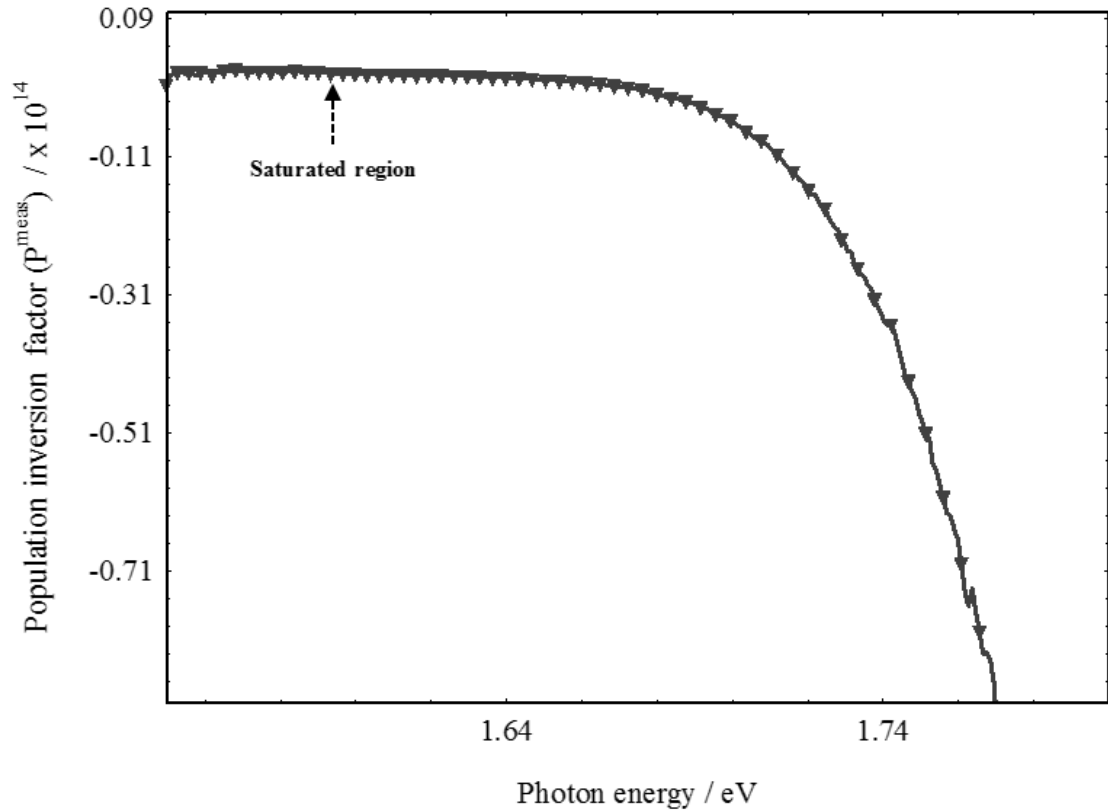
Figure 3:24 Population inversion spectrum of the InAsP QD materials at room temperature at 380 A.cm^{-2} of the driven current density.

From Figure 3:24 the region where *P=1* can be recognized by the region where takes its maximum value and saturates with increaing current density and this usully takes place at low photon energy. The calibration factor *C* can be used to calibrate the spontaneous emission and also to investegate the carrier distribution using the technique shown in section 2.7 in Chapter two. the spontaneous emission spactra in real unit is related to uncalibrated spontaneous emission by the relation:

$$ \underline{} \qquad \qquad 3:12 $$

3.8 Summary

This chapter introduced the device structures that have been used in this study and the experimental techniques used in this work. The chapter started with growing wafers and explaining the materials used, along with the samples that were fabricated and prepared. Several significant measurements for the wafers, such as Transmission Electron Microscopy (TEM), Photoluminescence measurements (PL) and the Calibration of P and As fraction in quantum dot structre were displayed in this chapter. The chapter also presented the experimental techniques and equipment used to collect data in this work, in addition to some important raw data. These include Current-Voltage-Light (IVL) temperature, near-field, spectrum and Edge-Photo Voltage Spectroscopy (E-PVS) measurements. Additionally, the Segmented Contact Method (SCM) technique is illustrated in detail in this chapter with several key equations used to process the data.

3.9   References

Asryan, L., and Suris, R. **1998**. Temperature Dependence of the Threshold Current Density of a Quantum Dot Laser. IEEE Journal of quantum electronics 34(5), pp.841–850.

Blood, P., Lewis, G., Smowton, P., Summers, H., Thomson, J., and Lutti, J. **2003**. Characterization of Semiconductor Laser Gain Media by the Segmented Contact Method. IEEE journal of selected topics in quantum electronics , 9(5), pp.1275–1282.

Coleman, J. J. **2000**. Strined-layer InGaAs quantum-well heterostructure laser.IEEE Journal on selected topics in quantum electronics **6**(6), pp.1008-1012.

Korucu, D. **2010**. Temperature and series resistance effect on the forward bias current-voltage (I-V) characteristics of In/p-InPSchottky barrier diode (SBD). Journal of optoelectronics and advanced materials 12(11), pp. 2194 - 219.

Ribeiro, E., Maltez, R. L., Carvalho, W., Ugarte, D. and Medeiros-Ribeiro, G. **2002**. Optical and structural properties of InAsP ternary self-assembled quantum dots embedded in GaAs. Applied Physics Letters 81(16), pp.2953-2955.

Shutts, S., Smowton, P. M.and Krysa. A. B. **2013**. InP quantum dot lasers with temperature insensitive operating wavelength. Appl. Phys. Lett. 103, pp. 061106

Vail, E. C., Nabiev, R. F. and Chang-Hasnain, C. J. **1994**. Temperature dependence of light-current characteristics of 0.98-pm Al-free strained-quantum- well lasers. IEEE Photonics technology letters 6(I I), pp. 1303-1305.

Wang, Z. L. **2000**. Transmission Electron Microscopy of shape-controlled nanocrystals and their assemblies. J. Phys. Chem. B 104, pp.1153-1175.

Chapter (4) Characterisation of InP and InAsP QD lasers

4.1 Introduction

This chapter introduces the room temperature results of the laser samples of the InAsP and InP structures and the multi-section devices using several experimental techniques illustrated in Chapter three. The chapter starts with determining the threshold current densities of the devices and investigates the temperature dependency of the threshold current density of the samples. The emission wavelengths of the samples were determined in addition to the output optical power and the differential optical efficiency in this chapter. Subsequently, the chapter reveals the optical modal absorption and optical modal gain of the InP and InAsP materials besides the gain-current relations of the materials under TE polarisation condition. Finally, the chapter displays the available transitions in InP and InAsP quantum dot materials using the E-PVS technique under TE and TM polarisation conditions.

4.2 Threshold current density (I-L) characteristics of the laser samples

4.2.1 Room temperature (I-L) characteristics of InP and InAsP

As mentioned previously the (I-L) characteristics of the laser samples are incredibly important because they can help to determine the threshold current and hence, the threshold current density of the devices, considering the near-field of the devices and their cavity lengths. Moreover, it is also possible to calculate the external differential efficiency from these characteristics besides the temperature dependency of the threshold current density of the lasers. Here, there is a comparison between the two different quantum dot lasers (InP as a standard laser and InAsP as a desired laser) grown in the same conditions, as mentioned in Chapter three. Figure 4:1 shows the (I-L) characteristics at room temperature of the 1, 2, 3 and 4mm cavity lengths of both the InP and InAsP QD lasers for the average results of the tested devices.

Figure 4:1 illustrates the light intensity in arbitrary units as a function of the injection current using the (I-V-L) kit described in Chapter three. It can be clearly seen that the InAsP samples have a higher threshold current compared to the same length of InP samples. For example, the threshold current for the 1mm InP laser at room temperature is roughly 220 mA, whereas for the InAsP laser of the same length it is 330 mA. Similarly, for the 4mm InP laser the threshold current is approximately 370 mA, whilst for the 4mm InAsP laser it is roughly 410 mA. Therefore, in general, adding As to the InP quantum dot system increases the threshold current of the laser, as shown in Figure 4:1.

Figure 4:1 indicates the laser intensity as a function of the current. However, what is more important is to convert the current into the current density to determine the threshold current density of each sample ($J_{th}=I_{th}/A$), which is the important factor related to the semiconductor lasers.

The full width at half maximum (FWHM) of the near-field profile of each sample was considered as a width of the laser devices. The near-field of the tested devices was measured using the experimental setup shown in Figure 3:11 in Chapter three. The (FWHM) of the measured devices varied between (55 to 65µm).
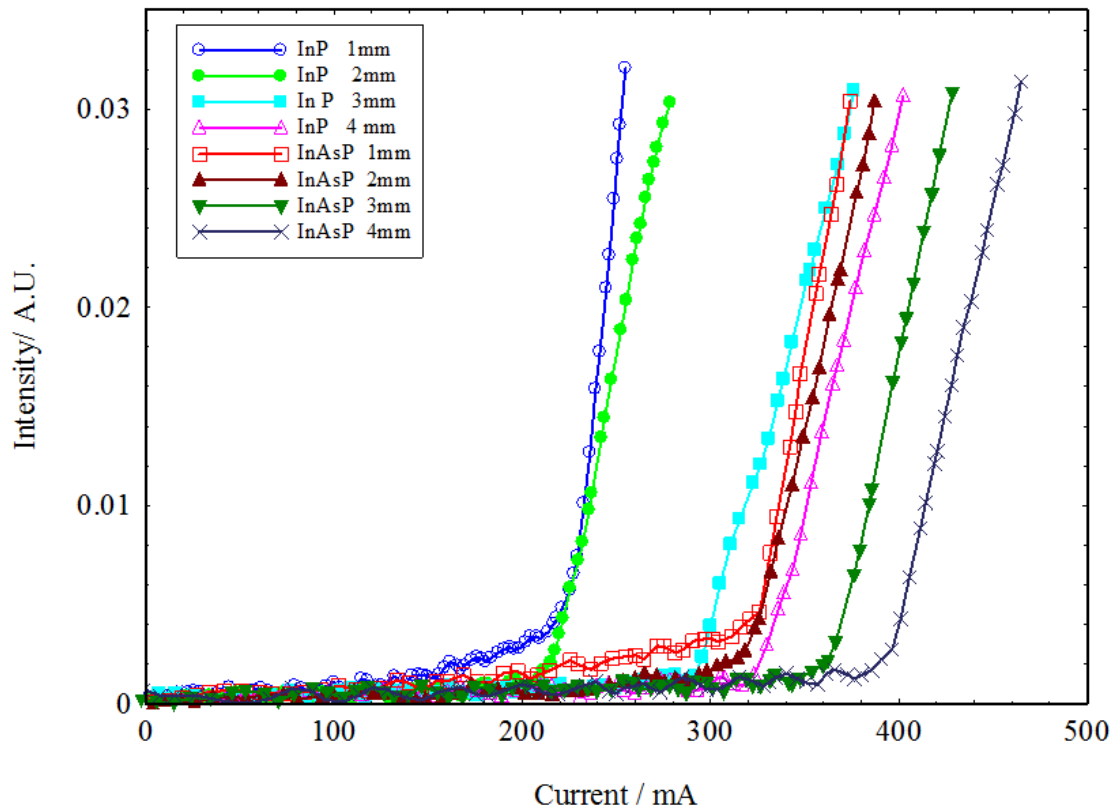
Figure 4:1 (I-L) characteristics of the 1, 2, 3 and 4mm lasers for both the InP and InAsP QD laser devices.

Figure 4:2 reveals the laser intensity of the devices as a function of the injection current density at room temperature of the 1, 2, 3 and 4mm cavity lengths of both the InP and InAsP QD lasers. From Figure 4:2, it is possible to estimate the threshold current densities of the devices as shown in Figure 2:7 in Chapter two. In general, the InAsP lasers display larger threshold current densities in comparison with InP materials, especially for short cavity length devices. For example, the 4mm cavity length laser of InP materials has a threshold current density of 110 A.cm^{-2}, whereas the same length of InAsP materials has a threshold current density of 145 A.cm^{-2}. This difference increases when the cavity lengths decrease. Table 4:1 shows the approximated threshold current densities of the devices estimated from Figure 4:2 at room temperature. Smowton et al. (2000), studied the effect of growth temperature on a InP QD laser with a similar structure to the InP QD laser in this work. For the growth temperature at 730 ^{0}C, they established that the 2mm cavity length device has a threshold current density

of 165 A.cm^{-2}, which is consistent with the result shown in Table 4:1 for the same length cavity of lasers.
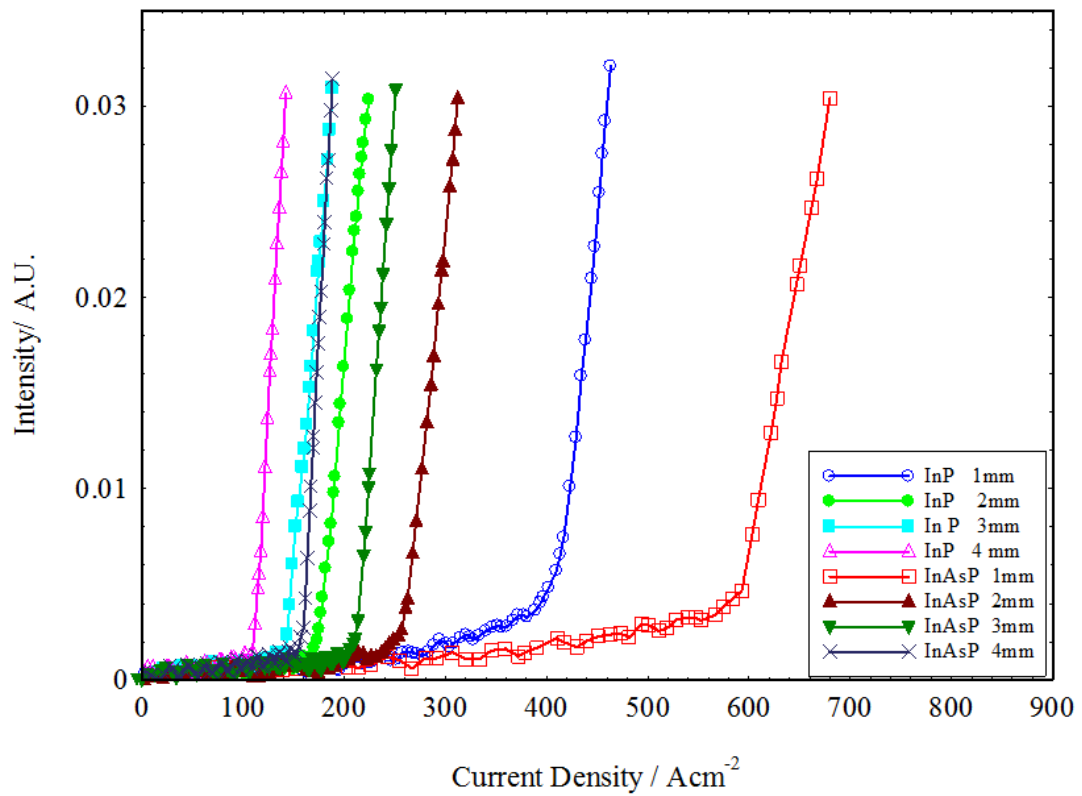
Figure 4:2 (J-L) characteristics of the 1, 2, 3 and 4mm lasers for both the InP and InAsP QD laser devices.

Makarimi et al. (2005), studied thermal carrier spreading in InP Quantum Dot Lasers, although with a growth condition that was slightly different to the InP QD laser in this work. They ascertained that for the 2mm cavity length device the threshold current density is approximately180 A.cm^{-2} at 300 K.

Devices lengths(mm)	Threshold current density (A.cm^{-2})	
	InP	InAsP
1	410	620
2	175	260
3	135	210
4	110	145

Table 4:1 Threshold current density of the 1, 2, 3 and 4 mm lasers for both InP and InAsP QD devices.

The higher threshold current densities for the InAsP QD material could be due to either increasing the non-radiative recombination, increasing the optical loss or broadening the optical gain. This will be discussed later in this chapter.

4.2.2 Temperature dependence of the threshold current density of the devices

The less temperature sensitivity of the QD lasers in comparison to the quantum well, Quantum wire and bulk materials makes them a good candidate for many applications, including biophotonics and mode-locking. The (I-L) characteristics of the devices were measured at different temperature ranges (150-400 K). Figure 3:8 in Chapter three specifies the (I-L) curves at different temperatures for the 1mm InP laser.

The threshold current increases non-linearly when the temperature increases, whilst the slope efficiency also decreases with temperature. Figure 4:3 reveals the temperature dependency of the threshold current density for 1, 2, 3 and 4mm cavity lengths of both the InP and InAsP lasers at range of temperature (150 -380 K).

In general, at temperature levels between 150-290 K there is a slight increase in the threshold current density with temperature. Meanwhile above this temperature, there is a rapid increase in the J_{th} with temperature. Figure 4:3 also confirms that the threshold current density is larger for the InAsP material along the entire range of temperatures. In addition, longer length devices are less temperature dependent for both materials.

The J_{th} of 1mm InAsP demonstrates that it is slightly more temperature dependent compared to the InP material, whereas for the rest of the cavity lengths, the InAsP material shows less temperature dependence in relation to the threshold current density.

The most important detail that Figure 4:3 reveals, is that operation up to at least 380 K is easily achieved for both materials. The rapid increase of the threshold current density of the QD lasers above 300 K is due to the increase of the non-radiative current density, which requires the device to be driven hard to maintain the threshold gain requirements (Smowton et al. 2008).
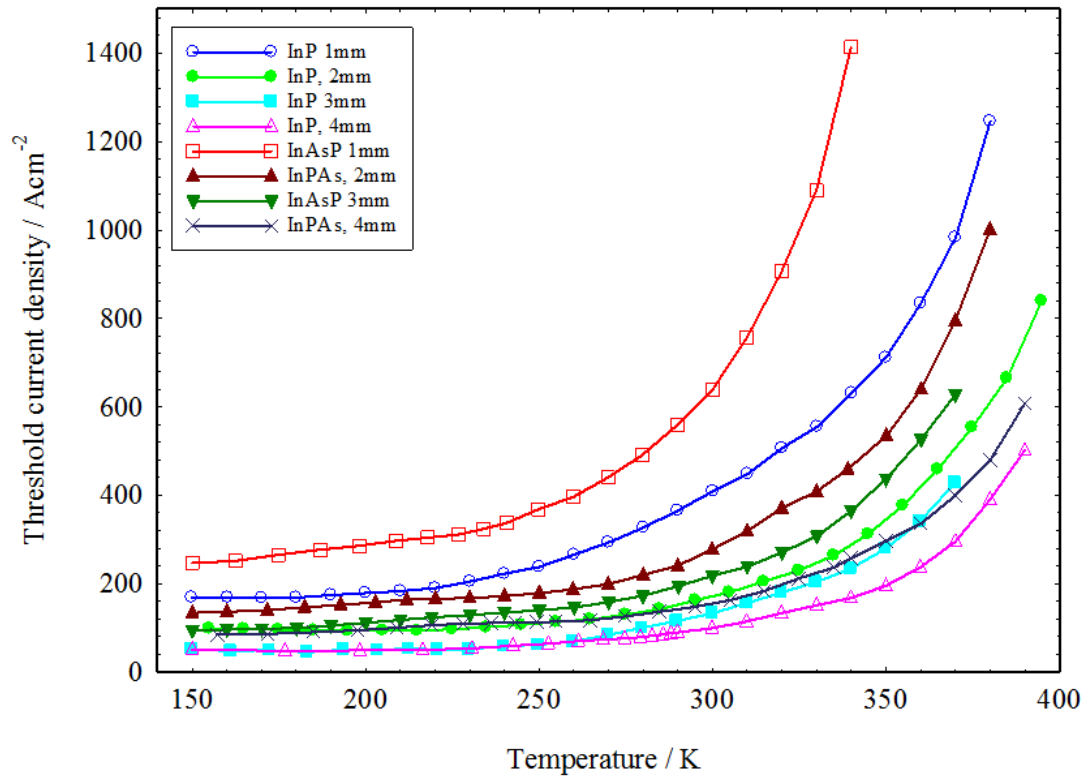
**Figure 4:3 Temperature dependency of the threshold current density of the
1, 2, 3 and 4mm lasers for both InP and InAsP QD devices.**

To determine the characteristic temperature (T_0) mentioned in Chapter three, the plot of $\ln(J_{th})$ versus temperature in the ranges of (290-350 K) and (350-380 K) for 2mm length devices is depicted in Figure 4:4 to measure the characteristic temperature (T_0) of the devices, using Equation 3:1 in Chapter three. A significant expected advantage of semiconductor quantum dot lasers over the conventional quantum well lasers is the extremely weak temperature sensitivity of the threshold current density.

Ideally QD laser should remain unchanged with the temperature and the characteristic temperature T_0 should be infinitely high. This would be so if the overall injection current go entirely into the radiative recombination in QDs and if there was charge neutrality in QDs. In fact, because of the presence of free carriers in the optical confinement layer (OCL), a fraction of the injection current is wasted there. This fraction goes into the recombination processes in the OCL (in the barrier regions. Hence, recombination in the OCL gives rise to one more component of J. The latter component, associated with the thermal excitation (leakage) of carriers from QDs to

continuous-spectrum states in the OCL, depends exponentially on T. leads to a T-dependence of the J component associated with the radiative recombination in QDs. As a result, J should become temperature dependent, especially at high T (Asryan and Suris 1997) The high value regarding characteristic temperature indicates that it is more thermally stable when operating the device.

Figure 4:4 illustrates that T_0 is approximately 80 K for both InP and InAsP QD laser in the ranges of (290-350 K), whereas in the ranges of (350-380 K) T_0 decreases from 53 to 47 K for 2mm InP and InAsP devices respectively. However, T_0 is not the most suitable way to define temperature dependency, as it is depends on the magnitude of J_{th}. The rapid increase in J_{th} with T at a high temperature in QD lasers is thought to be because of the thermally activated loss of carriers from the dots. InAsP dots with, a greater confining potential of the dots would be expected to be a have thermally activated loss and demonstrate a slower rate of increase of J_{th} at the same Fermi-level separation.
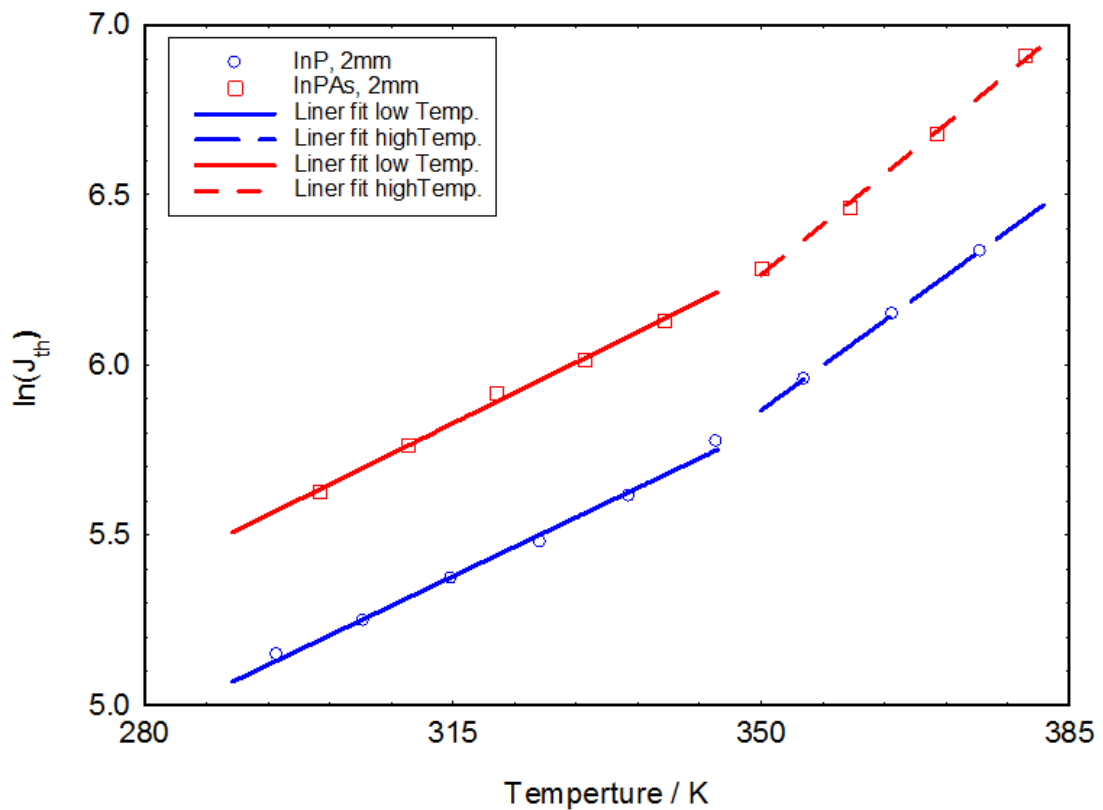

Figure 4:4 Characteristic Temperature of 2mm long of InP and InAsP QD lasers.

4.3 Wavelengths of the devices

The emission spectra of the laser samples were measured using the spectrum analyser setup described in Chapter three Figure 3:14. The measurement was conducted at 1.1 times the threshold current for each laser and at the same value of the resolution (0.5 nm) at room temperature. Figure 4:5 shows the emission spectrum of the InP and InAsP QD laser devices at room temperature. The peak lasing wavelength varies between 760-774nm for the InAsP QD lasers as compared with 716-725nm for the InP QD lasers. This difference of approximately 50nm (110 meV) is expected due to the arsenic incorporation but the magnitude may be less than expected from the predicted change in bulk band gap.

 It is important to mention that the long wavelength shift of 50 nm (110 meV) of the InAsP QDs is considerably smaller than expected from the arsenic fraction derived from the Theta-2theta diffraction scans and the corresponding bandgap reduction of InAsP. This discrepancy can be explained by a smaller average InAsP QD size seen in TEM images in comparison to InP QDs, as suggested by Vinokurov et al (1998).

  However, it demonstrates the longer wavelength laser can be produced while maintaining reasonable threshold currents. Figure 4:6 depicts the emission wavelength as a function of the cavity length of the 1,2,3 and 4mm laser devices for both InP and InAsP QD samples. In general, when the device becomes longer, the peak wavelength shifts toward longer wavelengths and the InAsP dot material shows a larger range of emission wavelengths with cavity lengths between 1-4 mm. This could be a sign of greater gain saturation in the dots, which will be discussed in Section 4.6.2.

 Moritz et al. (1996) studied the optical gain and lasing in self-assembled InP QD laser using the same well and barrier material that used in this work. They found that the peak emission spectrum takes place at 705 nm for 0.5mm cleaved sample. On the other hand, InP quantum dot lasers have been studied in order to extend the wavelength coverage of semiconductor disk lasers into the applications-rich spectral gap between 690 and 780nm. Multiple layers of InP QDs embedded within InGaP QWs were incorporated into an AlGaInP gain region grown on top of an AlGaAs distributed Bragg reflector. Laser emission from $716 - 739$ nm with wavelength tuning up to 26nm was demonstrated using different samples from a spatially graded gain structure.
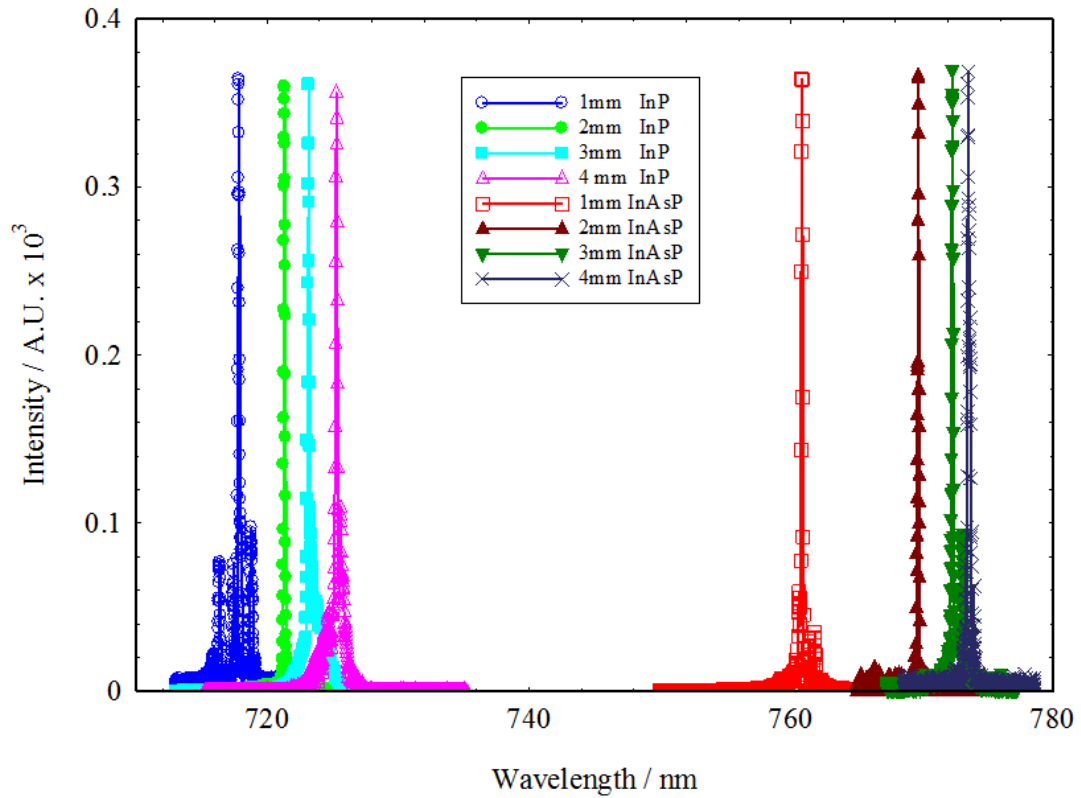
Figure 4:5 Emission spectra of the 1, 2, 3 and 4mm lasers for both the InP and InAsP QD devices.

The shifting toward a longer wavelength for InAsP gives a signal for deeper dot confinement of the InAsP structure. This will be studied in this chapter more thoroughly using the E-PVS technique in Section 4.7. It has been alleged recently that the deeper dots with high energy barriers can support mode-locking in a monolithic semiconductor laser by reducing the pulse duration (Finch et al. 2013). Figure 4:5, also confirms that the ground state dominates the emission wavelength in the cavity lengths between 1 and 4mm. This gives the potential to control the ratio of the gain to absorption section for the mode-locked device on this cavity length range.

Moreover, the longer wavelength for InAsP QD laser devices make them good candidates in biophotonic application, where longer wavelengths towards 780nm transmit deeper into blood (Roggan et al. 1999), tissue and microvasculature (Bashkatov et. al 2005).

Table 4:2 shows the peak emission wavelengths at 1, 2, 3 and 4mm cavity length lasers for both the InP and InAsP QD lasers at room temperature.
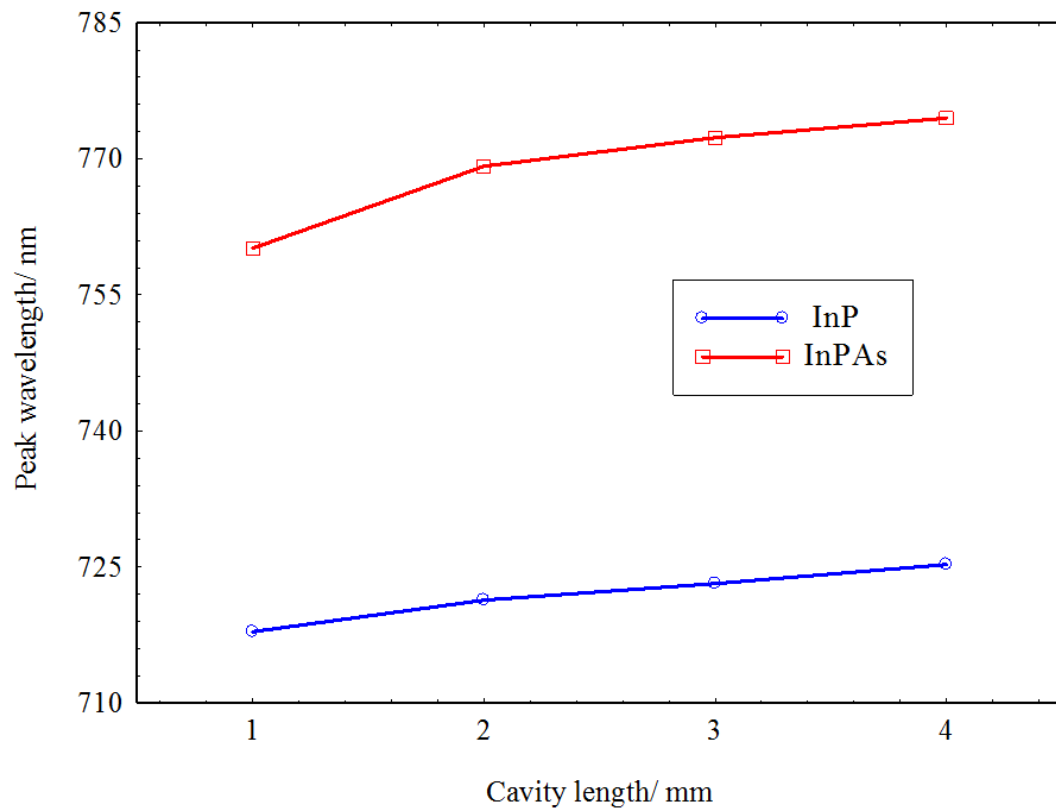
Figure 4:6 Lasing wavelengths as a function of the cavity length of lasers for the both InP and InAsP QD devices.

Devices lengths (mm)	Peak wavelength (nm)	
	InP	InAsP
1	716	760
2	720	769
3	723	772
4	725	774

Table 4:2 Emission wavelengths for 1, 2, 3 and 4mm lasers for both InP and InAsP QD materials.

4.4 Optical Power and the efficiency of the devices

To measure optical output power in (mW), the calibrated integrated sphere was used. Figure 4:7 illustrates the power-current (P-I) characteristics at room temperature of 1 and 4mm long devices for both samples. The output peak pulse powers beyond 300 mW were achieved without any sign of rollover for both the InP and InAsP lasers.
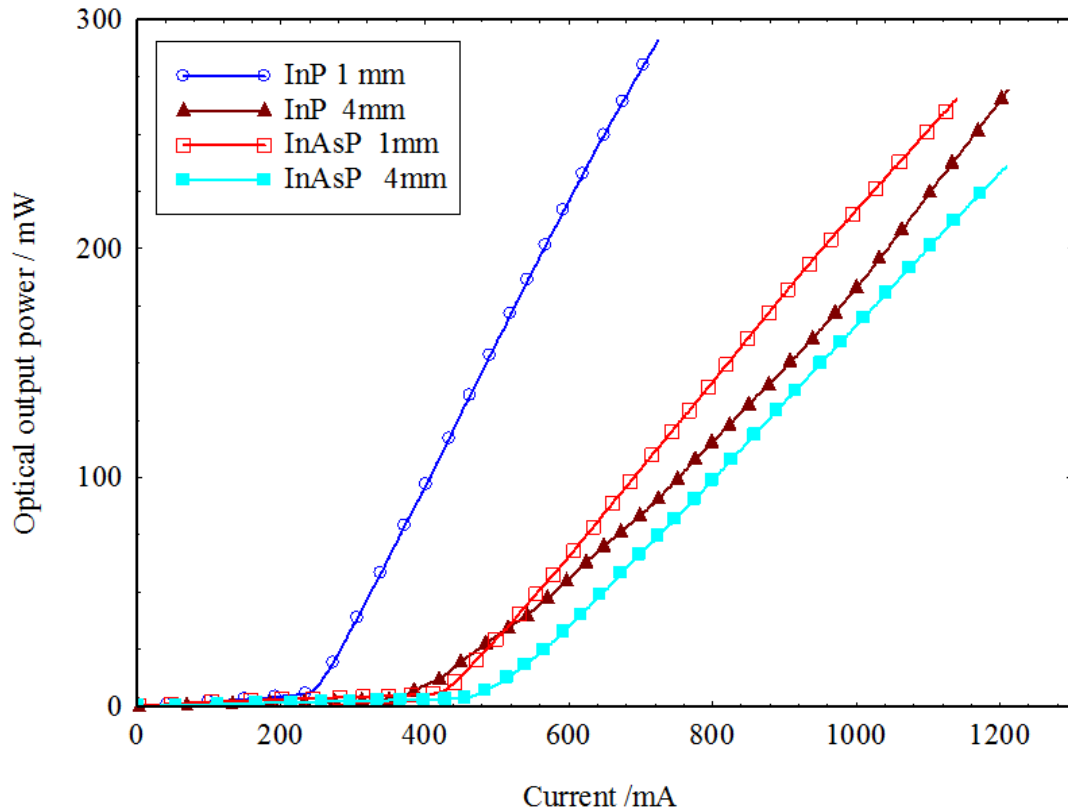
Figure 4:7 Pulse peak power-current characteristic of the 1 and 4mm long lasers for both the InP and InAsP devices.

The InAsP 4mm laser shows increase in the slope efficiency at high pumped current (see Figure 4:7). This behaviour was also found in InGaAs QD laser at 80 K (Sugawara et al. 2000) and In InAs QD laser (Gao et al. 2015). This could indicate that the high pumped current could activate more energy states to participate in emission, hence, increasing the radiative recombination in the laser. Moreover high pumped current sometimes leads to switch between the longitudinal modes inside the laser cavity which in turn causes instability in (I-P) characteristics (Ascent 2007).

Using Equation 2:12 from Chapter two, it is possible to calculate the differential quantum efficiency of the devices (   ), as long as the wavelength of each device has been determined. Figure 4:8 is the plot of the reciprocal differential quantum efficiency against the cavity length of the devices.
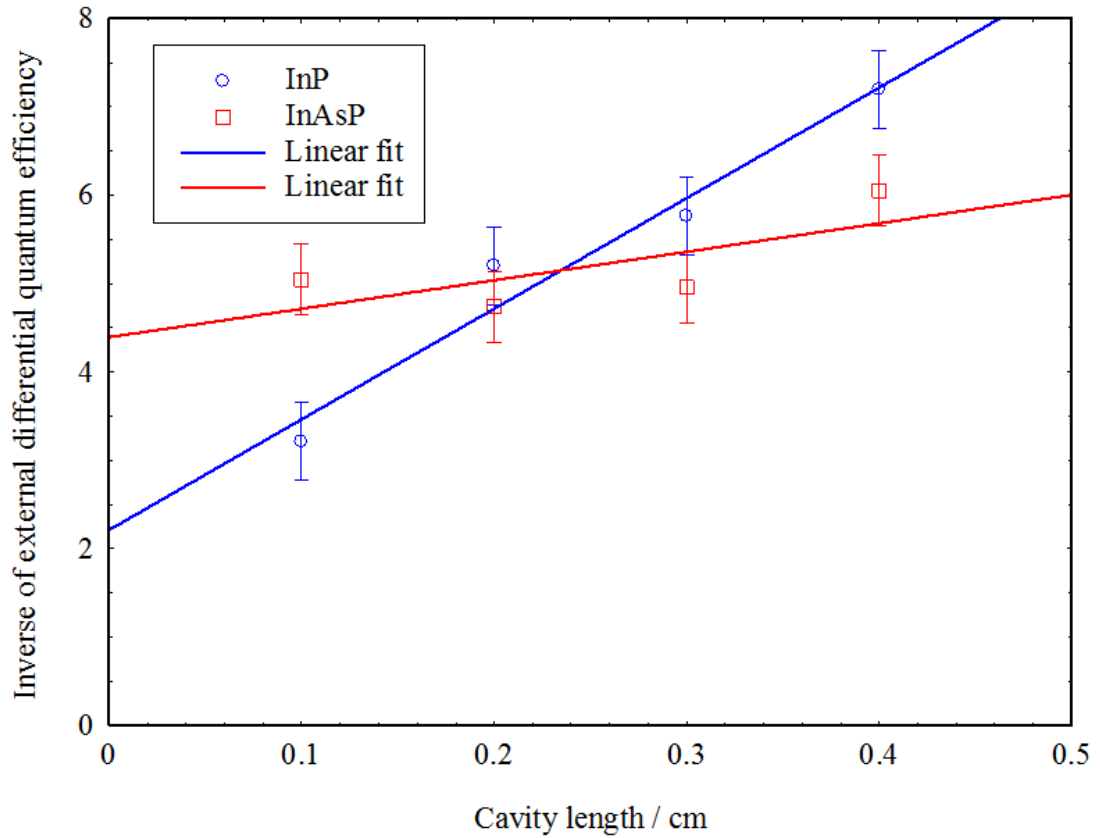
Figure 4:8 Cavity length dependence of the inverse differential quantum efficiency of both the InP and InAsP devices.

By fitting the data in Figure 4:8 to Equation 2:13, it is possible to determine the internal optical loss (   ) and the internal differential quantum efficiency (η) of the lasers. From Figure 4:8, the   for InP is 45%, whereas for InAsP it is 22%. Additionally, the (   ) is 6.5 cm^{-1} for InP and 1.2 cm^{-1} for InAsP material. In fact this method of calculation is not appropriate for the reason that it relies on the assumption that   and   do not depend on cavity length, as mentioned in Chapter two (Inada et al. 2008). The   of the InP and InAsP materials will be measured precisely using the segmented contact method from the modal gain and absorption spectra in the following sections.

4.5 Modal absorption of the InP and InAsP materials

The modal absorption spectra of the materials were measured using the segmented contact method described in Chapter three by means of Equation 3:8. The modal absorption is a function of available transitions between states in the material when the material is not pumped. This will depict the difference in the states between InP and InAsP materials. Figure 4:9 describes the positive modal absorption spectra at room temperature of the both the InP and InAsP QD materials under TE polarisation.

As expected from the solid molar fraction of arsenic of roughly 25%, the available transitions are shifted toward a longer wavelength by less than 120 nm in comparison with the InP bulk material.

However, the smaller than expected lengthening of the wavelength, roughly 60 nm is most probably because of the smaller dot size of the InAsP material observed in the TEM images (see Figure 3:4).
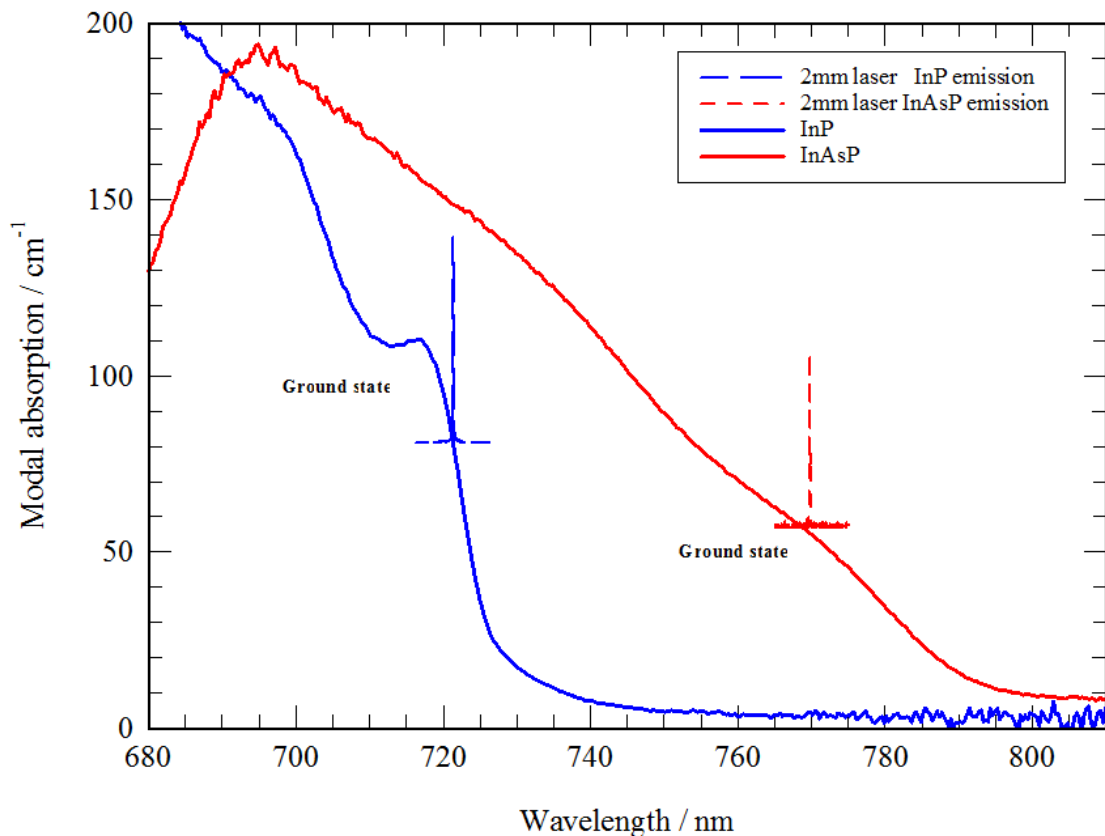

Figure 4:9 The positive modal absorption spectra for the InP and InAsP dot samples at room temperature. Lasing wavelengths of 2mm lasers (in arbitrary units) are added for both samples.

The ground state of the InAsP material is less well defined, which indicates a greater degree of inhomogeneous broadening. These results are also compatible with the photoluminescence measurements taken at room temperature as shown in Figure 3:5 in Chapter three. The greater degree of inhomogeneous broadening for the InAsP material could be due to the dot size variation shown in the TEM image (see Figure 3:4).

The absorption spectrum of the InAsP is appreciably broader, while the magnitude of the ground state is significantly reduced to approximately 55 cm^{-1}. This could be less available gain from the ground state when the carriers are present. This will be discussed in the subsequent section. Finally, the enhanced degree of inhomogeneous broadening in the InAsP materials implies broadening in both the optical gain spectra and emission spectra, where these can support mode-locking in InAsP material by producing short pulse duration (Finch et al. 2015).

4.6 Modal gain spectra of the InP and InAsP materials

4.6.1 Net modal gain as a function of pumped current density

The optical gain spectra of the materials are studied at room temperature using the segmented contact method by means of Equation 3:9. The modal gain spectra as a function of photon energy at room temperature are plotted in Figure 4:10 and Figure 4:11 for InP and InAsP dot materials respectively at room temperature, under TE polarisation. These are taken at different pumped levels.

In general, when the pumped current density increases the gain bandwidth broadens and the gain magnitude intensifies along with the peak of the gain spectrum, which indicates the emission energy of the ground state shifts toward a lower wavelength.

The gain shown arises entirely from the quantum dots with the tensile strained $Ga_{0.54}In_{0.46}P$ quantum well having a band gap of 1.03 eV.

InAsP gain spectra which are shifted toward a longer wavelength are broader than the InP dot spectra, which could help to produce a shorter pulse width in the case of using the material in the mode-locking laser. In contrast, InAsP dot spectra require more current density to achieve the same peak for the InP dot spectrum. This is expected due

to higher threshold current density for the InAsP lasers, where this makes threshold conditions occur at a higher current density.

Moreover, the energy position of the peak gain spectra of the InAsP dot increase (wavelength decreases) more rapidly with increasing current density. This is consistent with the cavity length dependency of the wavelength observed in Figure 4:6, which is a signal of high gain saturation.

The internal optical loss that has been calculated earlier in this chapter via the reciprocal quantum efficiency method (see Section 4.4) can now be deduced more precisely from the low energy part of the gain spectra, which agrees with the low energy part of the absorption spectra in Figure 4:10 and Figure 4:11. It is determined that is around 2.5±1.5 cm^{-1} for the InP dots material, whereas it is slightly higher for the InAsP dots material, approximately 3.5±1.7 cm^{-1}.
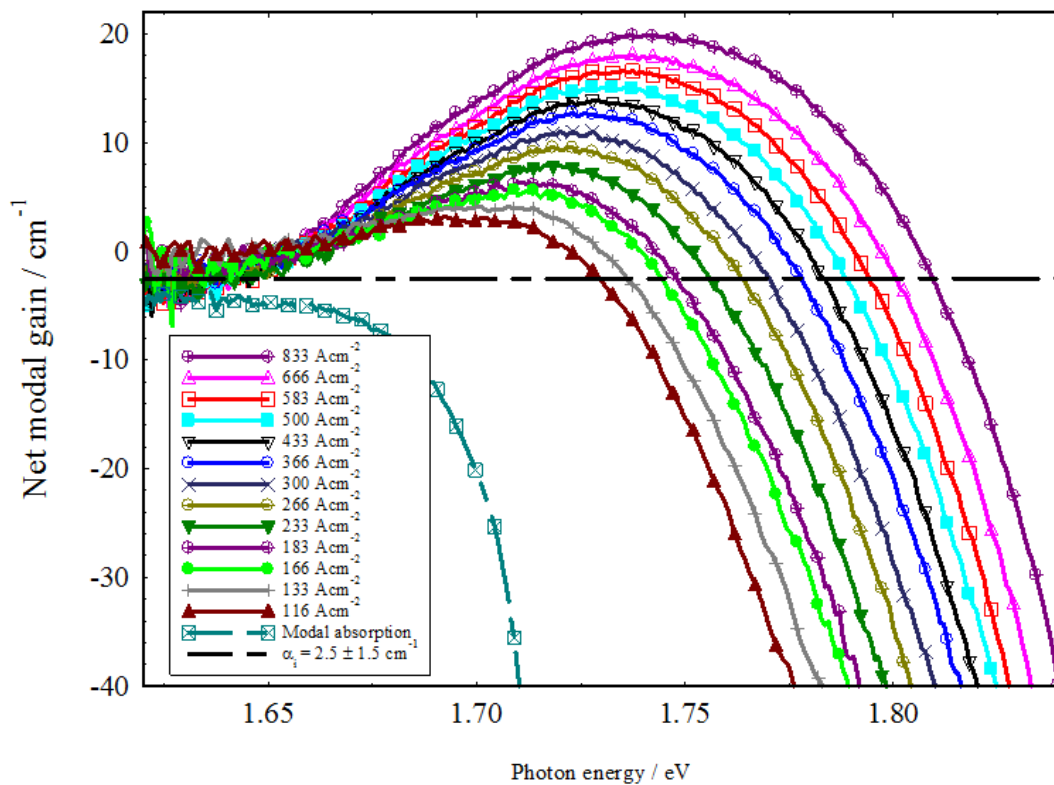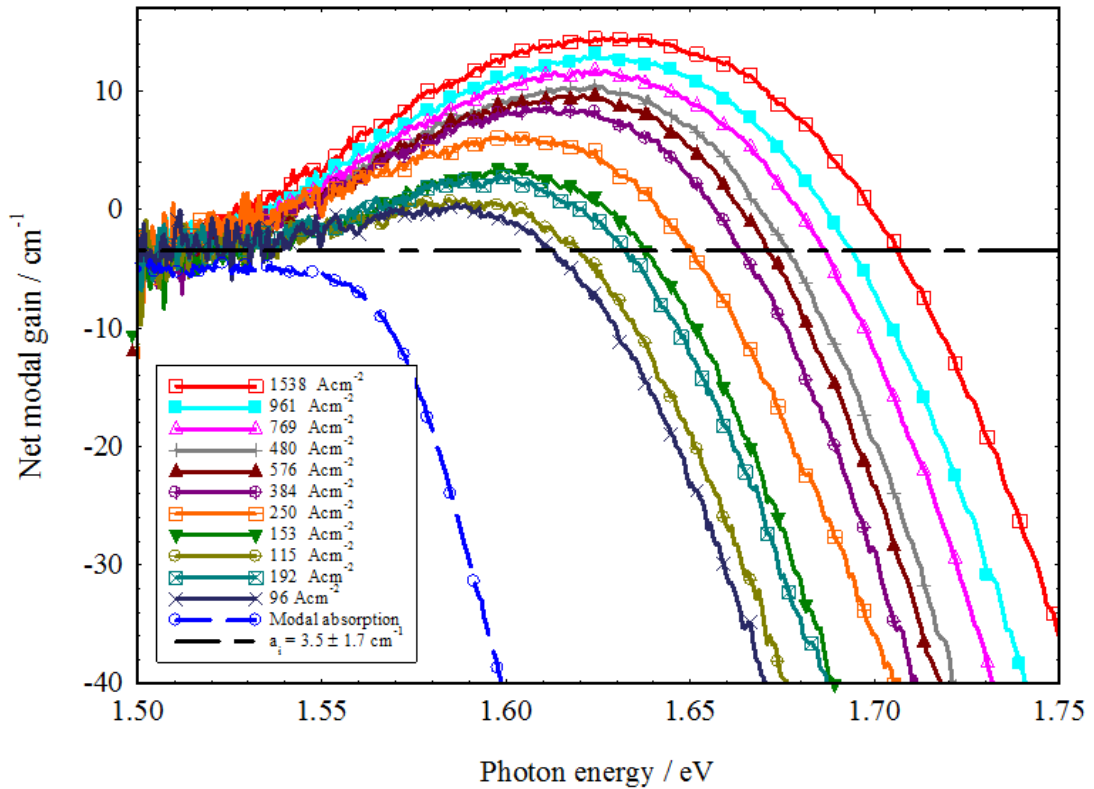

Figure 4:10 Modal gain spectra for the InP dot sample at different pumped levels with modal absorption at room temperature.

**Figure 4:11 Modal gain spectra of the InAsP dot sample at different pumped levels
with modal absorption at room temperature.**

The optical gain of InAsP QD material is wider than the InP QD one at a fixed gain coefficient. This is studied precisely in Chapter five at different value of temperature. On the other hand, the optical gain spectra of the QD lasers are much broader than the optical gain spectra of the Quantum well lasers, and also the QD structures have lower value of the internal optical loss (α_i) than the QW structures (Smowton et al. 2011). The relatively broader gain spectra for InAsP QD material can support tunable or multi-wavelength sources that can be useful in bio-photonic applications. Finally, the semiconductor optical amplifiers (SOAs) which are usually used in coarse wavelength division multiplexing (CDWM)(Uskov 2005) and the superluminescent diode (SLD) which commonly used in a high-resolution optical coherence tomography (OCT) have a gain bandwidth at 3dB of approximately 80nm at high pumped level (Ozaki 2016). In comparison to the gain in Figure 4:10 and Figure 4:11, the 3dB for InP QD is about 31nm whereas, for InAsP QD is roughly 42nm at high current density level. Such 3dBs of InP and InAsP QD materials have a potential in biophotonic sensing and telecommunications, across wavelengths from red to mid-infrared.

4.6.2 Gain-curent relation

The net peak gain for both the InP and InAsP materials is plotted versus current density at room temperature in Figure 4:12. The result shows that the InP dot material required less current density to achieve the same peak modal gain as the InP dot material. For example, to achieve 6 cm^{-1} of the net peak modal gain, which is corresponding to the threshold gain requirement of the 2mm length laser, according to Equation 2:18 in Chapter two. InP quantum dot materials needs 170 A.cm^{-2} pumped level. Meanwhile, the InAsP quantum dot material needs 250 A.cm^{-2}, as shown in Figure 4:12. And these values of current densities (indicated by the arrows in Figure 4:12) are consistent with the values of the threshold current densities of the 2mm long cavity laser at room temperature of both InP and InAsP QD lasers displayed in Table 4:1.Conversely, Figure 4:12 signifies that the peak modal gain of the InP dot is more sensitive to pumped current density (the differential gain is higher in InP QD material) and the gain saturation is more obvious in the InAsP quantum dots. In the other words, (   ) is lower for InAsP QD material than the InP QD material which means InAsP QD materials can be better for stabilized passive mode-locked laser system according to Equation 2:36 and Figure 2:23 in Chapter two.
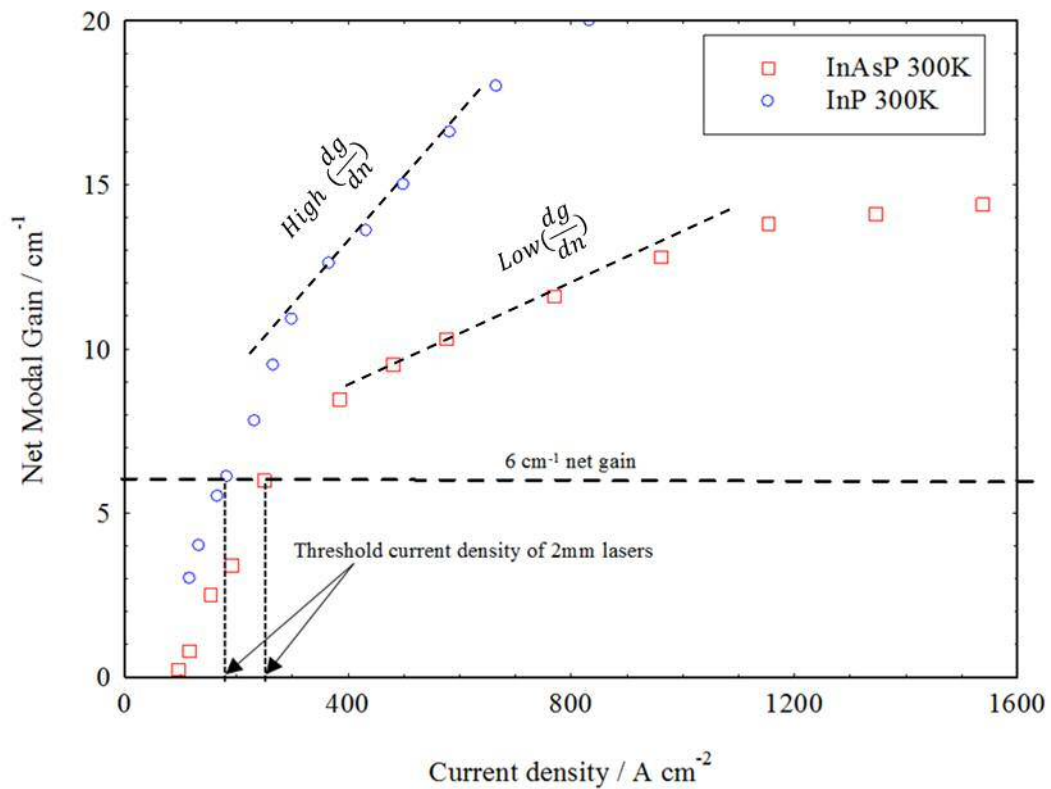

Figure 4:12 Gain-current relations for the InP and InAsP materials at room temperature.

4.7 Transition energy using E-PVS

The transition energies of the InAsP and InP materials have been measured using polarisation sensitive E-PVS described in Section 3.6 in Chapter three. This measurement allows determining the energies of both the quantum well states and quantum dot states of the materials and the separation energy between them. However, the intensity of the spectrum is in arbitrary units.

Figure 4:13, shows the transition energy of both the TE and TM polarised photovoltage signal for the InP and InAsP quantum dot materials using 2mm laser devices. The energy separation between quantum well states to the quantum dot states (ground state) is about 200 meV for the InP, whereas for the InAsP is approximately 300 meV. This indicates that the InAsP dots are confined deeper in the quantum well layers by approximately 100 meV, which means that there is the potential for the non-thermal occupation of the carriers. This is a positive point with respect to mode-locking.
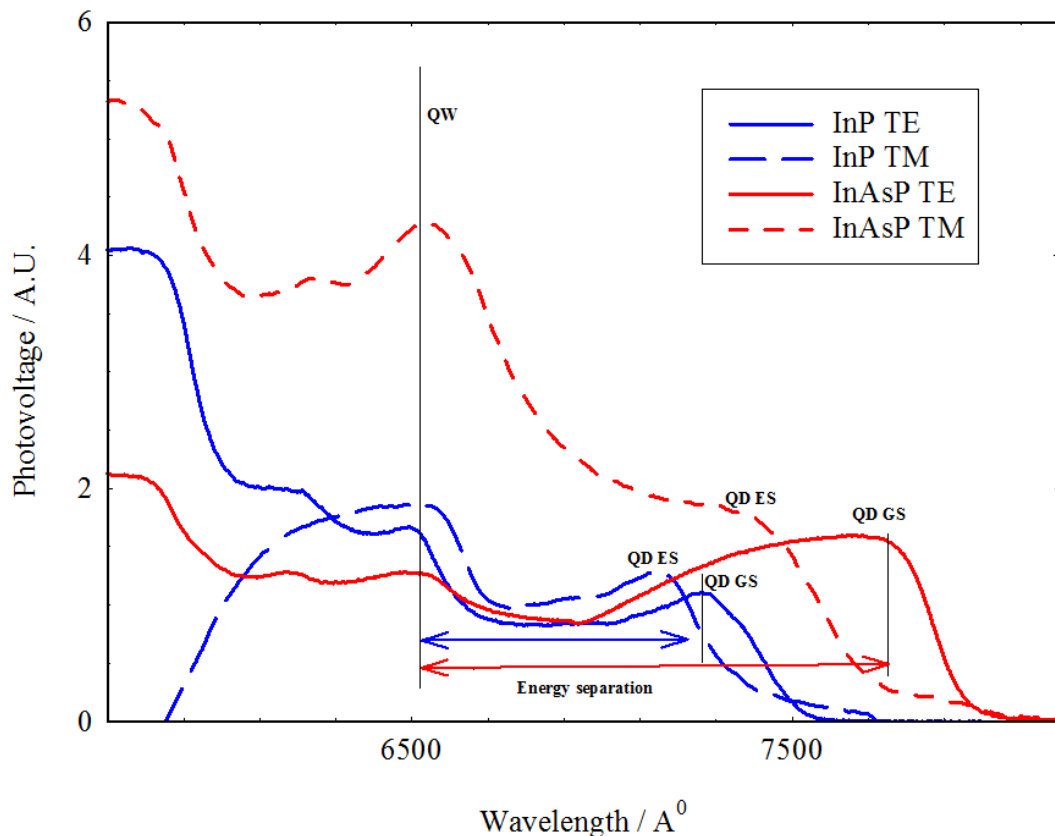

Figure 4:13 E- PVS measurements at room temperature for the InP and InAsP QD materials under TE and TM polarisation.

4.8 Summary

In this chapter, the characteristics of the InAsP QD lasers were determined and compared with the standard device (InP QD laser), such as threshold current density, laser efficiency, lasing wavelength and temperature dependency of the threshold current density for different cavity lengths (1, 2, 3 and 4mm) for both the InP and InAsP QD.

The results illustrate a shifting in the emission wavelengths for the InAsP QD lasers by approximately 55 nm toward longer wavelengths, while maintaining useable threshold current density and laser efficiency. Moreover, both samples delivered optical powers of at least 250 mW. Edge-photo voltage spectroscopy (E-PVS measurements) confirmed deeper dot confinements for the InAsP materials by 103 meV. Finally, the absorption measurements reveal a greater degree of inhomogeneous broadening for the InAsP QD material, while the gain-current measurements reveal differential gain for the InAsP QD materials.

4.9 References

Acsente, T. **2007** laser diode intensity noise induced by mode hopping. Romanian Reports in Physics 59(1), pp. 87–92.

Asryan, L.V. and Suris, R.A. **1997**. Characteristic temperature of quantum dot laser. Electronics letters 33(22), pp. 1871-1872.

Bashkatov, A., Genina, W., Kochubey V. and Tuchin V., **2005**. Optical properties of human skin, subcutaneous and mucous tissues in the wavelength range from 400 to 2000nm. Journal of physics D: Applied physics 38, pp 2543–2555.

Finch, P., Blood, P., Smowton, P. M., Sobiesierski, A., Gwilliam, R. M., and O'Driscol, I. **2013**. Femtosecond pulse generation in passively mode locked InAs quantum dot lasers. Applied Physics Letters 103(131109), pp.1–3.

Finch, P., Hutchings, M., Blood, P., Sobiesierski, A., Smowton, P., and O'Driscoll, I. **2015**. Improving the Optical Bandwidth of Passively Mode-Locked InAs Quantum Dot Lasers. IEEE journal of selected topics in quantum electronics 21(6). pp. 1900507

Gao, F. Luo, S. Ji, H. M. Yang, X. G. Liang, P. and Yang, T. **2015**. Broadband tunable InAs/InP quantum dot external-cavity laser emitting around 1.55 μm. Optics Express 23(14), pp. 18493- 18500.

Inada, S., Yoshita , M., Okano, M., Hara, T., Akiyama, H. and Zhangi, L. **2008**. Measurements of Cavity-Length-Dependent Internal Differential Quantum Efficiency and Internal Optical Loss in Laser Diod. Japanese Journal of Applied Physics, 47(4), pp.2288–2290.

Kasim, M., Elliott, S., Krysa, A. and Smowton, P. **2015**. Reducing Thermal Carrier Spreading in InP Quantum Dot Lasers. IEEE Journal of selected topics in quantum electronics, 21(6).

Moritz, A., Wirth, R. and A. Hangleiter **1996**. Optical gain and lasing in self-assembled InP/GaInP quantum dots Appl. Phys. Lett. 69 (2), pp. 212-214.

Ozaki, N., Childs, D., Sarma, J., Roberts, S., Takuma Yasuda, Shibata, H., Ohsato, H., Watanabe, E., Ikeda, N., Sugimoto,Y. and. Hogg R. A. **2016**. Superluminescent diode with a broadband gain based on self-assembledInAs quantum dots and segmented contacts for an optical coherence tomography light source. Journal of applied physics 119, 083107.

Roggan, A., Friebel,M. Do¨ rschel, K. Hahn, A. and Mu¨ ller,G. **1999**. optical properties of circulating human blood in the wavelength range 400 – 2500 nm. Journal of biomedical optics 4(1), pp.36–46.

Schlosser, P. J., Hastie, J.E., Calvez, S., Krysa, A. B. and Dawson, M.D. **2009**. InP/AlGaInP quantum dot semiconductor disk lasers for CW TEM00 emission at 716 – 755 nm. Optics Express 17(24), pp. 1-6.

Smowton, P., Al-Ghamdi, M., Shutts, S., Edwards, G., Hutchings, M., and Krysa, A. 2010. Effect of growth temperature on InP QD lasers. IEEE Photonics Technology Letters, 22(2), pp.88–90.

Smowton, P., George, A., Sandall, I., Hopkinson, M., and Liu, H-W. **2008**. Origin of Temperature-Dependent Threshold Current in p-Doped and Undoped In (Ga) As Quantum Dot Lasers. IEEE journal of selected topics in quantum electronics, 14(4), pp.1162–1170.

Sugawara, M., Mukai, K. Nakata,Y.and Ishikawa, I. **2000**. Effect of homogeneous broadening of optical gain on lasing spectrab in self-assembled In_xGa_{1-x}/GaAs quantum dot lasers. Physical review B 61(11), pp. 7595 -7603.

Smowton, P. M, Stella, N. E., Samuel, S., Al-Ghamdi, M. S. and Krysa, A.B. **2011**. Temperature-Dependent Threshold Current in InP Quantum-Dot Lasers. IEEE Journal of selected topics in quantum electronics 17(5), pp.1343-1348.

Uskov, A.V., O'Reilly, E.P., Laemmlin, M., Ledentsov, N.N and Bimberg, D. **2005**. On gain saturation in quantum dot semiconductor optical amplifiers. Optics Communications 248, pp. 211-19.

Vinokurov, D. A., Kapitonov, V. A., Kovalenkov, O. V., Livshits, D. A. and Tarasov, I. S. **1998**. Self-organized nanosize InP and InAsP clusters obtained by metalorganic compound hydride epitaxy. Technical physics letters 24(8), pp.623-625.

Chapter (5) Effect of temperature on the optical gain peak in InP and InAsP materials

5.1 Introduction

It is possible that the temperature of a laser device changes under operation, by means of both internal self-heating and external mechanisms like surrounding environment temperature. Furthermore, several parameters, which are critical to the mode-locked laser regime, can be modified using temperature. Therefore, it is important to quantify the temperature dependent behaviour of the InP and InAsP QD materials.

In the previous chapter, the modal gain of InAsP and InP QD materials were investigated at room temperature. However, in this chapter the modal gain of the InAsP and InP QD materials are studied as a function of temperature; specifically, (150, 200, 250, 300, 350, 400 K). It is important for the mode-locked laser regime to study the gain-current relation as a function of temperature, where several crucial parameters can be determined such as differential gain, gain saturation, transparency current density, in addition to optical gain bandwidth and inversion level.

This chapter begins by presenting the modal optical gain of the materials as a function of the driven current density at each studied temperature, whilst the gain- current relations are also studied at different temperatures. The comparison of the bandwidth of the optical gain spectra at a fixed peak gain (6 cm^{-1} which is corresponding to the threshold gain of 2mm long cavity lasers) was studied for the materials at each measured temperature. Moreover, the chapter evaluates the effect of temperature on the inversion level of the InP and InAsP QD materials Finally, it concludes with the effect of temperature on the lasing wavelength of the materials from the gain modal spectra and absorption edges.

5.2 Temperature effect on modal gain spectra

The segmented contact technique (described in Chapter three) was also used to determine the modal gain spectra for the InP and InAsP materials at different values of driven current and temperature; specifically, 150, 200, 250 300,350, 400 K. Figure 5:1 represents the modal gain spectra taken in TE polarisation as a function of driven current density at 150 and 400 K for InP QD sample, whereas Figure 5:2 demonstrates the optical modal gain spectra of the InAsP QD sample at the same temperatures.

A number of interesting conclusions can be inferred from Figure 5:1 and Figure 5:2. In general for both samples; particularly the InP and InAsP and for all temperatures, when the driven current density increases, the peak net gain increases and the gain curves become wider. Similarly, the peak gain position shifts toward higher photon energy (shorter wavelengths). Conversely, as the temperature increases, the gain spectra become broader at a fixed amplitude gain and the peak of the gain shifts to lower photon energy at fixed gain peaks (to longer emission wavelength), when the temperature increases. For example, the InP spectrum at 6 cm^{-1} of the peak gain amplitude (which is the threshold gain of the 2mm cavity length of the laser sample), the peak position energy, is at 1.77 eV at 150 K, meanwhile at 400 K it is at 1.68 eV (shifted by approximately -90 meV).

Figure 5:1 and Figure 5:2 also confirm that the InAsP material has wider gain spectra for all temperatures measured. When the temperature increases it requires a higher drive current density to achieve the same gain peak. For instance, for the InP QD materials at 150 K, just 100 A.cm^{-2} is required to achieve 6 cm^{-1} of the peak amplitude, whereas at 400 K it needs up to 1160 A.cm^{-2} to achieve the same gain peak.

This is consistent with the fact that the threshold current density increases exponentially with temperature (see Figure 4:3; temperature dependency of the threshold current density for InP and InAsP lasers); therefore, the threshold condition occurs at higher current density when the temperature rises, especially above 300 K. Moreover, the peak gain becomes less sensitive to the driven current density at high temperatures, which will be discussed Section 5.3. Net modal gain against driven current density can be formed by plotting peak net modal gain as a function of the driven current density at each temperature.
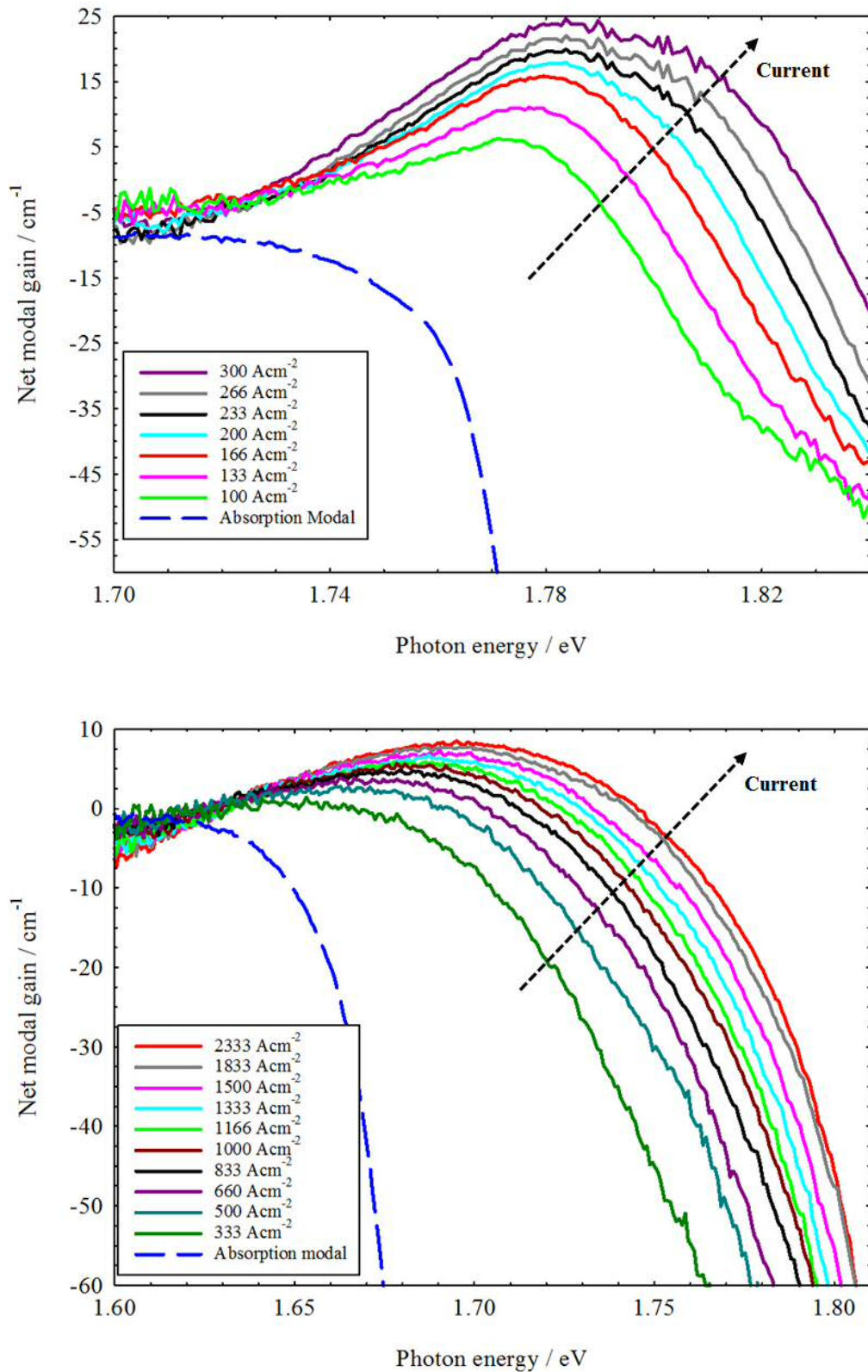
Figure 5:1 Gain spectra as a function of the driven current density for InP QD material at 150 K (top figure) and 400 K (bottom figure). The symbols marked on each curve are a guide for the eyes.
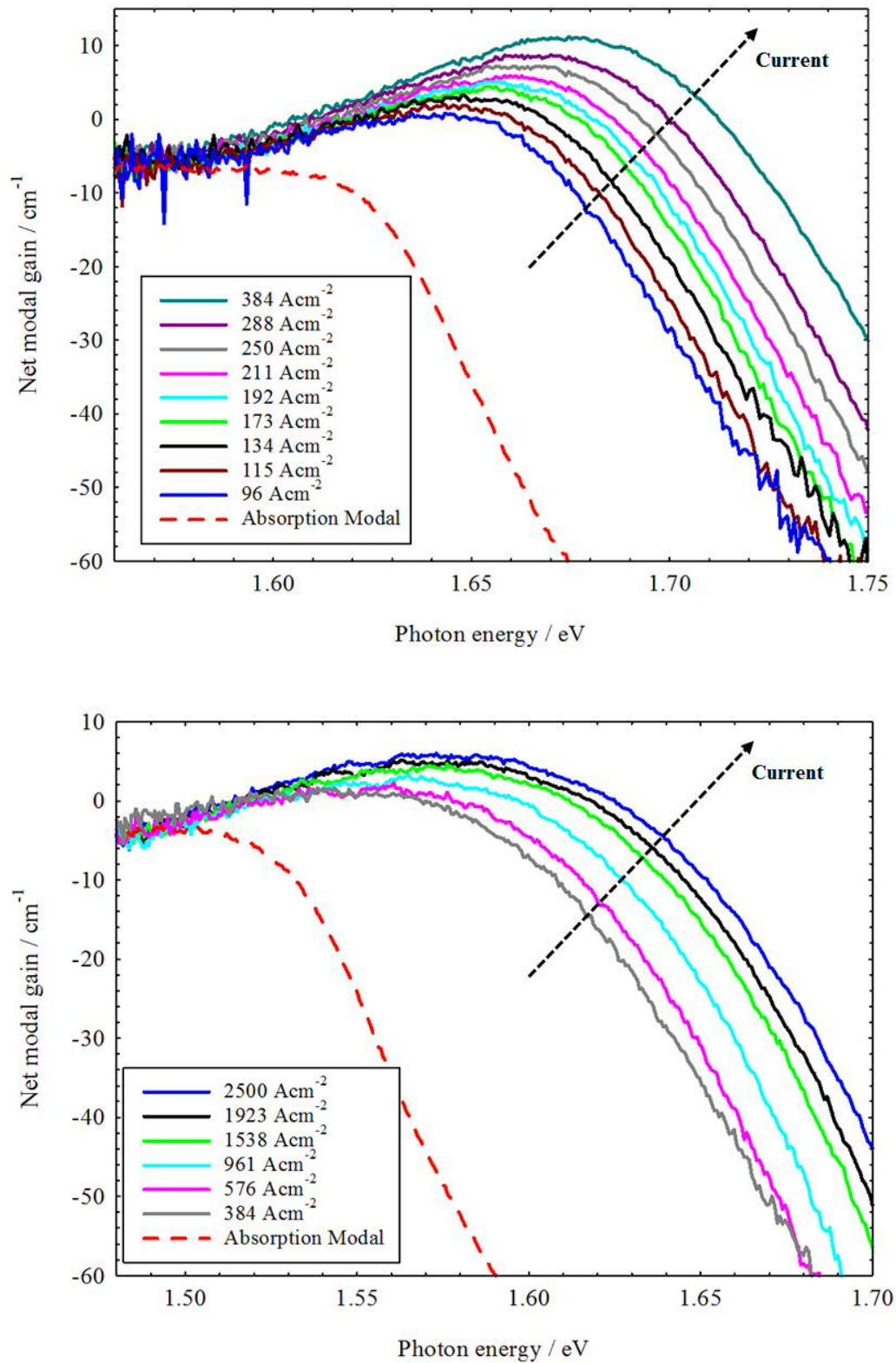
Figure 5:2 Gain spectra as a function of the driven current density for InAsP QD material at 150 K (top figure) and 400 K (bottom figure). The symbols marked on each curve are a guide for the eyes.

In fact, when the laser is operated at an elevated temperature, the thermal spread of the carriers among the available energy states will increase, which causes an increase in the threshold current density (Kasim et al. 2015). This effect can be seen clearly in the gain spectra plotted in Figure 5:3, which indicates the shifting in the transparency point (quasi Fermi-level separation) required to maintain the fixed peak gain from 250 K to 300 K.

Regarding the InAsP QD material the transparency point is shifted by 7 meV over the range of 50 K. The increase in the quasi Fermi-level separation with temperature associated with a broadening of the gain spectrum, for the fixed junction level, lowers the gain amplitude.

The increase of the injection required to offset the fixed gain amplitude also affects the gain peak wavelength. This is described in detail later in this chapter in Section 5.6. Figure 5:3 also confirms that to achieve the same gain peak magnitude at higher temperature, a higher current density is required to achieve 6 cm^{-1}, which is the threshold gain peak corresponding to the 2mm laser device. It requires 173 A.cm^{-2} at 250 K, whereas for 300 K it requires approximately 250 A.cm^{-2} and for 350 it needs 960 A.cm^{-2}. This is consistent with the temperature dependence of the threshold current density measured for 2mm long cavity laser samples in Chapter four (see figure 4:3, 2 mm cavity length device of InAsP QD laser).

The injection level indicated in Figure 5:3 (the value of the quasi-Fermi level separation minus absorption edge which was introduced in Chapter three Section 3.7.2), was studied as a function of the temperature for both the InAsP and InP materials. Figure 5:4 shows the injection level as a function of temperature for the materials at the fixed (6 cm^{-1}), which is the threshold requirement of the 2mm laser cavity length. The InAsP material demonstrates higher injection level value.

This arises from the results shown earlier in this chapter, which indicated that the InAsP material has wider gain spectra than the InP one, specifically at low temperature. Figure 4:5 also shows that the injection level becomes more sensitive to the temperature above 300 K.

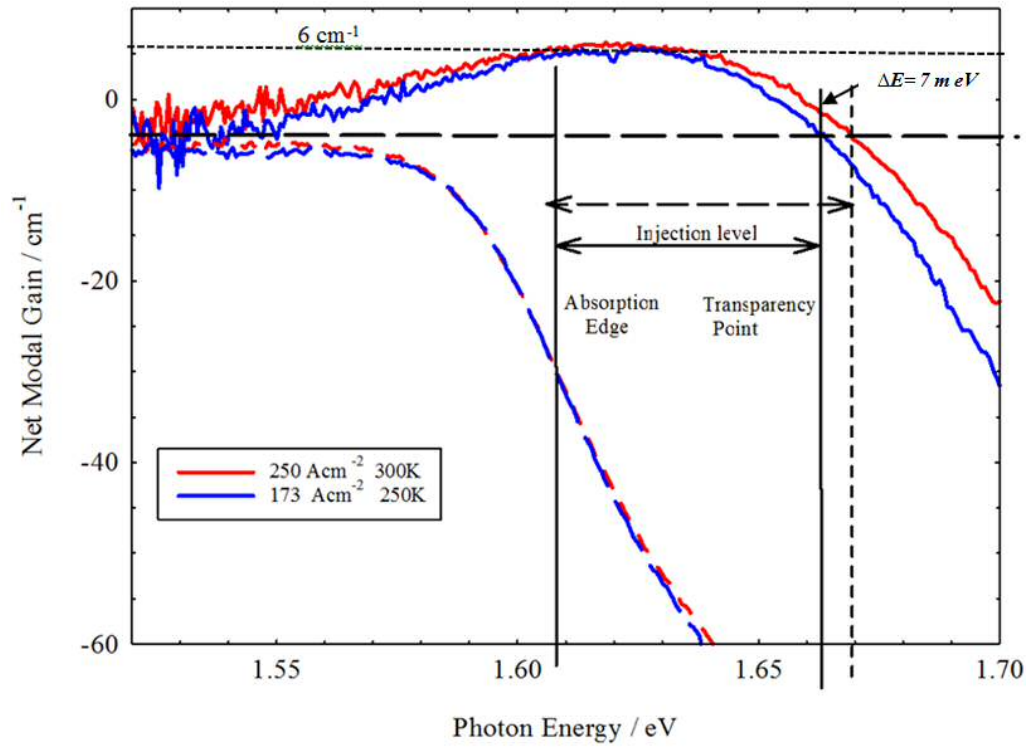**Figure 5:3 Modal gain spectra for the InAsP QD material measured at fixed peak gain (6 cm^{-1}) at 250, 300 and 350 k with absorption spectra. The absorption spectra have been shifted to point out the changing in the band-gap with temperature.**
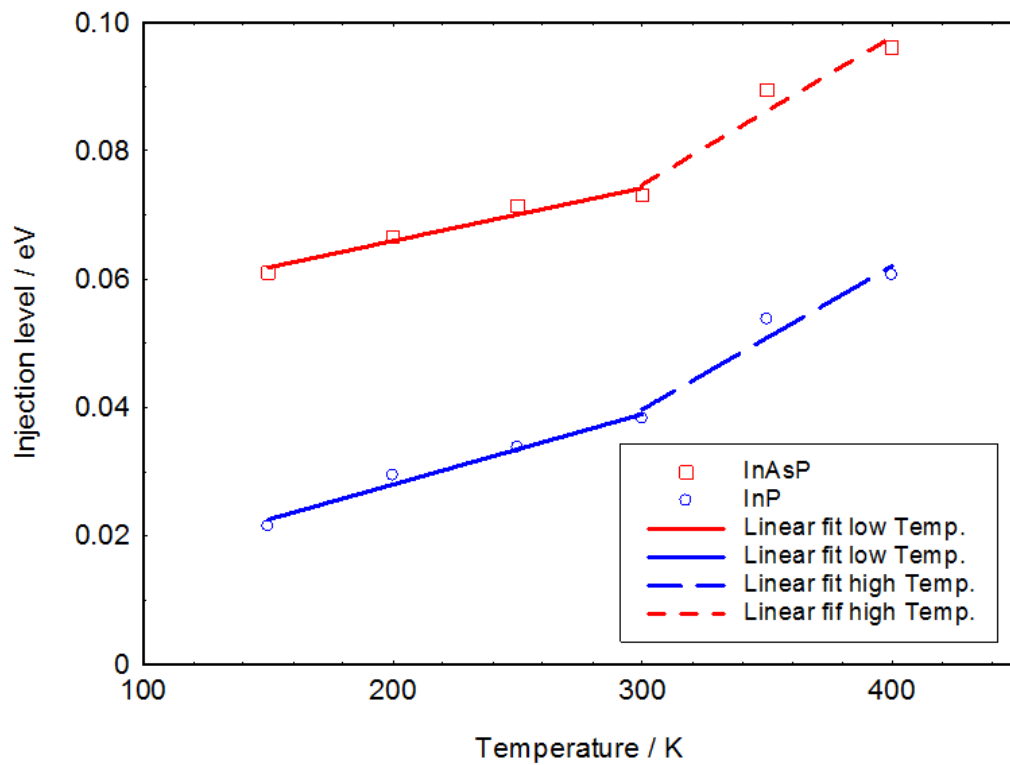

Figure 5:4 Injection level as a function of temperature for the InP and InAsP QD materials.

5.3 Gain-current relation as a function of temperature

To study the differential gain, gain saturation and transparency current of the samples, gain-current relationships are plotted at different studied temperatures. Figure 5:5 and Figure 5:6 represent the gain-current relationship for the InP and InAsP materials respectively, measured by the segmented contact method at different value of temperatures; specifically, 400, 350, 300, 250 and 150 K. As was mentioned in Chapter four (Figure 4:12, gain-current relationship at room temperature for the InP and InAsP at room temperature), but in Figure 5:5 and Figure 5:6 the y-axes is the peak optical gain which is the net optical gain plus α_i .the peak optical gain for the InAsP material is less sensitive to drive the current density. Figures 5:5 and 5:6 confirm this for all the temperature values measured. Additionally, the same temperature for the InAsP material requires more current to achieve the same modal gain peak. Moreover, Figure 5:5 and Figure 5:6 illustrate that the gain saturation effect increases when the temperature rises. This behaviour in the quantum dot materials was attribute to increasing carrier occupation of the well layer with increasing temperature (Smowton et al. 2004).
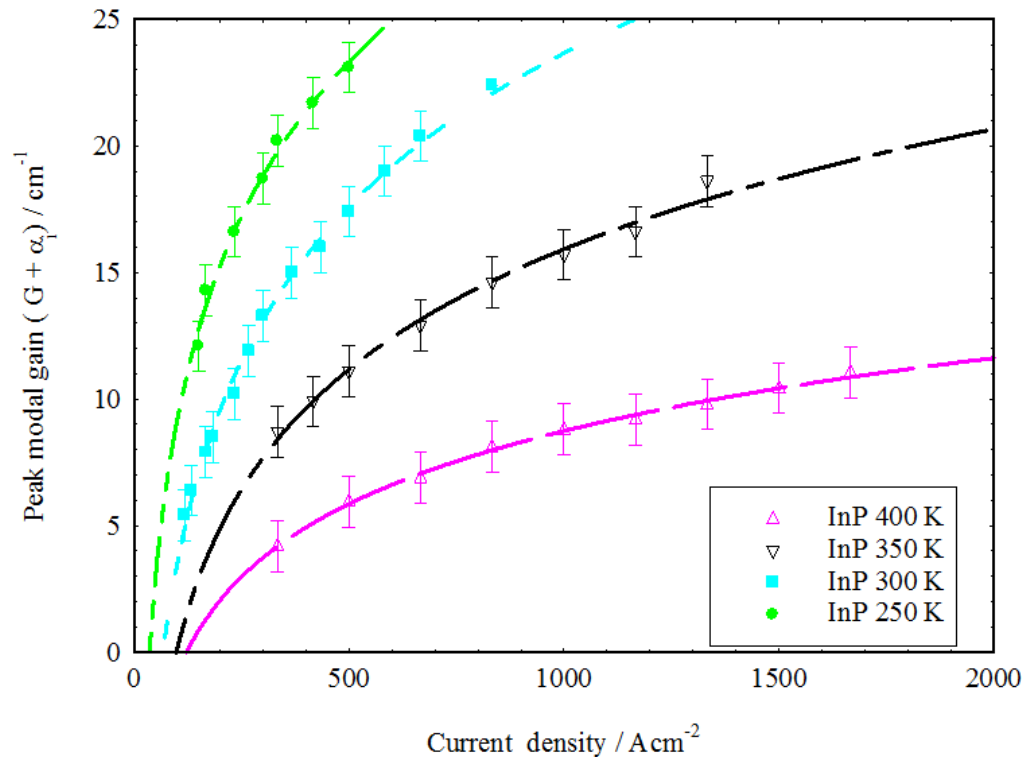

Figure 5:5 Gain–current relations for the InP QD laser at different temperatures.
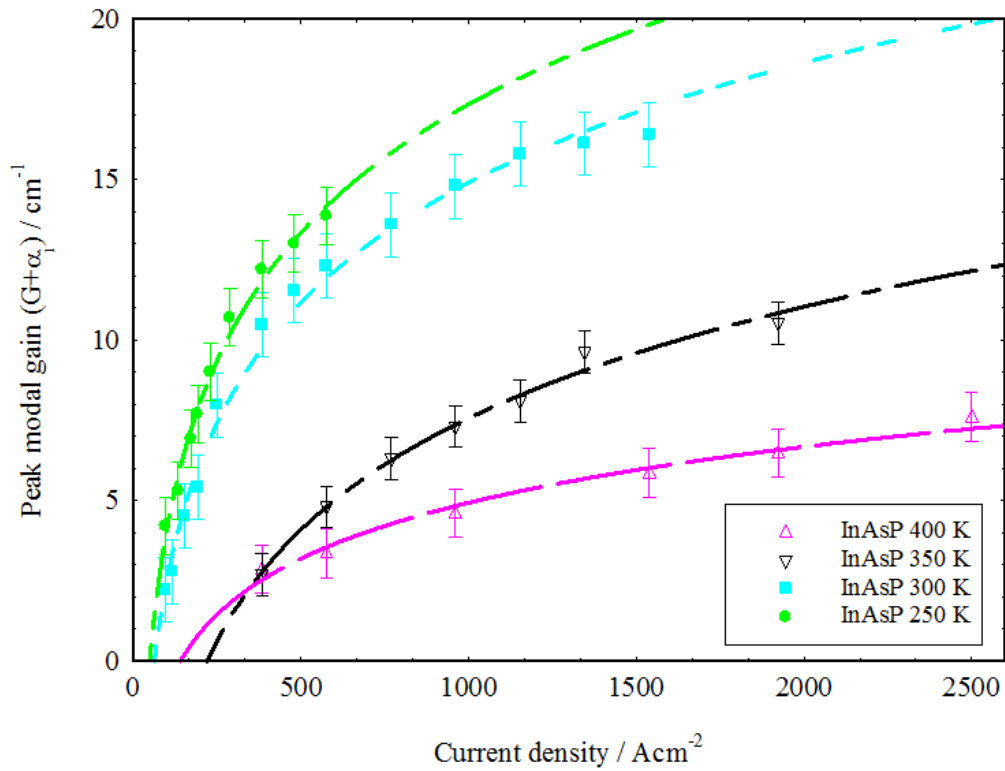
Figure 5:6 Gain–current relationship for the InAsP QD laser at different temperatures.

The differential gain (*dg/dJ*) decreases when the temperature increases. The curves on Figure 5:5 and Figure 5:6 were fitted to Equation 2:26 from Chapter two, to determine the important parameters of the gain-current relationship. Table 5:1 reveal the values of the gain saturation and the transparency current density for the InP and InAsP QD materials for 150, 200, 250, 300, 350 and 400 K.

Temperature(k)	G^{sat} (cm^{-1})		J_t (A.cm^{-2})	
	InP	InAsP	InP	InAsP
250	8.79	5.76	35	49
300	8.75	5.4	66	63
350	6.85	5	97	221
400	4.15	2.52	122	141

Table 5:1 The values of the gain saturation and the transparency current density for the InP and InAsP materials for 150, 200, 250, 300, 350 and 400 K.

Regarding Table 5:1, the InAsP QD material displays a lower gain parameter (G^{sat}) than the InP one. In the other words, *(dg/dn)* is lower for InAsP QD material than the InP QD material at all measured temperature which means InAsP QD materials can be better for stabilized passive mode-locked laser system according to Equation 2:36 and Figure 2:23 in Chapter two. And this can be understood from Figure 4:9 in Chapter four, where the lower amplitude of the absorption for InAsP QD material is due to greater degree of inhomogeneous broadening.

The transparency current density increases when the temperature rises. In general, when the temperature increases, both materials require more driven current density to achieve the same gain peak, as mentioned in Figure 4:3, Chapter four, temperature dependency of threshold current density.

5.4 Temperature effect on the modal absorption

Figures 5:7 and 5:8 show the modal absorption of the InP and InAsP QD materials respectively at different measured temperatures; specifically, 400, 350, 300, 250, 200 and 150 K. When the temperature increases the peak energy of the ground and excited states shift linearly towards lower photon energy (the emission wavelength shifts towards longer by approximately 0.17 nm/K for both the InP and InAsP structures. This is mostly owing to the thermal tuning of the band gap. The temperature dependency of the emission wavelength is less for InP and InAsP QD material in comparison to it in 1.55 μm InAs QD which is approximately 0.55 nm/K in pulse condition (abdollahinia 2018).

On the other hand, the inhomogeneous broadening is still the same at all temperatures measured, as shown in the Figure 5:7 and Figure 5:8. This is for the reason that it arises from dot size variation in the quantum dot system, as revealed in Section 2.4.4 in Chapter two, which does not change with temperature.

The absorption of the ground state and the excited state have a slight change with magnitude with temperature, especially for the InP spectra. This is possibly due to error in a small number of thermally excited carriers in the unpumped absorbing section at higher temperature, which partially blocks the absorption and also due to experimental uncertainty that can change the α_i region.
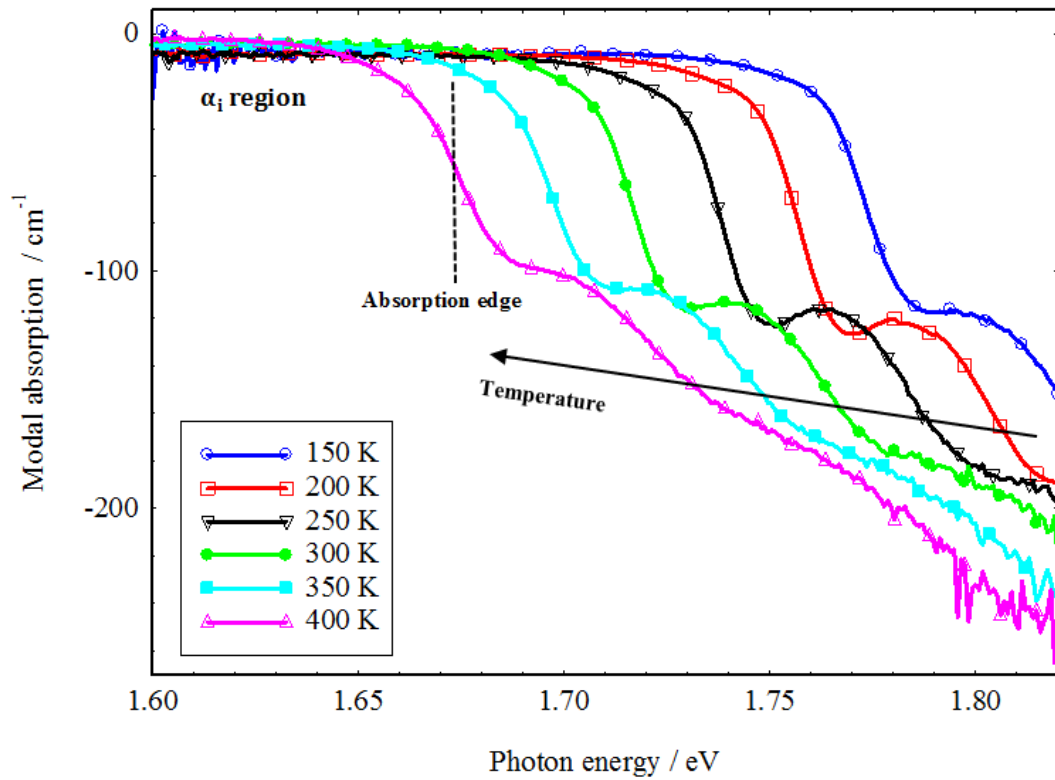
Figure 5:7 Modal Absorption spectra of the InP QD material at different temperatures.
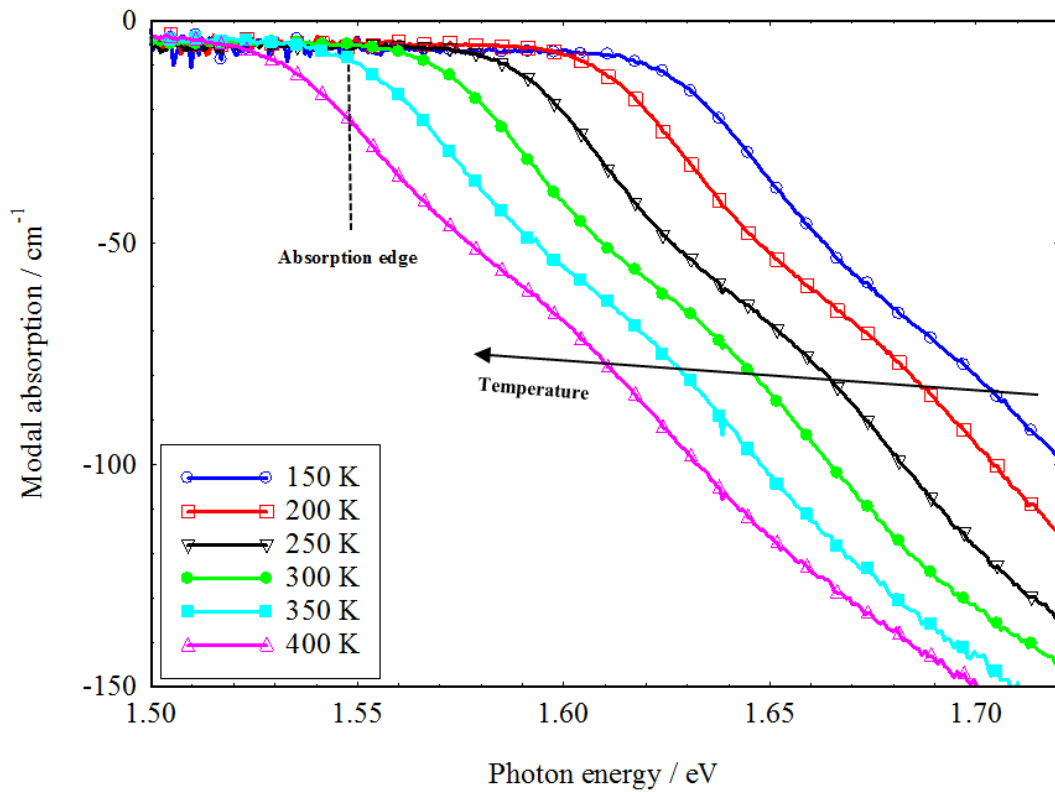

Figure 5:8 Modal Absorption spectra of the InAsP QD material at different temperatures.

Figure 5:9 is the plot of the internal optical losses as a function of temperature for both InP and InAsP QD materials. It is evident from Figure 5:9 that the internal optical losses for the InAsP materials is almost the same for all measured temperatures, roughly 3 cm^{-1}, except the 150 K which is higher. However, the InP QD material reveals variable values of internal optical loss at different temperatures.

Pikhtin et al. in (2010) shown that the temperature delocalization of charge carriers leads to an increase in the carrier concentration in the waveguide layers of the laser heterostructure. So the scattering by free charge carriers in active region changes which varies the value of the. On the other hand (Smowton et al. 2011) claimed that the internal optical loss is temperature invariant in the InP QD laser. However the values of internal optical loss αi in Figure 5:9 are the same at the different temperatures within the experimental uncertainty.
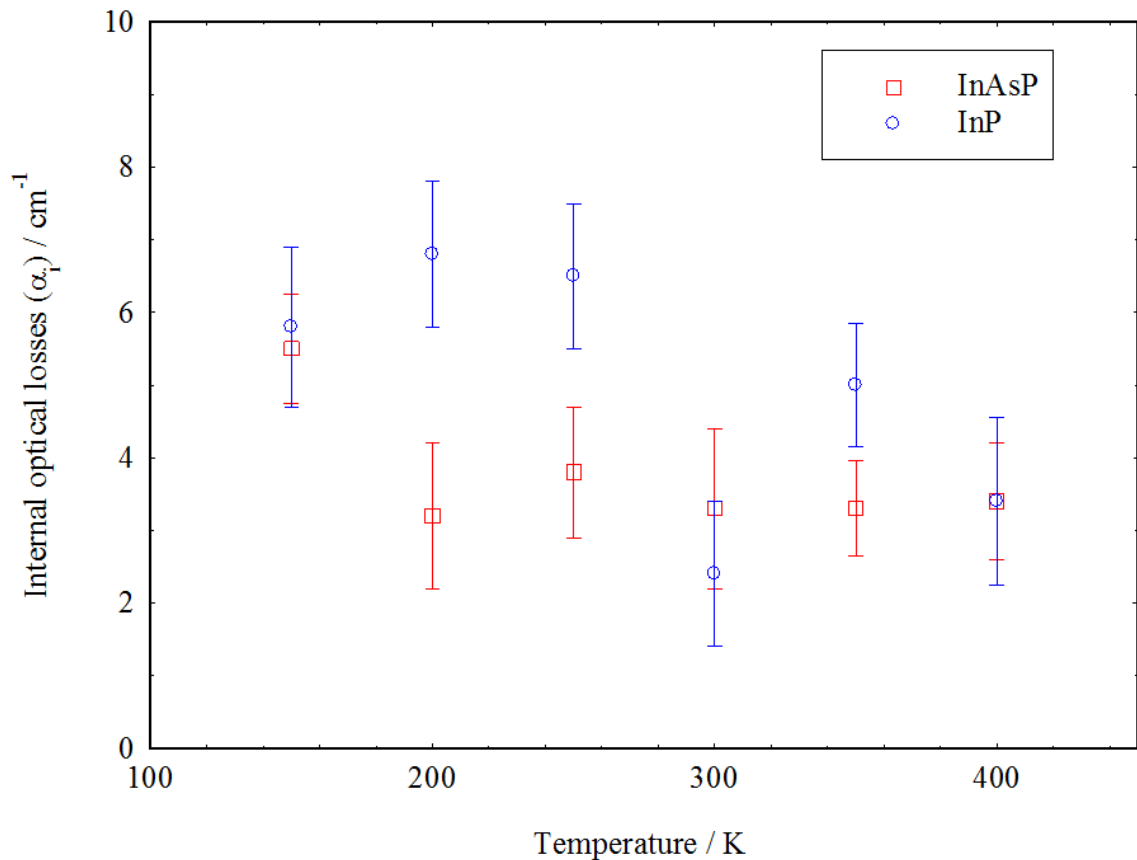

Figure 5:9 Internal optical losses (α_i) as a function of temperature for the InP and InAsP QD materials.

## 5.5 Temperature on the bandwidth of the modal gain spectra

It is beneficial here to study the optical bandwidth of the InP and InAsP QD materials as a function of temperature to identify what optical bandwidth can be covered with these materials. Figure 5:10 represents the comparison of the bandwidth of the modal gain spectra for the InP and InAsP QD materials at different temperatures; particularly 400, 350, 300, 250, 200,150 K at approximately the same level for peak gain (6 cm^{-1}), which is the gain threshold of the 2mm cavity length device. The InAsP modal gain is shifted by around 55nm toward the shorter wavelength for comparison purposes.

It can be clearly seen from Figure 5:10 that the amplifier optical bandwidth (FWHM) for InAsP quntum dot material is wider for all measured temperature specially at 150 K where the FWHM of the optical gain is more than doubled for InAsP than the InP sample. This could be a sign of non-thermal distribution of the carriers at this temperature. However, the carrier distribution will be study in the next Chapter to ensure if the InAsP QD regime tends to non-thermal distribution at this temperature.

On the other hand, The optical gain bandwidth as a function of temperatures is plotted in Figure 5:11 for both the InP and InAsP QD materials (the FWHM is converted to THz in Figure 5:11 where the pulse duration of the mode locked laser (Δt) in inversely proportion with the optical gain bandwidth ($\Delta \omega$) $\Delta t.\Delta \omega$=constant, where the wider optical bandwidth can produce shorter pulse duration (Derickson et al. 1992)).

It is obvious from Figure 5:11 that the InAsP material has wider bandwidth especially at low temperature. For example, at 150 K the gain bandwidth (the Full Width at Half Maximum) for the InP is 5 THz, whereas the InAsP material is doubled to approximately 12 THz.This difference decreases when temperature increases. As a result, the InAsP could be a good material to produce short pulse width in the case of using these materials in mode-locking regime. Moreover, the fact that the gain bandwidth can be modified by the temperature offers the potential for manipulating the pulse width in case of mode-locking.

However, what is crucial to improve the mode-locking system is the occupational probability of the carrier in the quantum dot system, as stated in Chapter two, where the random and non-thermal distributions can improve the mode-locking. This will be studied comprehensively in the next chapter.
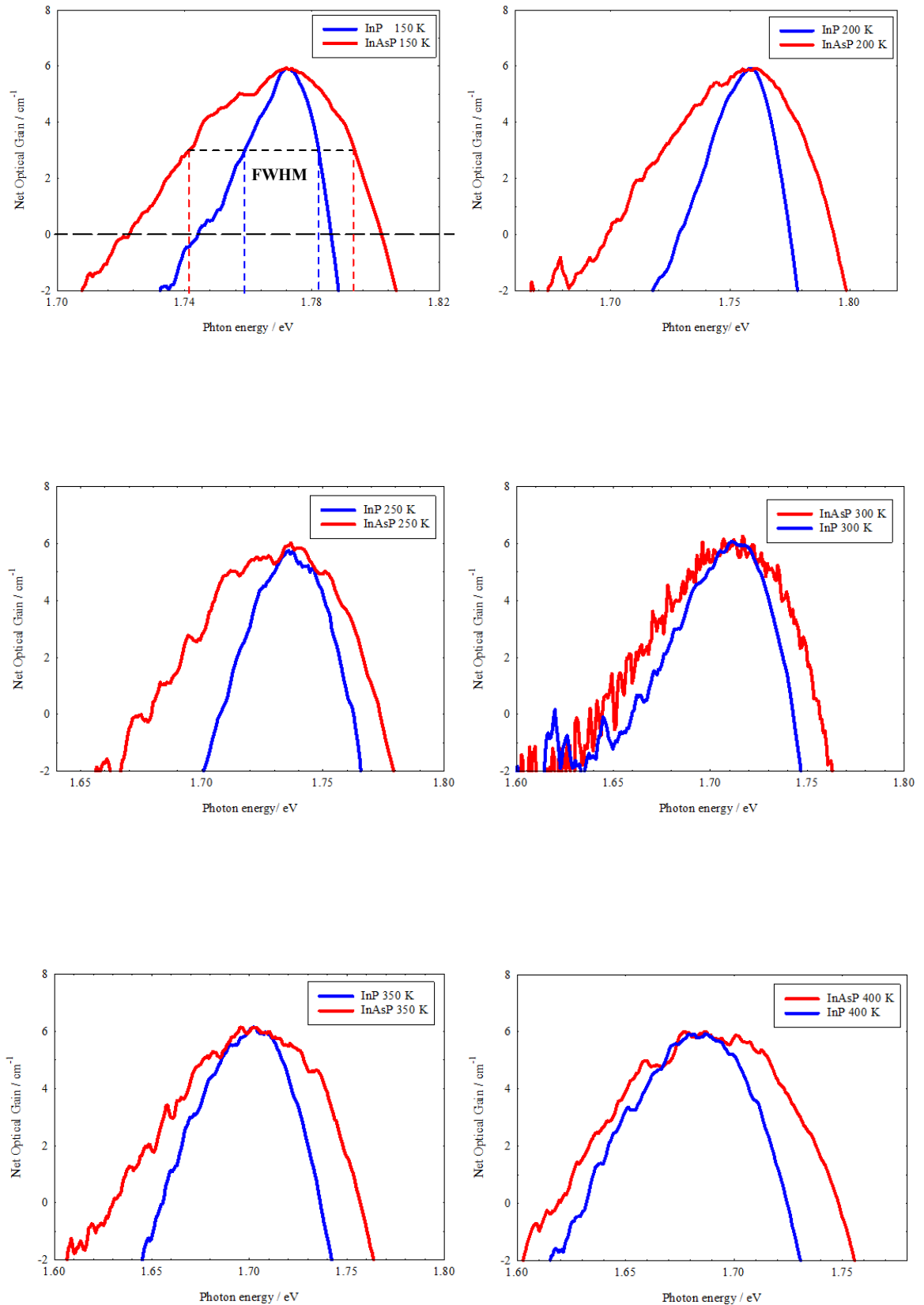
Figure 5:10 Bandwidth modal gain spectra for the InP and InAsP materials at different temperatures at approximately the same level of gain peak 6 cm⁻¹. The InAsP spectra were shifted by roughly 55 nm to allow comparison.
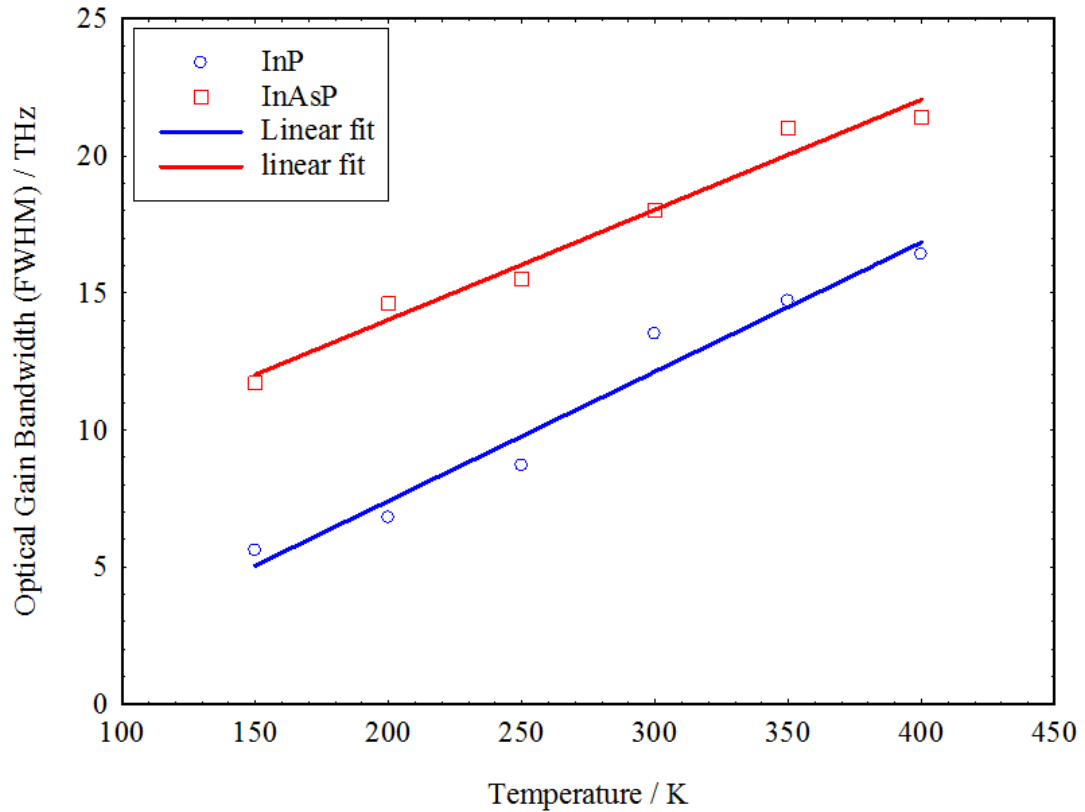
**Figure 5:11 Optical gain bandwidth as a function of temperature for
the InP and InAsP materials.**

5.6 Temperature effects on emission peaks

Gain peak energy and absorption edge energy as a function of temperature for the InP and InAsP materials is shown in Figure 5:12 at fixed peak model gain position 6 cm^{-1}, which corresponds to the threshold requirement of the 2mm long cavity devices, whereas for the modal absorption the absorption edge position was considered, as displayed in Figure 5:7 and Figure 5:8. In general, it can be clearly seen that the photon energy linearly decreases as the temperature increases and the absorption result is consistent with the gain one. This signifies that the energy gap of the materials decreases when the temperature increases, according to the Varshni Equation:

5:1

(Varshni, 1976)

where Eg (T) is the energy gap at temperature T, Eg (0) is the energy gap at 0 K, while α and β are adjustable parameters.

In fact, the decrease in the energy band gap with temperature can be understood when it is considered that the interatomic spacing of the semiconductor materials increases when the amplitude of the atomic vibrations increases owing to the increased thermal energy . An increased interatomic spacing decreases the potential seen by the electrons in the material, which in turn reduces the size of the energy band gap(O'Donnell and Chen 1991).

Table 5:2 depicts the temperature dependence coefficient of the emission energy for both the absorption and gain results calculated from Figure 5:12 for both InP and InAsP QD materials.

Materials	$\Delta E/\Delta T$ (meV/K)	
	Absorption edge	**Gain spectra peak at 6 cm^{-1}**
InP	-0.39	-0.37
InAsP	-0.36	-0.36

Table 5:2 Shows the temperature dependency coefficient of the emission energy for both absorption and gain results.

The energy ranges from 1.77 eV to 1.67 eV for the InP, whereas the InAsP ranges from 1.65 eV to 1.56 eV when the temperature changes from 150 to 400 K. Consequently, this corresponds to the emission wavelengths range from 700 nm to 742 nm for the InP and from 751 nm to 794 nm for the InAsP. The results at 300 K agree with laser spectral results for 2mm long cavity devices taken at room temperature (see Figure 4:5).The InAsP QD materials show a similar temperature dependence of emission energy to the InP QD.
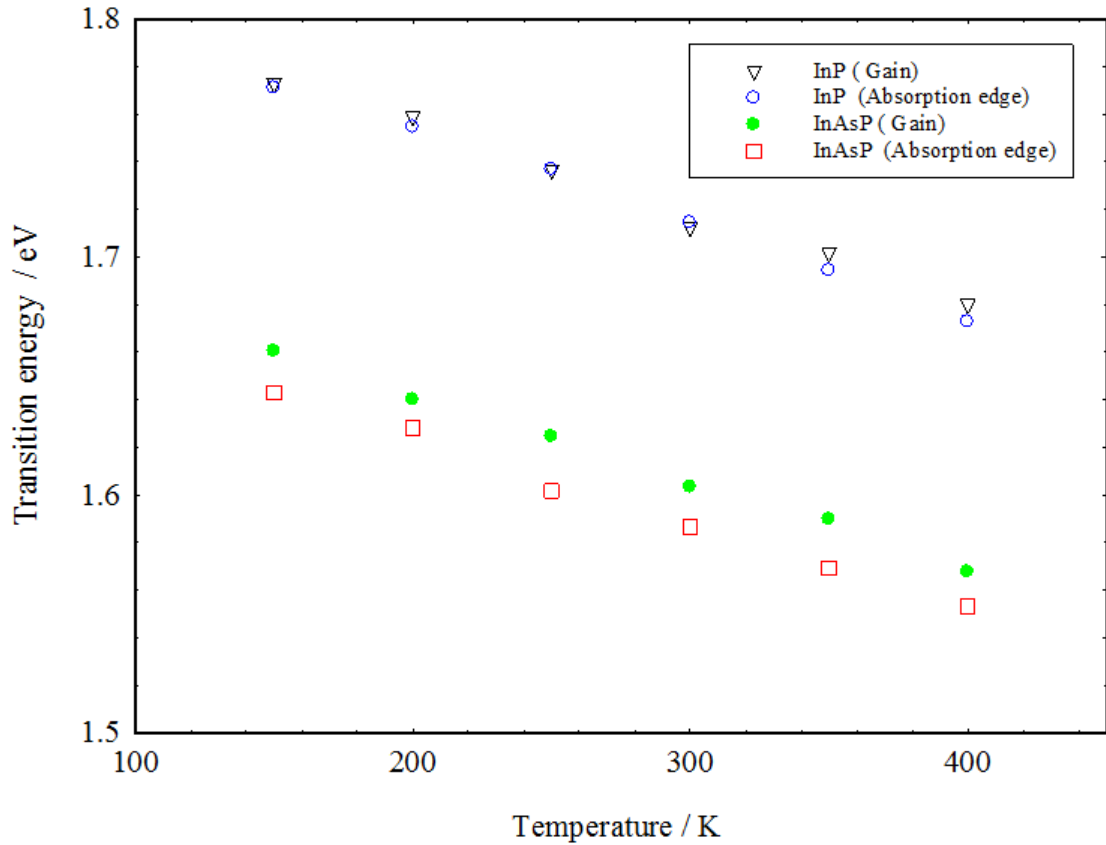
**Figure 5:12 Absorption edges and emission energies as a function
of the temperatures for the InP and InAsP QD materials.**

5.7 Summary

In this chapter, the modal gain and modal absorption of the InAsP and InP QD materials are studied as a function of temperature; namely, 150, 200, 250, 300, 350, 400 K. The results in this chapter illustrate that the InAsP QD materials have a wider amplifier bandwidth optical gain in comparison with the InP material at all the studied temperatures. This makes InAsP QD laser promising materials for the mode-locking laser. The results in this chapter also reveal that the temperature dependence of the emission energy is almost the same for both materials. Similarly, the InAsP QD structure depicts a slightly higher internal optical loss. Finally, the injection level of the InAsP QD materials displays less temperature sensitivity at low temperature, whereas it shows higher temperature sensitivity at a high temperature in comparison with the InP QD material.

5.8 References

Abdollahinia, A., Banyoudeh, S., Rippien, A., Schnabel, F., Eyal, O. Cestier, I., Kalifa, I., Mentovich, E., Eeisenstein, G. and Reithmaier, J.P. **2018**. Temperature stability of static and dynamic properties of 1.55 μm quantum dot lasers. Optics Express 24(5), pp.6056-6066.

Derickson, J., Helkey, J., Karin, R.,. Wasserbauer, G., and Bowers, E. **1992**. Short pulse generation using multisegment mode-locked semconductor lasers. IEEE Journal of quantum electronics 28(10). pp.2186-2202.

Kasim, M., Elliott, S., Krysa, A. and Smowton, P. M. **2015**. Reducing thermal carrier spreading in InP quantum dot Lasers. IEEE ournal of selected topics in quantum electronics, 21(6).

O'Donnell, K. P. and. Chen, X. **1991**. Temperature dependence of semiconductor band gaps. Appl. Phys. Lett. 58 (25), pp. 2924-2926.

Pikhtina, N. A. Slipchenkoa, S. O., Shashkina, I. S., Laduginb, M. A., Marmalyukb, A. A. Podoskina, A. A. and Tarasova I. S. **2010**. The Temperature Dependence of Internal Optical Losses in Semiconductor Lasers (λ = 900–920 nm). Semiconductors 44(10), pp. 1365–1369.

Smowton, P. M., Pearce, E., Lutti, J., Matthews, D., Summers, H.D., Lewis, G., Blood, P., Hopkinson, M. and Krysa, A. **2004**. Carrier distribution, spontaneous emission and gain in self assembled quantum dot lasers. In Proceedings of SPIE - The International Society for Optical Engineering, 5365. pp. 86–95.

Smowton, P. M, Stella, N. E., Samuel, S., Al-Ghamdi, M. S. and Krysa, A.B. **2011**. Temperature-Dependent Threshold Current in InP Quantum-Dot Lasers. IEEE Journal of selected topics in quantum electronics 17(5), pp.1343-1348.

Varshni, Y.P. **1976**. Temperature dependence of the energy gap in semiconductors. Physica, 34(1), pp.149–154.

Chapter (6) Carrier distribution in InP and InAsP quantum dot lasers

6.1 Introduction

As mentioned in Chapter two, the carrier distribution plays a significant role in a mode-locked laser, where the non-thermal and random distribution can support mode-locking. In fact, the deeper dot potential pertaining to the InAsP QD material shown in Section 4.7 in Chapter four could indicate that this material is more likely to demonstrate non-thermal distribution. Moreover, the faster carrier dynamic makes recovery time of the absorber section faster which is positive point for mode-locking.

This chapter focuses on carrier distribution in InP and InAsP QD materials at different studied temperatures; namely, 150, 200, 250, 300, 350, and 400 K. This chapter reveals how temperature affects the occupational probability of the carriers in both the InP and InAsP QD materials. The first section of the chapter demonstrates the unamplified spontaneous emission spectra of the materials and the effect of temperature, besides the driven current density on the spontaneous emission spectra. In the following sections the population inversion factor is calculated at each studied temperature, while the carrier temperatures are also studied. After that spontaneous emission spectra are measured in a real unit and radiative currents in QD materials are studied, the internal quantum efficiencies are also calculated for the materials.

6.2 Spontaneous Emission

6.2.1 Unamplified spontaneous emission of InP and InAsP materials

Using the segmented contact method, the spontaneous emission spectrum was measured by means of Equation 3:10 under transverse electric (TE) polarisation as a function of the driven current density at different temperatures; specifically, 150, 200, 250, 300, 350 and 400 K for both the InP and InAsP QD materials.

Figure 6:1 and Figure 6:2 represent the unamplified spontaneous emission spectra in arbitrary units as a function of driven current density for the InP and InAsP QD materials respectively at 150 K. In general, the spontaneous emission amplitude increases when the driven current density increases and the peak energy of the spectrum (the distribution is due to the inhomogeneous broadened QD states) shifts towards higher energy emission (shorter wavelengths). This is consistent with shifting of the peak modal gain with pumped current density seen in Figure 5:1 and Figure 5:2 in Chapter five. The blue shift of the spectra wavelength with increasing of the injected carrier density is due to state filling effects.

Moreover, the spontaneous emission spectra for the InAsP QD materials are wider than these for the InP QD materials at fixed threshold gain. This is a result of the greater degree of inhomogeneous broadening in the ground state shown in the absorption spectra in Figure 4:9. The area under the curve which is related to the spontaneous radiative recombination rate also increases with injected current density.

However, the unamplified spontaneous emission spectra should be measured in real units in order to determine the area under the curves in real units. This requires the calibration factor mentioned in Section 3:7.4 in Chapter three, This will be determined later in this chapter in Section 6.3.1.
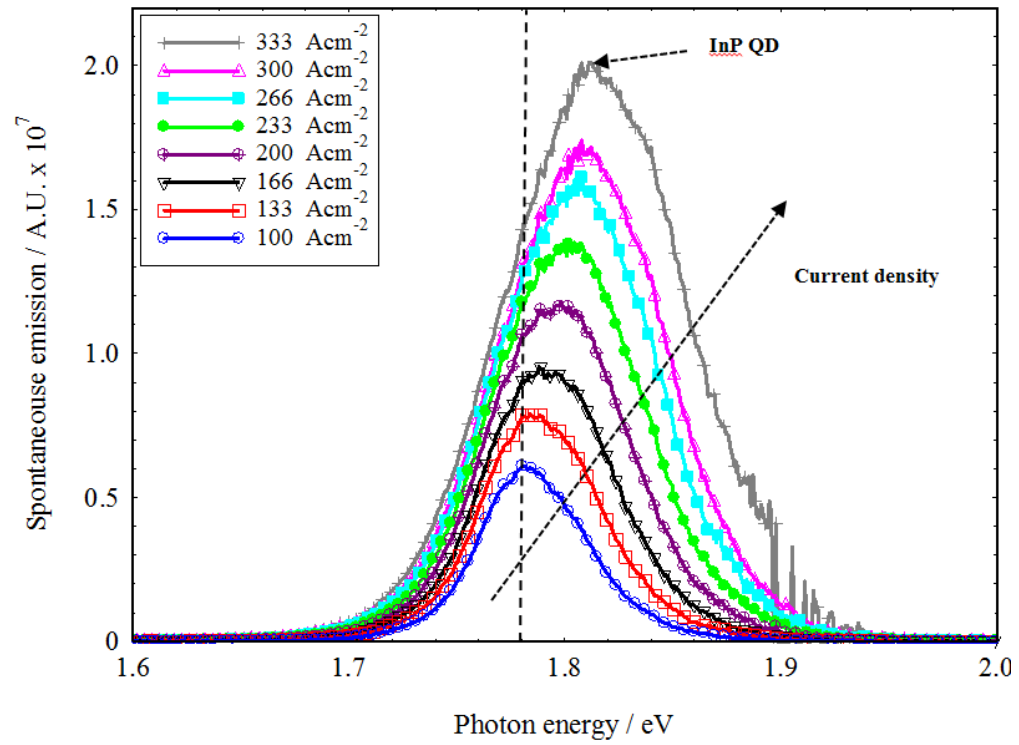
Figure 6:1 Unamplified spontaneous emission spectra as a function of driven current density for InP QD at 150 K.
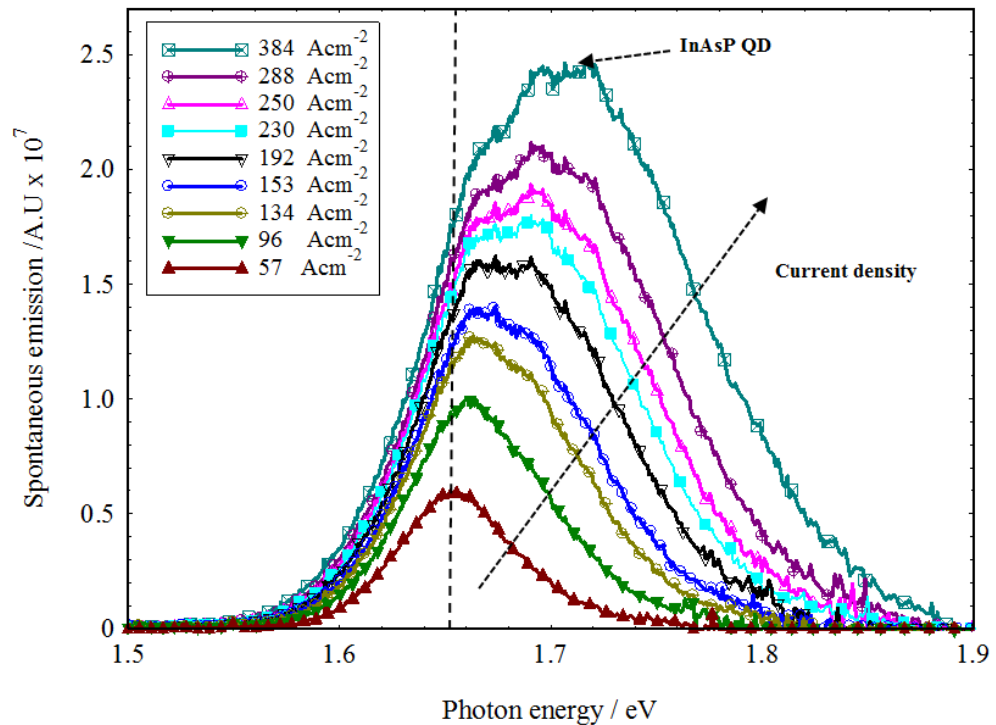

Figure 6:2 Unamplified spontaneous emission spectra as a function of driven current density for InAsP QD at 150 K.

6.2.2 Temperature effect on unamplified spontaneous emission

Figure 6:3 and Figure 6:4 show the profile of the normalised spontaneous emission spectra corresponds to the distribution of charge carriers among the available energy states for InP and InAsP QD material, at each studied temperature; namely, 150, 200, 250, 300, 350 and 400 K at a fixed optical gain coefficient (6 cm^{-1} which corresponds to the threshold of a 2mm laser) calculated by means of Equation 3:10 under transverse electric (TE) polarisation.

The emission peak shifts toward lower photon energy positions (longer wavelengths) when the temperature increases. This is consistent with the shifting of the modal gain peak and absorption edges with the temperature described in Section 5.6 in Chapter five which is due to the shrinking in the mean energy gap of the semiconductor materials when temperature increases. Moreover, as the temperature increases the breadth of the profile spectrum increases due to thermal spread of the carriers amongst dot states.
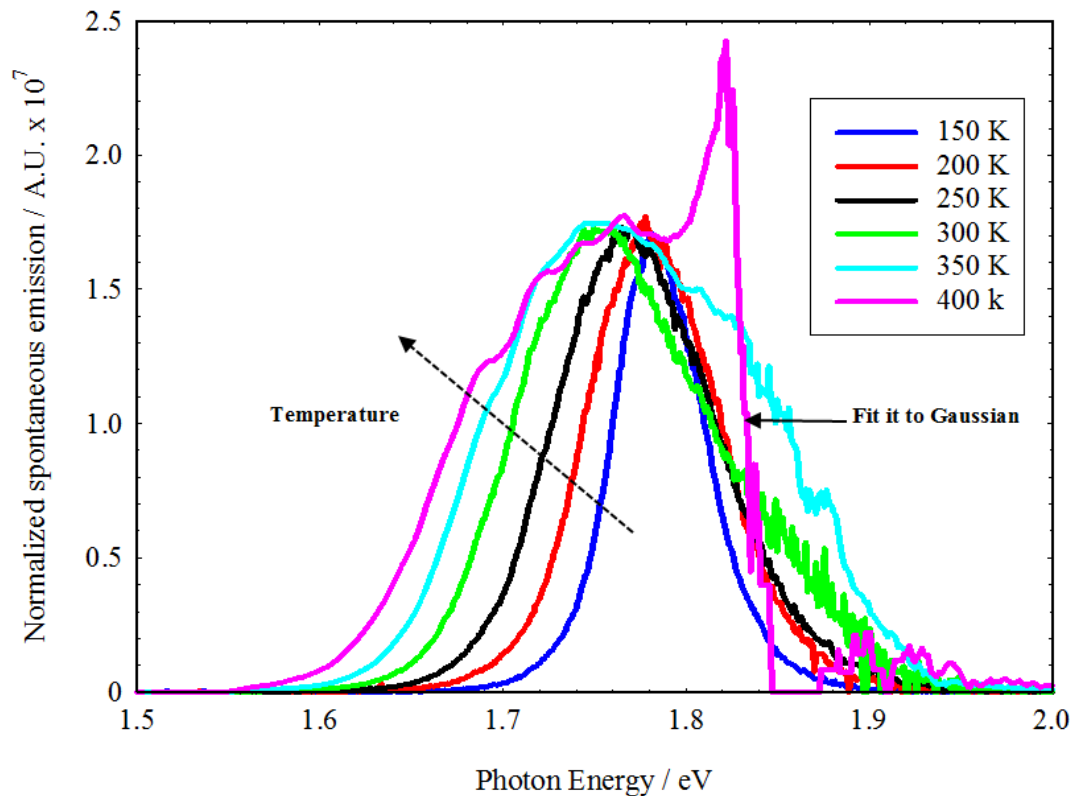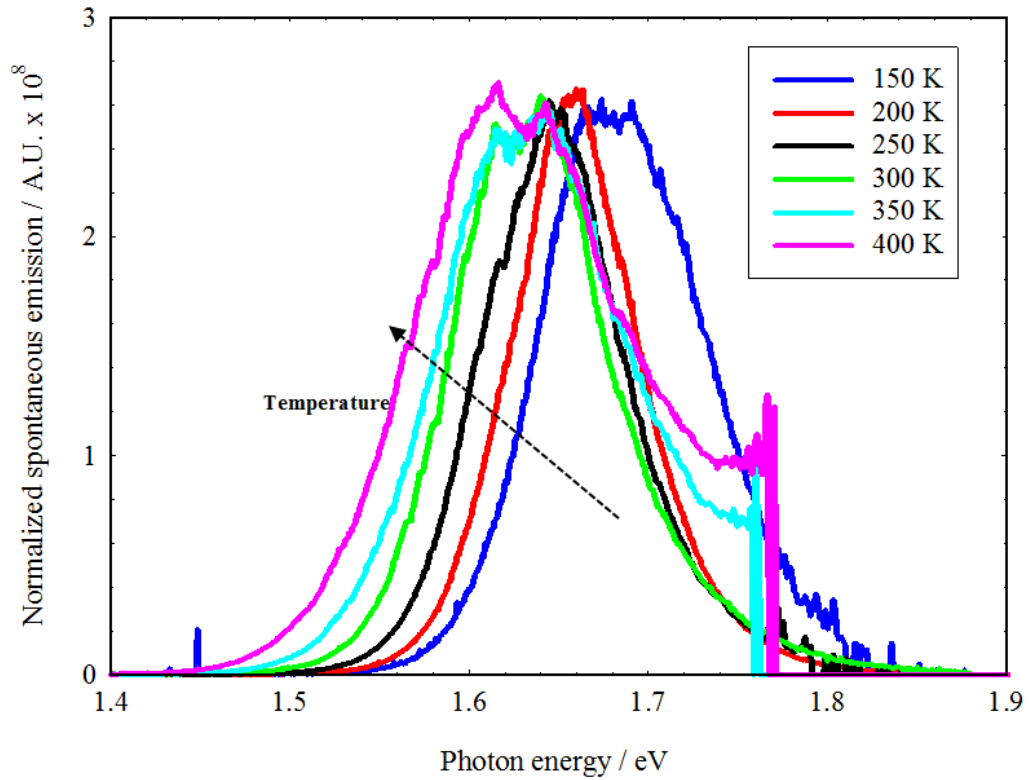

Figure 6:3 Normalised spontaneous emission spectra for InP at 150, 200, 250, 300, 350,400 K at a fixed optical gain coefficient (6 cm^{-1}).

Figure 6:4 Normalised spontaneous emission spectra for InAsP at 150, 200, 250, 300, 350,400 K at a fixed optical gain coefficient (6 cm⁻¹).

It is beneficial here to study the (FWHM) of the spontaneous emission spectra peak as a function of temperature and compare this with the temperature dependence of the threshold current density of 2mm lasers for the InP and InAsP QD lasers shown in Figure 4:3. This FWHM is plotted as a function of temperatures along with threshold current density for the InP and InAsP materials in Figure 6:5 and Figure 6:6 respectively.

The FWHM of the spontaneous emission spectra in the InP quantum dot state increases with the temperature, similar to their threshold current density, whereas in the InAsP structure, the FWHM of the spontaneous emission spectra decreases when the temperature moves from 150 K to 200 K and subsequently increases with a temperature similar to their threshold current density.

The broadening of the spontaneous emission spectra with increasing temperature is likely to be due to an increasing spread in the carrier distribution with temperature and it is likely that this is ultimately responsible for increasing threshold current density with increasing temperature.

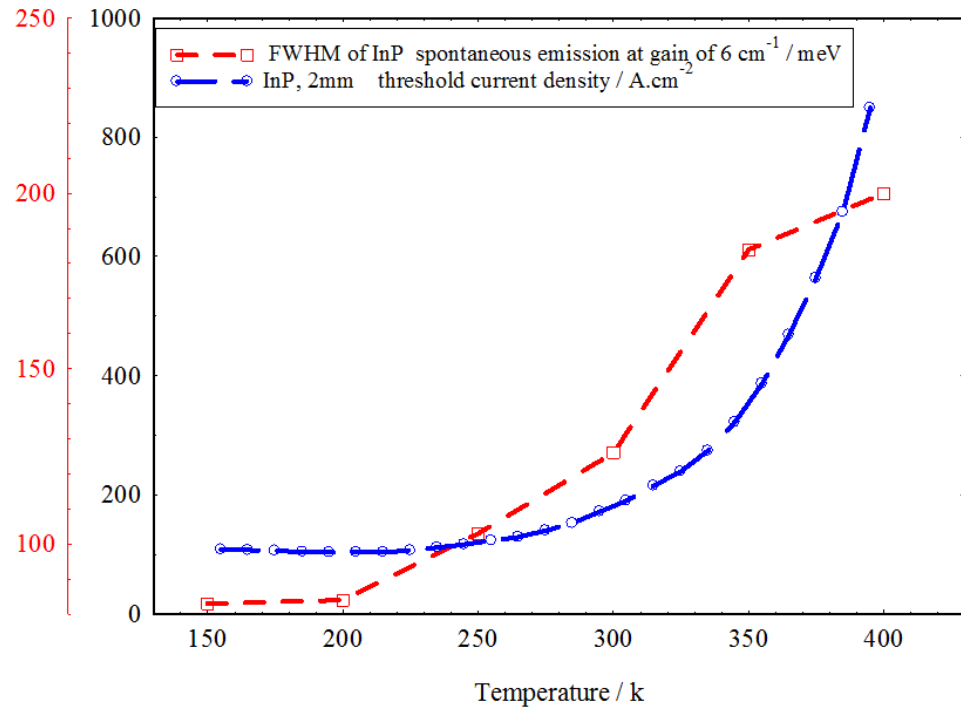**Figure 6:5 (FWHM) of the spontaneous emission spectra peak as a function of temperature, compared with the temperature dependency of the threshold current density of 2mm lasers for the InP QD.**
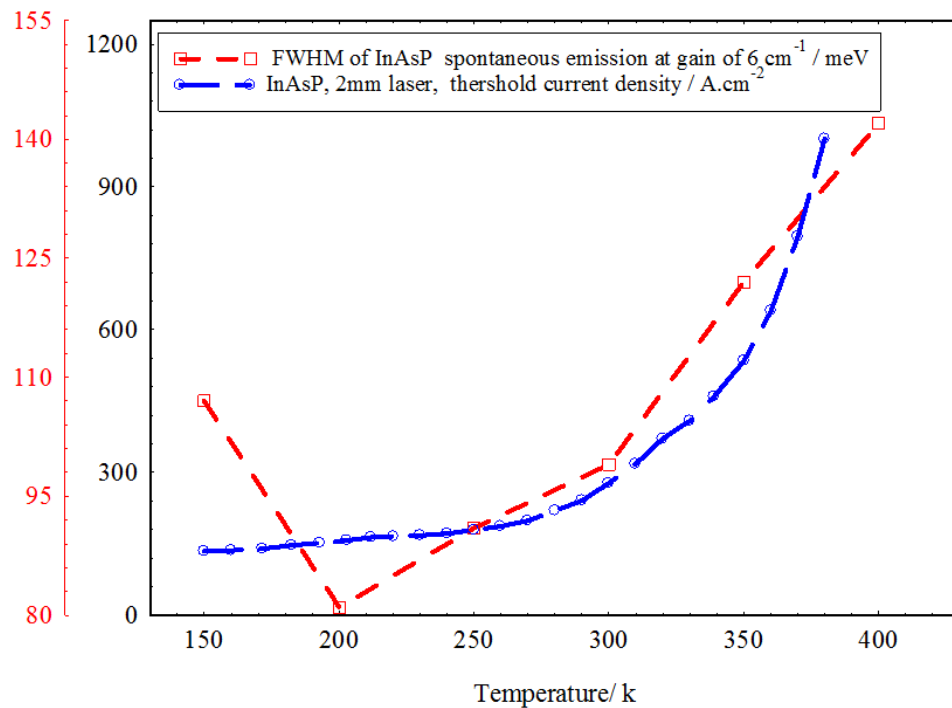

Figure 6:6 (FWHM) of the spontaneous emission spectra peak as a function of temperature and compare this with the temperature dependency of the threshold current density of 2mm lasers for the InAsP QD.

The most important point indicates in Figure 6:6 is that the the InAsP QD material at 150 K show significant broadening which is not flow the behaviour of the threshold current dependency of the laser device and this could indicate non-thermal distribution of the carrier for this material at 150 K. this is studied more precisely in the Section 6.3.2.

6.3 Population inversion and carrier temperature

6.3.1 Population inversion and calibration factor

To study how the carriers populate the available states of a semiconductor material, the population inversion factor $P^{meas}(hv)$ is a key quantity. It is a number which consists of only the occupational probabilities of states that have a certain energy separation hv (Summers 2001). This factor was introduced in Section 3.7.4 in Chapter three and was clarified how it can be determined using the segmented contact method.

Population inversion factor $P^{meas}(hv)$ was calculated for both the InP and InAsP samples as a function of the driven current density at different temperatures (150, 200, 250 300, 350 and 400 K), in order to investigate the distribution of the carriers in the materials at these temperatures. Moreover, it was also calculated to find the calibration factor (C) mentioned Section 3.7.4 in Chapter three with the aim of calculating the emission temperature of the QD materials. Subsequently, the carrier distribution within the OD states was investigated and the spontaneous emission spectra in real units were calculated and calibrated.

Figure 6:7 represents the $P^{meas}(hv)$ factor, calculated by means of Equation 3:11 over a range of injection levels (384, 480, 770, 960 and 1150 A.cm^{-2}) for InAsP QD lasers at 300 K, as a function of photon energy.

In Figure 6:7, $P^{meas}(hv)$ takes its maximum value (lowest photon energy region) and saturates with respect to increasing current. From this region, the calibration factor can be determined, whereas for the InAsP at 300 K, the inverse of the calibration factor is calculated as 2.1 x 10^{12} eV^{-1}.sec^{-1}.cm^{-2}.
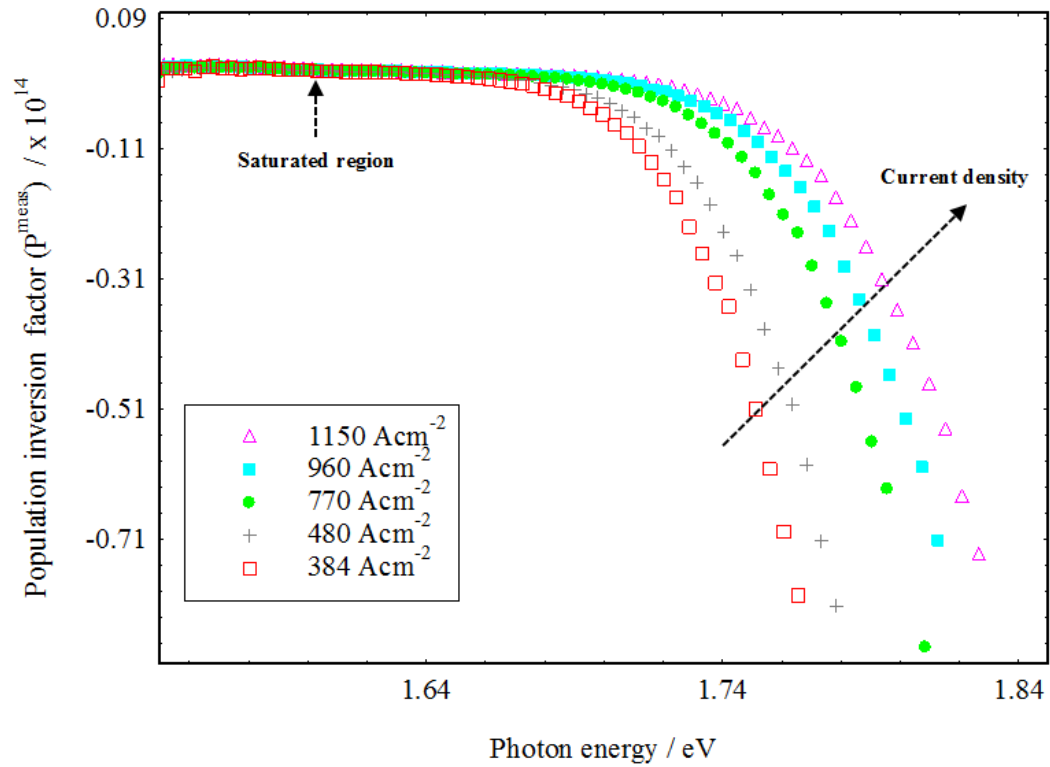
Figure 6:7 P factor spectra over a range of injection levels for the InAsP QD lasers at 300 K.

In a similar way the calibration factor is calculated at each studied temperature for both the InP and InAsP QD materials. Table 6:1 represents the inverse calibration factors for the InP and InAsP QD materials at each temperature.

Inverse of the calibration factor: 1/C ($eV^{-1}.sec^{-1}.cm^{-2}$)		
Temperature (K)	InP	InAsP
150	1.77×10^{13}	5.4×10^{12}
200	2.06×10^{13}	9.86×10^{11}
250	7.54×10^{12}	9.1×10^{11}
300	1.2×10^{13}	2.1×10^{12}
350	7.12×10^{12}	1.5×10^{12}
400	6.5×10^{12}	5.23×10^{11}

Table 6:1 the inverse of the calibration factor at each studied
temperature for both the InP and InAsP QD. materials.

Table 6:1 reveals that the calibration factor varies from material to material and also when temperature changes for the same material. This arises from the fact that the calibration factor depends on the experimental circumstances. For example at each temperature the experimental set up needs to be realignment as well as the wavelength and the near-filed profile vary with temperature.

Now after calculating the calibration factor it is possible to determine the $P^{meas}(hv)$ spectra in real units ($eV^{-1}.sec^{-1}.cm^{-2}$) as well as the spontaneous emission spectra in real units.

6.3.2 Occupation probability and carriers temperature

As mentioned in Chapter two the carrier distribution in the quantum dot system could be distributed in three different modes: thermal, non-thermal and random distribution. Here, Equation 2:33 in Chapter two described a technique able to study carrier distribution in QD materials which was introduced by (Hutchings et al. 2014), used to investigate the occupation probability of the carriers in the quantum dot system for the InP and InAsP QD lasers at different temperatures; specifically, 150, 200, 250, 300, 350 and 400 K.

Figure 6:8 is the plot of $ln(1-p^{meas})$ against photon energy for the InAsP materials at 300 K at different levels of the current density. Figure 6:8 reveals a set of linear plots in specific spectra regions which have almost similar gradients.

The linearity of the plots indicates that the occupation probability within the QD states can be described by Fermi-Dirac statistics. From the gradients, it is possible to calculate a single emission temperature (T_E) at each injection level from Equation 2:33 in Chapter two. These plots give an average slop of 33 ± 4 eV^{-1} which is corresponding to the emission temperature (T_E) of (330 ± 25 K).
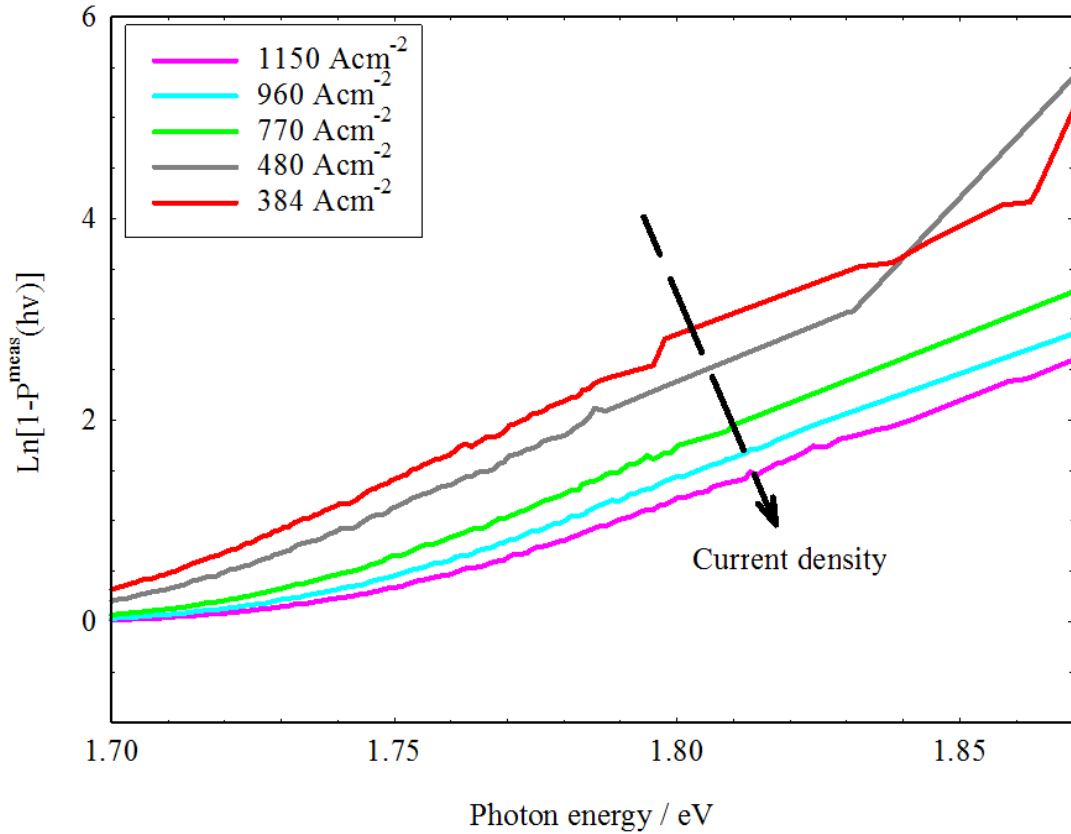
Figure 6:8 Plot of the ln(1-p^m) against photon energy for the InAsP materials at 300 k at different levels of the current density.

the emission temperature is slightly higher than the lattice temperature by approximately 30 K and this is due to homogeneous broadening in the quantum dot system (which mostly arises from Coulomb carrier-carrier correlation and dynamics of carrier capture and emission in QD structure (Uskov 2001), so, in this case, the emission temperature is almost consistent with lattice temperature which is 300 K This indicates that the carriers are distributed thermally in the quantum dot system at this temperature (300 K), according to the definition of this technique (see Section 2.6 in Chapter two).

To investigate the occupation probability of the carriers at all studied temperatures for both the InP and InAsP materials, the plots of $\ln(1-p^{meas})$ against photon energy at each studied temperature; specifically, 150, 200, 250, 300, 350 and 400 K at a fixed peak gain, which is 6 cm^{-1}, are shown in Figures 6:9 and 6:10 for the InP and InAsP QD materials respectively.

**Figure 6:9 Logarithmic plots of [1-P(hv)] versus photon energy for InP QD
at different temperatures at a fixed peak gain (6 cm⁻¹) with the liner fitting.**

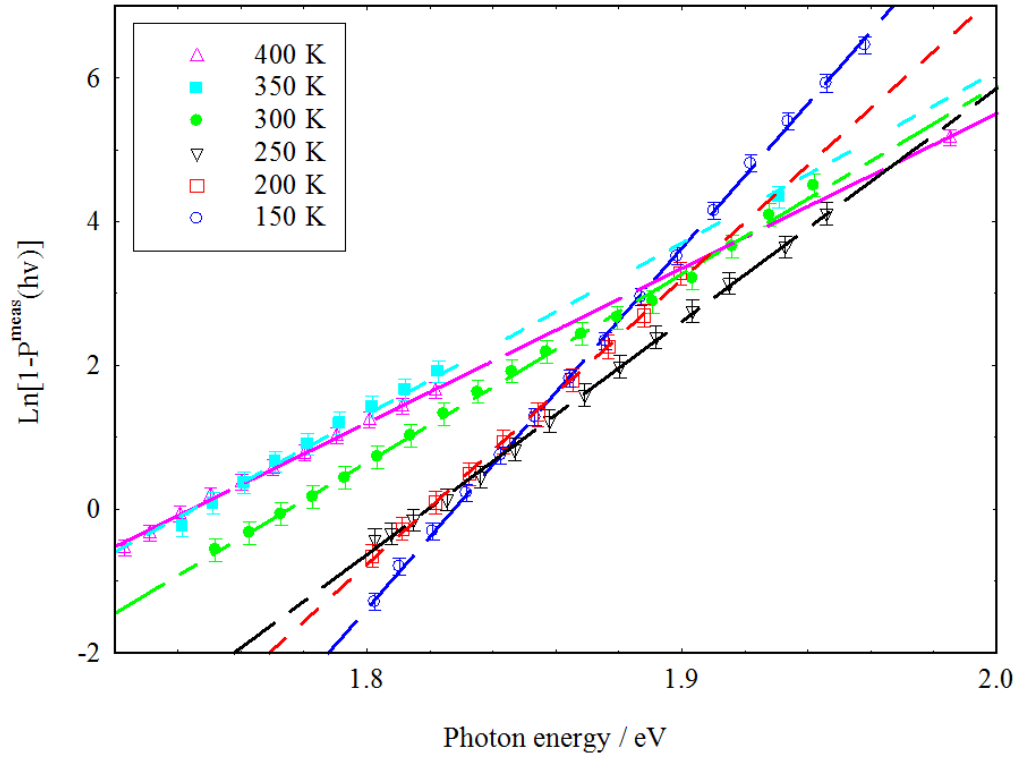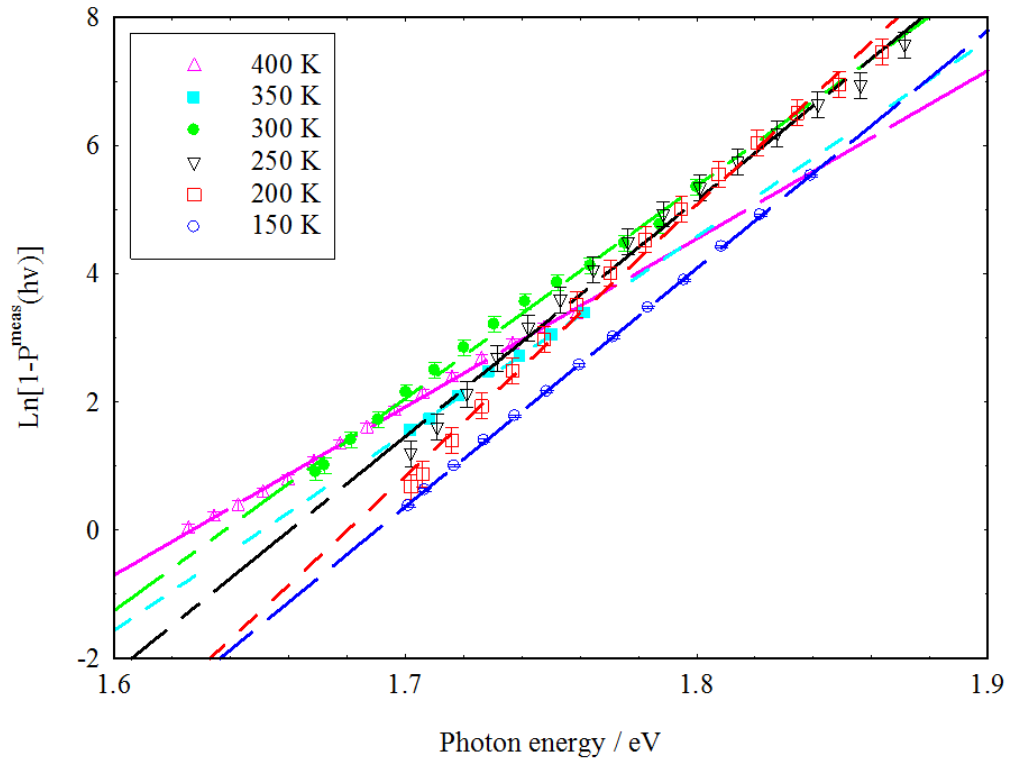**Figure 6:10 Logarithmic plots of [1-P(hv)] versus photon energy for InAsP QD
at different temperatures at a fixed peak gain (6 cm⁻¹) with the liner fitting.**

Table 6:2 reveals the result of the emission temperature calculated from Figure 6:9 and Figure 6:10. The results illustrate that for both InP and InAsP QD materials, the emission temperatures show higher values than the lattice temperatures in the rang range from 30 to 60 K and this is thought to be due to the homogeneous broadening effect, as similar effect were seen in InAs QD lasers (Hutchings et al. 2014). The only point which deviates from this behaviour is InAsP QD material at 150 K, where the emission temperature is more than doubled compared to the lattice, as it shown in Figure 6:11. This could indicate that the carrier distribution at 150 K tends to non-thermal equilibrium. This could be due to the higher energy separation between dot states and quantum well states for the InAsP QD material shown in the E-PVS measurements (see Figure 4:13 in Chapter four). This result is also consistent with Figure 5:10 and 5:11 at 150 K, where the InAsP QD material shown wider optical gain bandwidth than InP one by more than doubled In comparison with the rest studied temperatures, where the non-thermal distribution broadens both spontaneous emission and optical gain spectra. On the other hand, it is found that the elastic coulomb interaction with carriers in the barrier/wetting layer material in the QD materials is quenched below 150 K due to the decreased thermal occupation of the high-energy states with decreasing temperature (Borri et al. 2002), and this could be more obvious in the InAsP QD material due to deeper dot confinement

Lattice Temp.(K)	InP	InAsP
	Emission Temp. (K)	Emission Temp. (K)
150	200 ± 10	323 ± 5
200	255 ± 11	252 ± 22
250	285 ± 12	276 ± 25
300	350 ± 15	330 ± 25
350	405 ± 22	385 ± 17
400	470 ± 17	460 ± 21

**Table 6:2 Lattice and emission temperatures
for both the InP and InAsP QD materials.**

The non-thermal distribution of the carrier in the quantum dot system means that the rate of the carriers recombination from the dot states is faster than the thermal distribution of the carriers via the well states (Sugawara et al 1997). Therefore, the non-thermal distribution makes the lasing spectra wider, hence, shorter pulse duration can be obtained in case of using this material in monolithic passive mode-locked laser.
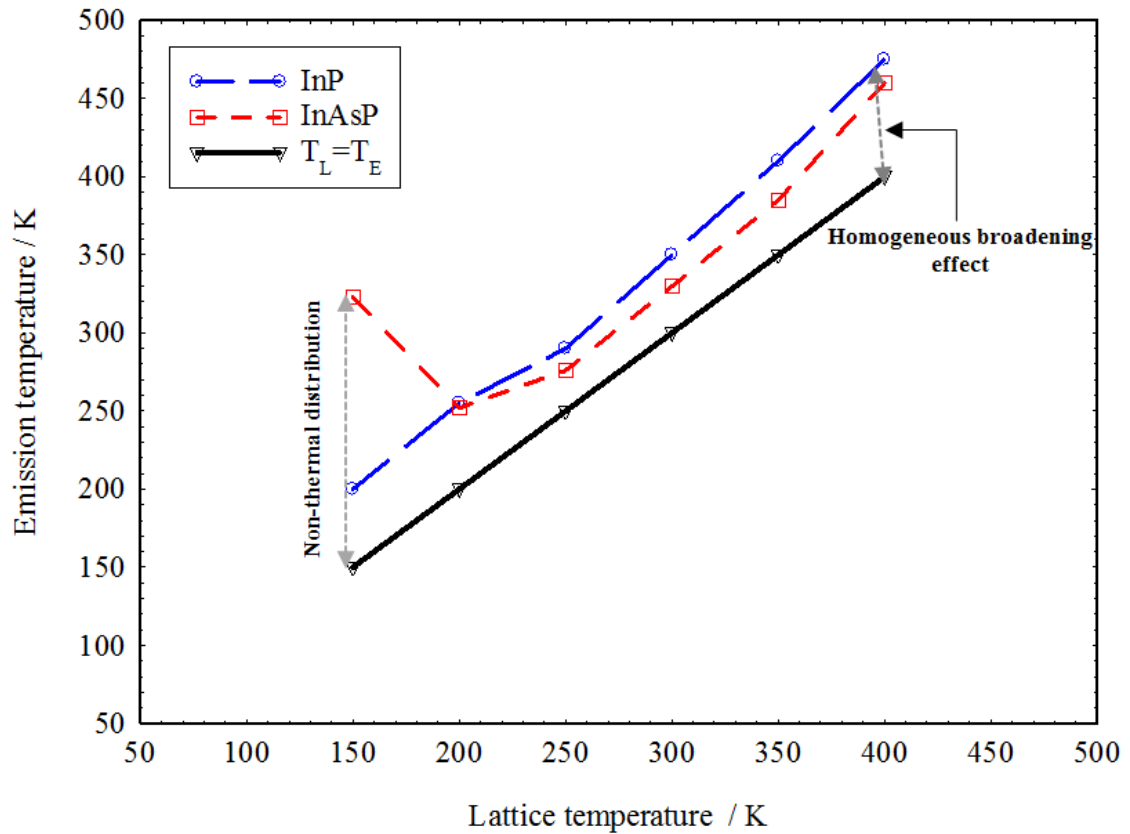

Figure 6:11 Lattice temperature against emission temperature for InP and InAsP QD materials at a fixed peak gain (6 cm^{-1}).

6.4 Spontaneous emission in real unit and quantum internal efficiency

Characterization of the vital optical properties such as radiative recombination current density and radiative efficiency is essential for developing new QD laser materials (Dang et al 2012) . The spontaneous emission spectra in Figure 6:1 and Figure 6:2 is in arbitrary units. Calculating the spontaneous emission spectra in real units, required calibration factors at each temperature. Subsequently, Equation 3:12 in Chapter three is employed to convert the spontaneous emission into real units. Figures 6:12 represents

the spontaneous emission spectra for InAsP QD material at 150 K in real unit. The area under the spontaneous emission spectrum gives the radiative carriers rate, by ultiplying this rate by the electron charge gives the radiative carriers in the QD material.
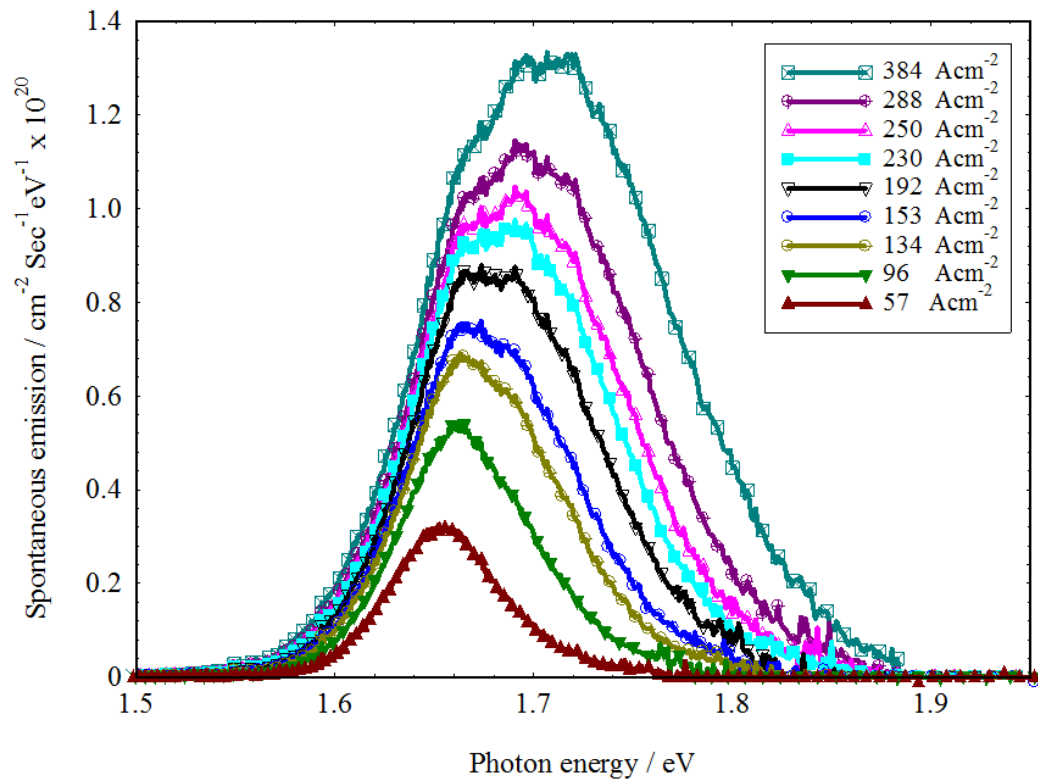

Figure 6:12 Unamplified spontaneous emission spectra in real units as a function of driven current density for InAsP QD at 150 K.

Figure 6:13 plots the radiative current density calculated for spontaneous emission spectra in real units, as a function of the driven current density for the InP and InAsP QD materials at 300 K. The gradients of the plots give the radiative efficiency (total radiative current divided by total current) of the materials, which for InP is roughly 11%, whereas for the InAsP materials it is lower, approximately 5%. This signifies that the non-radiative recombination in the InAsP is faster (where the radiative current rate inversely proportional with carrier life time (Hetitz et al 1997)). Consequently, this could be a sign that the recombination rate for the InAsP structure is faster than the one for the InP structure. This could make the InAsP QD material a suitable material for mode-locked regime where the recovery time of the absorption section will be faster (Guina et al. 2007) due to faster curriers dynamic in InAsP QD material.
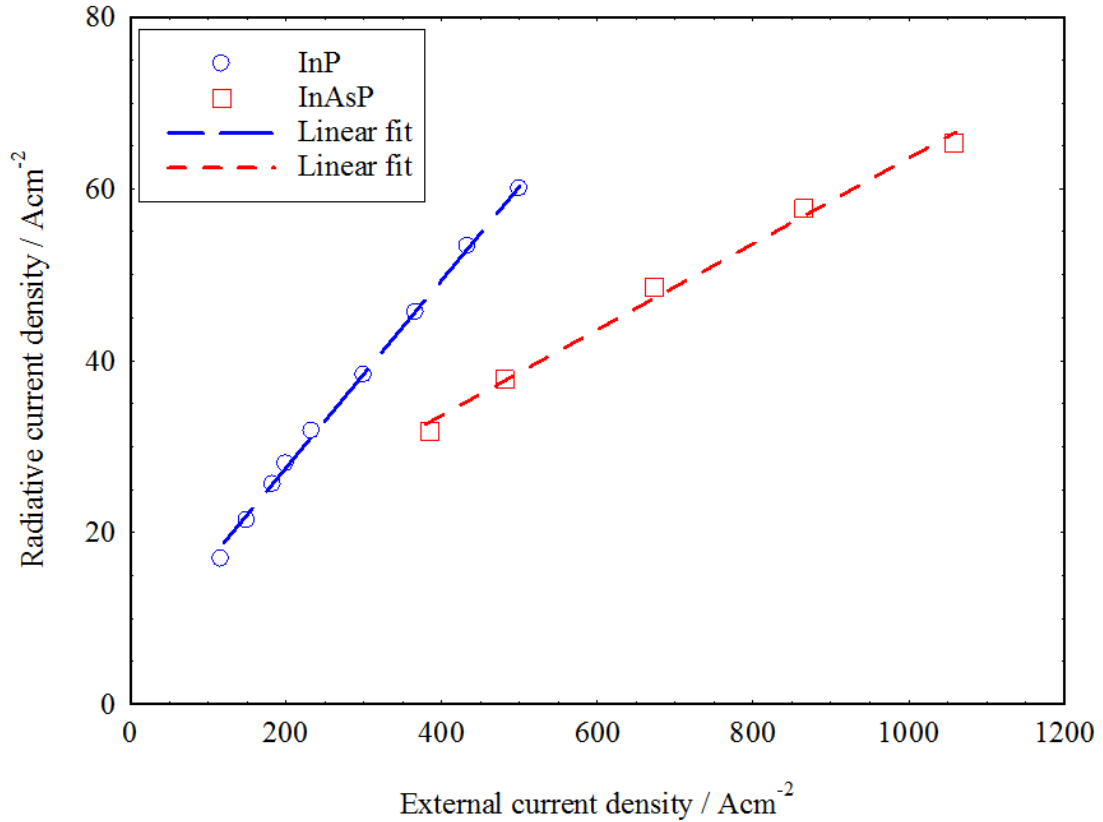
**Figure 6:13 Radiative current density versus external current
density at 300 K for the InP and InAsP QD lasers.**

6.5 Summary

This chapter has focused on carrier distribution in the InP and InAsP QD materials at
different studied temperatures; namely, 150, 200, 250, 300, 350, and 400 K. The
investigation of the carrier distribution in this chapter reveals that the InAsP QD
materials tend to populate non-thermally at 150 K. This is a positive sign in the case of
using this material in a mode-locked regime. Furthermore, another important aspect
displayed in this chapter is that the InAsP QD material demonstrates a faster
recombination rate than the InP. This can also support passive mode-locking, which
makes the recovery time for the absorption section quicker.

6.6 References

Borri, P., Langbein, W., Schneider, S., Woggon, U., Sellin, R. L., Ouyang, D. and Bimberg, D. **2002**. Exciton relaxation and dephasing in quantum-dot amplifiers from room to cryogenic temperature. IEEE Journal of selected topics in quantum electronics 8(5), pp.984-991.

Dang, C., Lee, J., Breen, C., Steckel J.S., Coe-Sullivan, S,.and Nurmikko, A. **2012**. Red, green and blue lasing enabled by single-exciton gain in colloidal quantum dot films. Nature Nanotechnology 7(5) pp.335-339.

Guina, M., Tuomisto, P., Okhotnikov, O. G., Marcinkevicius, S., Mizohatad K. and Keinonen, J. **2007**. Semiconductor saturable absorbers with recovery time controlled through growth conditions," SPIE Proc. 6451, pp.113–1 -113–7.

Heitz, R., Veit, M. N., Ledentsov, N., Hoffmann, A.and Bimberg D. **1997**. Energy relaxation by multiphonon processes in InAs/GaAs quantum dots. Physical Review B 56(16), pp.10435-10444.

Hutchings, M., O'Driscoll, I., Smowton, P. M., and Blood, P. **2014**. Fermi-dirac and random carrier distributions in quantum dot lasers. Applied Physics Letters 104(031103), pp.1-4.

Sugawara, M., Mukai, K. and Shoji, H. **1997**. Effect of phonon bottleneck on quantum-dot laser performance. Appl. Phys. Lett. 71(19), pp.2791-2793.

Summers, H., Thomson, J., Smowton, P. M., Blood, P. and Hopkinson, M. **2001**. thermodynamic balance in quantum dot. Semiconductor science and technology 16, pp.140–143.

Uskov, A.V. **2001**. Line broadening caused by Coulomb carrier -carrier correlation and dynamics of carrier capture and emission in quantum dots. Applied Physics Letters 97(11), pp.1679-1681.

<u>Chapter (7) Conclusion and further work</u>

7.1 Summary and conclusions

In this thesis, new quantum dot materials were introduced (InAsP) that are compatible with InP QD laser structure and grown in appropriate conditions for standard InP QD laser with regards to biophotonics and monolithic systems applications.

The InAsP QD lasers demonstrate a good performance, even though the threshold current density of the InAsP QD lasers is higher. For example, the 2mm long cavity of the InAsP QD laser shows an increase of 100 A.cm^{-2} compared to the same cavity length of reference InP QD laser at room temperature. The higher threshold current densities for InAsP QD devices is due to; the increase in internal optical losses shown in Chapter four, increases in the optical gain bandwidth shown in Chapter five and increase of the non-radiative recommendation rate observed in Chapters six. However, the temperature sensitivity of the InAsP QD lasers is similar to the InP ones, while peak power in the pulse above 250 mW is achieved with negligible reduction in slope efficiency compared to the InP reference structure. Moreover, the main factor behind this material, was to extend the emission wavelength toward longer wavelengths, where in relation to the InP QD laser there is a limitation in the growing due to the large dot size required to extend the operation wavelength. Additionally, the InAsP QD materials reveal a shift of approximately 55 nm towards longer wavelengths (out to almost 780 nm is possible with this material), which consequently, makes this InAsP QD material a prospective QD laser that can be applied in biophotonic applications.

The InAsP material display several positive points that make it an attractive candidate for generation of mode-locked, ultrashort pulses; for instance, the greater degree of inhomogeneous broadening shown in modal absorption which is due to dot size variation seen in the TEM images. Moreover, the modal gain measurements at different temperatures 150, 200, 250, 300, 350 and 400 K, reveal a wider amplified optical bandwidth for the InAsP QD materials, at all studied temperatures.

Similarly, the InAsP QD material illustrates faster recovery time regarding the absorption. What is more, the currier distribution study shows that the InAsP QD material has a tendency to non-thermal distribution at 150 K and this could be due

to higher energy separation between the QD states and QW states seen in the E-PVS measurements (EPVS measurements confirmed deeper dot confinement for the InAsP QD materials by approximately 103 meV than the InP QD material). All these factors can make the InAsP QD a good candidate material when used in monolithic passive mode-locked regime. In addition, the deeper dot confinement for InAsP QD material could be the reason of the sign of the non-thermal distribution only at 150 K. So much deeper dot confinement could make the carriers to be distributed non-thermally above 150 K.

Finally, the compatibility of the InP and InAsP structures can open the door to growing both dots in the same structure. This will give extremely broad optical gain which brings several advantages, such as mode-locking, tunability resources, in addition to monolithic regimes.

7.2 Future work

The work in this thesis has introduced an original QD material for QD laser applications compatible with standard InP QD lasers. From the results and discussion presented in the previous chapters, future work can be classified as follows:

- Growth of the InAsP QD material was performed under conditions appropriate for InP QD. The relatively small increase in threshold current density of the InAsP dot lasers may be improved following growth optimisation, such as changing the growth temperature of the dot and adjacent layers for the InAsP dots.

- There is a possibility of growing both InP and InAsP dots in the same structure, creating broadband or extensively tunable sources.

- Studying the effect of fraction of As in the InAsP QD materials would extend the operation wavelength range of the InP QD lasers more towards longer wavelengths and also would create much deeper dot confinement for.

- As the InAsP QD material show non-thermal distribution at 150 K, it would be beneficial to study the carrier distribution below this temperature, up to 20 K, to investigate whether the system demonstrates random population. (Finch et al. 2013) concluded that optical pulse duration can be significantly reduced by operating in the random population regime which was below 50 K for for InAs QD lasers and they observed a pulse width as short as 290 fs at 20 K.

- As InAsP QD material shows a few positive points that can support monolithic passive mode-locking such as broadening in the both homogenous distribution and optical gain bandwidth as well as the faster recombination rate. It is suggested to employ this material in mode-locked laser regime.

7.3 References

Finch, P., Blood, P., Smowton, P. M., Sobiesierski, A., Gwilliam, R. M. and O'Driscol, I. **2013**. Femtosecond pulse generation in passively mode locked InAs quantum dot lasers. Applied Physics Letters 103(131109), pp.1–3.